Model and experimental validation of a PEM fuel cell for performance, durability, signal optimisation and exergoeconomic evaluation

Abdelnasir Omran

A PhD Thesis

ASTON UNIVERSITY

December 2023

© Abdelnasir Omran, 2023

Abdelnasir Omran asserts his moral right to be identified as the author of this thesis. This copy of the thesis has been supplied on the condition that anyone who consults it is understood to recognise that its copyright rests with its author and that no quotation from the thesis and no information derived from it may be published without proper acknowledgement.

Aston University

Model and experimental validation of a PEM fuel cell for performance, durability, signal optimisation and exergoeconomic evaluation

Abdelnasir Omran

PhD Thesis

2023

Thesis abstract

In this research, experimental data and simulation models were utilised to examine the performance, efficiency, signal optimisation and exergoeconomic evaluation of PEM fuel cell. The work was conducted through experiments carried out on 0.5 kW and 1.2 kW PEM fuel cells, in addition to three MATLAB/Simulink models here developed. A steady state Simulink model was created for the 0.5 kW fuel cell, and a M. Script model was built for the 1.2 kW fuel cell to perform an exergoeconomic analysis, in addition to a MATLAB/Simulink model to optimise voltage, current and power signals. Model and experiments of the 0.5 kW fuel cell revealed the maximum overall system efficiency of around 47.5% at 50% of the rated power. It is recommended that the system of 1.2kW operates at a stoichiometric ratio of less than 4 to optimise the relative humidity level in the product air and avoid the membrane drying out at higher operating temperatures. The predicted hydrogen price of 1.9 $/kg will improve the exergy cost by about 15 $/GJ, which is a decrease of 12% compared with today's price. In terms of voltage values of the Power Electronic Interface of 1.2kW, it settled the voltage at 42V with less steady state error while Nexa settled it at 38V. Both managed to settle their output voltage in less than 18 ms, corresponding to less than 0.1 s sampling period, indicating that the optimisation model here presented can be used for devices that entail swift change of load requirements.

Keywords: Hydrogen Fuel Cell, Fuel Cell Performance, Mathematical Modelling, Numerical Simulation, Exergoeconomic Analysis, Signal Optimisation.

بِسْمِ اللَّهِ الرَّحْمَٰنِ الرَّحِيمِ

وَسَخَّرَ لَكُم مَّا فِي السَّمَاوَاتِ وَمَا فِي الْأَرْضِ جَمِيعًا مِّنْهُ ۚ إِنَّ فِي ذَٰلِكَ لَآيَاتٍ لِّقَوْمٍ يَتَفَكَّرُونَ ﴿١٣﴾

He 'also' subjected for you whatever is in the heavens and whatever is on the earth-all by His grace. Surely in this are signs for people who reflect.

[The Glorious Quran (Al-Jathiyah) (13)

This thesis is dedicated to:

My Parents.

My Family.

My colleagues and friends.

Acknowledgements

ALL PRAISES ARE DUE TO MY LORD, THE LORD OF THE UNIVERSE, THE ENTIRELY MERCIFUL, THE ESPECIALLY MERCIFUL.

I am grateful to my supervisor Dr Jose Sodre for sharing knowledge and experience with me and for his patience and endless support. I would also like to convey my most profound appreciation to my associate supervisors, Dr Abed Alaswad and Dr Amirpiran Amiri, for their support during my PhD project. I also appreciate my teachers, Mr David Smith, and Dr Tabbi Awotwe, for all their technical advice and laboratory support. I want to thank Dr Laura Leslie for her help and the teaching opportunity she honoured me with to enhance my teaching skills. I am grateful to all academic and supporting staff for their support and kindness.

I am thankful to all my colleagues, students, and friends for their immense support. Finally, I would like to convey my great gratitude to my wife and children for always supporting, advising, and encouraging me.

Contents

List of Figures

List of Tables

Nomenclature

ACC	annual capital cost, US$
c	cost, US$
CF	capacity factor, dimensionless
CRF	capital recovery factor, dimensionless
$\dot{E}_{aux}$	auxiliary load, kW
E_e	electrical power output, kW
$\dot{E}_{ext}$	external load from reactant consumption, kW
ex	total exergy transfer per unit mass, kW/kg
ex_{CH}	chemical exergy per unit mass, kW/kg
ex_{PH}	physical exergy per unit mass, kW/kg
$\dot{E}x$	exergy, kW
F	Faraday constant (96,485 C)
h	specific enthalpy, kJ/kg
i_r	annual interest rate, dimensionless
I_{fc}	fuel cell stack current, A
I_m	measured current, A
$\dot{m}_{H_2}$	hydrogen mass flow rate, kg/s
n_{H_2}	number of moles of hydrogen consumed per mol of oxidant in the reaction, mol
n_y	number of years, dimensionless
N	number of cells in the stack, dimensionless
P	pressure, kPa
s	specific entropy, kJ/kg.K
T	temperature, K
V_{fc}	fuel cell stack voltage, V
V_m	measured voltage, V
x_n	mole fraction of component n, dimensionless

Greek symbols

η	Fuel cell efficiency, %

Subscripts and superscripts

air	air
AC	alternating current
AFC	alkaline fuel cell
BEIS	the UK department of business, energy & industrial strategy
BEVs	battery electrical vehicles
BOS	balance of systems
C	capital
CCS	carbon capture storage
CCUS	carbon capture utilisation & storage
CFD	computational fluid dynamic
CO_2	carbon dioxide
CoS	city of Surry
DC	direct current
DI	deionisation
DMFC	direct methanol fuel cell
DOE	the US department of energy
E	exergy
EU	European union
FC	fuel cell
FCEBs	fuel cell electric buses
FCEVs	fuel cell electrical vehicles
FTA	the US department of transportation's federal transit administration
GDL	gas diffusion layer
GDP	gross domestic productions
GE	general electric
GHG	greenhouse gas

H	enthalpy
H_2	hydrogen
H_2O	water
HES	hydrogen energy systems
HT	high temperature
HVAC	high voltage alternating current
HVDC	high voltage direct current
I	investment
IC	internal combustions engines
IEA	the international energy agency
IPHE	international partnership for hydrogen and fuel cells in the economy
JLR	jaguar land rover
KOH	potassium hydroxide
LANL	Los Alamos national labrotarty
LCH	low carbon hydrogen
LPG	liquid petroleum gas
LT	low temperature
n	component in the reaction
NREL	the national renewable energy laboratory
NTS	national transmission system
MEA	membrane electrode assembly
MCFC	molten carbonate fuel cell
MoU	memorandum of understanding
OCV	open circuit voltage
OM	operation and maintenance
P	products
PEMFC	proton exchange membrane
PFI	per-fluorinated ionomer films
PI	proportional-integral
PiCG	plug-in car grant
PAFC	phosphoric acid fuel cell

PWM	pulse-width modulation
R	reactants
R&D	research and development
RH	relative humidity
S	entropy
Sinopec	China petroleum & chemical corporation
SOFC	solid oxide fuel cell
TRL	technology readiness level
UAVs	uninhabited air vehicles
UDDS	the urban dynamometer driving schedule
UK	United Kingdoms
VNT	variable nozzle turbine
Va	the immediate rise in voltage
Vr	the slow rise of voltage to OCV
YSZ	yttrium-doped zirconium oxide

1 Introduction

This chapter presents a background of fuel cells, particularly the proton exchange membrane (PEM) type, as well as the aims and objectives, research gap and novel contributions of this work.

1.1 Background

The excessive use of fossil fuels for decades has dramatically damaged the environment and life on earth [1]. Many countries have been increasingly putting pressure on the automotive industry through rigorous regulations to minimise emissions. These regulations seriously consider an alternative to internal combustion engines, which account for a big deal of air pollution and pollutants affecting breathing and cardiac health in many major cities worldwide [2]. With the successful commercialisation of battery electric vehicles (BEVs) in the last few years, fuel cell electric vehicles (FCEVs) has the potential to follow a similar step and provide additional solution to many of those problems.

A fuel cell is an apparatus that directly converts chemical energy into an electrical form [3], generally powered by hydrogen as fuel and air as an oxidant. The use of hydrogen and air is a significant advantage compared to any other thermal machine since the losses concerning the combustion and the conversion in mechanical energy systems are not apparent in fuel cells [4]. In addition to the higher efficiency, a fuel cell can guarantee free emission energy production [5,6]. While a fuel cell is running with hydrogen fuel, there are no local discharges since heat and water are the only by-products of the reaction [7].

Nevertheless, hydrogen is not accessible in free form, requiring it to be obtained from hydrogen-containing compounds such as water and hydrocarbons. The extraction process produces carbon dioxide, so the pollution concern is just shifted. For example, hydrogen can be obtained from electrolysis by electricity generated from green energy to avoid any discharges in the whole fuel cell lifecycles [8].

Figure redacted

(a)

(b)

Figure 1. Single cell image (a) and exploded view (b) of a fuel cell [9].

Figure 1 captures the several individual components of fuel cells in a simplified schematic. Fuel cells usually have two electrodes which are the anode and the cathode. Electricity is produced as consequence of an electrochemical reaction between a fuel and an oxidant, directing the evolution of heat and water as a by-product of the electrochemical reaction. The various categories of fuel cells differ based on the type of membrane/electrolyte used in the development of the cell. Most investigations in fuel cells are conducted mainly to ascertain the possibility of maximising the electrochemical process to guarantee that higher cell efficiency is obtained at a lower operating cost.

The initial demonstration of fuel cells was made by the English lawyer and scientist Sir William Robert Grove, in 1839. Experimenting with electrolysed water into hydrogen and oxygen by passing an electric current across it, he reversed the experiment by managing to recombine hydrogen and oxygen to produce an electric current. It took scientists a century-long to bring fuel cells into practice [10,11]. In the 1950s, General Electric Company (GE) started enhancing fuel cells. As a result, the company won the contract, which allowed it to build a 1 kW fuel cell system for the Gemini series of spacecraft in 1962 [12]. The system had 35 mg Pt/cm^2 platinum loading, and it had the performance of 37 mA/cm^2 at 0.78 V. Material science was not as advanced as today; the material used in the system was costly, and the fuel used was pure hydrogen and oxygen.

Further improvement was needed on the fuel cell. In 1966, an innovation was made through the development of Perfluorinated Ionomer (PFI) Nafion membranes [13]; this step was decisive for improving Proton Exchange Membrane (PEM) fuel cells at that time. Since then, research and development of Proton Exchange Membrane Fuel Cell (PEMFC) have lost momentum, and the focus was shifted elsewhere for decades. Recently, the innovation of material science and new laboratory technologies enabled scientists to reach a breakthrough. Some laboratories, such as Los Alamos National Laboratory (LANL), improved the catalyst effectiveness and moderated the quantity of platinum required in PEMFC [14].

A recent study showed that the transport sector around the globe emits about 7000 Mt CO_2 annually into the atmosphere, making it the second-largest pollutant of greenhouse gas

(GHG) emissions. In 2012, the transport sector in the UK was responsible for 21% of GHG emissions at 118 $MtCO_{2eq}$ and the road vehicles share was 68% of it. One of the measures the UK implemented to confront the emissions challenges in the transportation sector is the ultra-low emission vehicles (ULEVs) development strategies, financed via the Office for Low Emission Vehicles. The strategies aim to maintain the early market of the ULEVs [15]. In 2008, the American National Research Council of the United States mentioned hydrogen fuel cell vehicles as the best substitute for the GHG emissions reduction target [3]. In 2012, the UK government also considered FCEVs as one of the solutions to reduce GHG emissions. It established the UKH2Mobility (a private-public partnership) to develop FCEVs in the UK, starting in 2015 [16]. To overcome the GHG emissions complications, FCEVs could be one of the problem solutions for the transport division in the EU and worldwide.

PEMFCs are composed typically of a Nafion membrane holding positive ions H^+, operating on hydrogen as fuel and oxygen/air reactants. The polymeric membrane acts as an electrolyte. Thanks to fast start-up, elevated power density, lightness, compactness, and low operation temperature, PEMFCs are indicated for automotive applications [17]. Depending on the electrolyte used, it can work at a low temperature between 60–80°C (low-temperature PEMFCs) or a high range between 130–200°C (high-temperature PEMFCs). The advantages are the fast cold start and high efficiency, in addition to the fact that they can be simply assembled in stacks, thus giving higher energy production. The cathode is equipped with air, while the anode is packed with hydrogen.

If hydrogen is produced from fossil fuel reforming, it is essential to eradicate the existence of carbon monoxide (CO) to avoid catalyst poisoning in low-temperature PEMFCs. High-temperature PEMFCs are not susceptible to CO and do not need membrane hydration, which is vital for operating low-temperature PEMFCs. These must be provided with a water management system.

PEMFC has been preferred by the motor industry so far due to its numerous advantages compared with other types of fuel cells [18]. The need for more rapid start-up times,

recurrent starts and stops, and processes at low and high temperatures are reasons for PEMFC to be favoured [19]. FCEVs can become cost-competitive with internal combustion engine (ICE) automobiles and provide higher efficiency, producing fewer GHG emissions per-mile than ICE cars. In addition to that, FCEVs have zero exhaust emissions and have the ability to quick refilling just like ICE cars. With a full hydrogen tank of 5kg stored at 700 bar, they can drive over 500 km. Although the hydrogen infrastructure is not yet as it should be, many companies have already started commercialising FCEVs, such as Toyota and Hyundai; Honda and Daimler may follow soon.

FCEVs and BEVs are favourites to ICE vehicles to reduce pollutant and GHG emissions. FCEVs can boost car efficiency and reduce fossil fuel consumption and global GHG-zero emissions in major cities[20]. A recent review study covering the emissions problem in major urban cities shows that hydrogen fuel can be a sustainable option for road transportation. Many countries and private sectors strongly support hydrogen fuel as an alternative to conventional fuels in the transport sector [21].

Several car companies have developed FCEVs and started selling models, such as Toyota Mirai, Hyundai ix35, Hyundai Nexo and Honda Clarity. Other companies like Mercedes Benz, Audi and BMW are on the way to the market. One of the few commercially available FCEVs in the UK is Toyota Mirai (Figure 2). Some challenges new owners face are lack of enough hydrogen refuelling stations (less than 20 in the UK), high price of hydrogen, low durability and other mechanical problems. To overcome these problems, Toyota includes in the price the cost of fuel and it offers the car on lease only [22]. The cost and durability targets of the United State Department of Energy (U.S. DOE) are $30 per kW and 8000 h, respectively, for light-duty FCEVs, which are comparable with those of traditional automobiles. The Hyundai NEXO has a driving limit of 611 km and a stack power of 95 kW with 3.1 kW/L power density. Early in 2021, Toyota launched a redesigned second-generation Mirai with a price tag of about US$ 49500, driving range of 647 km, stack power 128 kW, and power density 4.4 kW/L [23].

Figure redacted

Figure 2. Toyota Mirai [22]

Due to the generation of hydrogen from non-renewable sources, FCEVs emit around 120 g/km of carbon dioxide (CO_2) over their lifecycle. Clean hydrogen will cut that to 60 g/km CO_2. In 2011, the Honda dealership in Wiltshire town in the UK was the first hydrogen station to produce pure hydrogen from solar power. In Swindon, there were two hydrogen stations and six FCEVs in 2018, and the company Arval planned to have 170 in 2020 but that has not been met. By January 2023 there were 300 FCEVs in the whole UK according to the Society of Motor Manufacturers and Traders and 15 hydrogen filling station. The market of FCEVs in the UK could value about £15.2 billion by 2030. Globally, Toyota, Daimler and BMW are on the top of the thirteen corporations devoting $10bn throughout the next ten years to emerging hydrogen equipment and substructure. The number of hydrogen stations in Germany reached 89 in 2023. In the UK, studies show that 1 TW renewable energy is wasted due to lack of storage; this could generate about 18,000 tonnes of hydrogen, which could fuel 90,000 cars for 12,000 miles [24].

Riversimple Rasa, a Wales firm, has built a lightweight (580 kg) car sourcing a carbon composite chassis and fibreglass body panels (Figure 3). It uses an 8.5 kW PEMFC, while normal FCEVs use 85 kW PEMFC. The company is planning to build 20 prototypes [25]. Under the name of project Zeus, a consortium of companies led by Jaguar Land Rover (JLR) in the UK is working on FCEVs prototype. The UK government funded the programme with £73.5 million aiming to uplift FCEVs supply chain in the country [26].

Figure redacted

Figure 3. Rasa Car from Riversimple firm in Wales [25]

The collaboration between companies, manufacturers and politicians has shaped an appropriate essential environment for hydrogen buses in numerous countries and cities worldwide. Recently, the public transport companies in Vienna started the test of hydrogen buses. The plan is to operate ten buses from 2023 (Figure *4*). Bus manufacturer Solaris made buses with 70 kW fuel cells and high-power batteries. The energy is also recovered by braking. There are two integrated electric motors of 125 kW each. The hydrogen tank is on the roof, offering a range of up to 400 km. In addition to the investment, the company and its partners plan to build an electrolysis plant in Vienna to produce green hydrogen from renewable power [27].

Figure redacted

Figure 4. Hydrogen buses in Vienna from 2023 [27]

This same company, Solaris, which uses Ballard 20 FCmove™ -HD modules, had 40 buses in 2021 in The Netherlands and soon will run buses in Germany and Italy. Starting from the 2nd quarter of 2023 the company had plans to deliver 10 buses of the Urbino 18-meter model to the Netherlands. Since 2019, Zhongzhi Hydrogen Fuel Cell buses (Figure *5*) have been

operational in China. More than 500 hydrogen buses served during the 2022 Winter Olympics, which was co-hosted by Beijing and Zhangjiakou [28].

Figure redacted

Figure 5. Hydrogen buses in China [28].

In the UK, Ryse Hydrogen Ltd, a subsidiary of Wrightbus based in Oxford, announced a plan to invest £500 million to build a 3000 PEMFC bus fleet in the Ballymena plant, Northern Ireland [29]. The buses will operate in major UK cities, 400 of them in Birmingham. These buses are reported to save around 280,000 tons of CO_2 annually, equivalent to the pollution from 107,000 conventional vehicles. Ryse is also building the first UK hydrogen generation plant employing electrolysers on the Kent coast, powered by a nearby offshore wind farm. The company plan to build four additional plants by 2025.

Modifications in fuel cell function mode and material structure are essential to make them marketable. Fuel cells can be maintained without any dependency on fossil fuels, which is subject to the source of hydrogen production. Avoiding conventional fuels would produce electricity from environmentally friendly fuel cells, primarily if the hydrogen gas is generated from renewable resources. Another reason for the environmentally friendly nature of fuel cells is that water is the derivative of the electrochemical reaction in the fuel cells, making it an ideal contender in the quest for fighting climate change. Fuel cells are further designed to have a quick start-up time compared to other sources of energy generation [30,31].

The non-existence of moving parts in fuel cells is another distinction between these energy-converting devices; this suggests that maintenance time and cost can be

reduced compared to other conventional mediums of energy conversion. The operation of fuel cells is also highly dependable, with virtually no form of vibration due to the nonexistence of moving components. The efficiency and power densities of fuel cells are also more remarkable than those of batteries and heat engines. Fuel cells commonly have extended life periods because they only generate electricity by introducing the reactants into the cell. Other electro-chemical devices like batteries tend to have shorter life spans since electrochemical reactions occur in the battery even when they are not producing electricity. Fuel cells are not usually corrosion-resistant like other energy devices [17,32].

The major drawback of fuel cells has to do with overall cost. The membrane, which is the centre of the cell, is often coated with a catalyst, primarily to pace up the electrochemical reaction. Various catalysts used are platinum and ruthenium. Nevertheless, loading these catalysts on the membrane significantly impacts the cell overall cost. The other major challenge of fuel cells is thermal and water management. Since fuel cell performance is proportional to cell operational temperature, the cell performance is expected to reduce if it operates below or above its recommended range of operating temperatures. It can sometimes be complex as frequently preserving a constant cell operating temperature becomes very tedious in managing the cell [33–35]. Mitigation strategies like improving the relative humidity of the reactants in the cell have been proposed in some studies. However, this often raises the system total cost. The readiness of the fuel, paired with its storage, is another encounter that must be factored into future research activities.

The universal hydrogen fuel cells market was US$2.6 billion in 2022. In 2023 it reached US$3.3 billion and expected to reach US$8.7 in 2028. The change in growth trend is generally due to the encouraging government strategies and grants for R&D and application such as fuel cell automobiles[36] . According to the report, Asia Pacific was the most significant territory in the hydrogen fuel cell market in 2021. North America was the second-largest marketplace in the hydrogen fuel cell market. The regions

encompassed in this statement are the Middle East and Africa, Asia-Pacific, Western Europe, Eastern Europe, North America and South America.

1.2 Aims and objectives.

This PhD project aims to develop a steady-state simulation model and an exergoeconomic model for a PEMFC system to investigate how temperature, pressure, humidity, fuel and air mass flow rates, and cell voltage and current can optimise the performance and efficiency, improve reliability, and reduce cost. The simulation model calculates the fuel cell output current, voltage and power, analysing the system response to different external loads, and is compared with experimental data from the commercial Horizon H-500XP fuel cell stack. The exergoeconomic model analysis was based on a 1.2 kW Nexa™ PEMFC at variable operating conditions, calculating the fuel and product exergy and the cost rates associated with these quantities. The output power of PEM fuel cell depends on the operating conditions, including hydrogen partial pressure, oxygen partial pressure and cell temperature [37]. Each of these conditions has a unique operating point with the highest output. To reach this point a close loop of PEM fuel cell, DC/DC boost converter and Proportional Integral Derivative (PID) controller has been designed and simulated in MATLAB/Simulink. The specific objectives are thus summarised:

1. Build a MATLAB/Simulink-based PEMFC simulation model to predict steady-state operation performance and efficiency parameters.
2. Experimentally validate the model using an H-500XP PEM fuel cell in laboratory tests with varying loads.
3. Apply the model to investigate the effects of temperature and pressure on the performance and efficiency of a PEM fuel cell.
4. Develop a MATLAB-based model using M. Script for exergoeconomic analysis of the fuel cell.
5. Experimentally validate the model using the Nexa™ 1.2kW PEMFC system in laboratory tests with varying loads.

6. Investigate the effects of temperature, pressure, air stoichiometric ratio, and cell voltage variation on exergy and energy efficiencies.
7. Investigate the exergy cost on Nexa™ 1.2kW PEMFC system at various operating temperatures, pressure, cell voltages and air stoichiometries.
8. Apply the exergoeconomic model to optimise the system for performance, efficiency, and costs.
9. Build a MATLAB/Simulink-based PEMFC simulation model to increase the power production using an improved power electronic interface.
10. Optimise the model signal using PID optimisation tool.

The project draws on existing literature in fuel cell systems modelling and parameter control and employ fluid flow, heat, and mass transfer principles to develop the MATLAB models. Both the H-500XP and Nexa™ 1.2 kW fuel cell system systems are available resources in Aston University laboratories. The models were validated by experiments monitored and controlled by LabVIEW software. The MATLAB simulation model was used to analyse the fuel cell performance, efficiency, and the effects of temperature and humidity changes to determine optimal operating conditions. The exergoeconomic model indicated the conditions of maximum performance and minimum costs, while the power enhancement model provided ways to increase the power production using an improved power electronic interface instead of adding more costly cells to the PEMFC stack.

1.3 Research gap and novel contribution of this work

The proton exchange membrane (PEM) is one of the most popular fuel cells commercially available. PEM fuel cells are already commercially applied, especially in the transportation and small appliances. Although these devices can offer a quick start-up, fast transient response, and high energy density, further research is still needed to improve their durability and performance and to maximise their conversion efficiency [38]. These achievements will help to make this technology more feasible and widespread in its application.

Temperature, pressure, air stoichiometry and cell voltage are some of the most significant factors affecting fuel cell performance and efficiency. Temperature increases result in improved membrane proton conductivity, enhanced electrode kinetics and increased mass transfer of the reactants, leading to higher performance. However, high temperatures can lead to membrane dehydration, hydrogen crossover, degradation of components and, consequently, shorter fuel cell lifetime. Another critical parameter is humidity, as appropriate water management is required to guarantee decent proton conductivity during fuel cell operation. Inadequate humidity lowers the conductivity of the membrane yielding low output currents. In contrast, excessive moisture leads to flooding of the electrode and reducing the yield current due to the electrochemically active area decrease [4,9,39] .

Temperature and humidity are intensely dependent on each other, and critically connected to water diffusion across the membrane. Water absorption and desorption dynamics are a function of the operating temperature; therefore, the optimal management of different component humidity and operating temperature must be decided together to maximise the system efficiency and improve its performance and durability. In addition to temperature and humidity, increasing pressure benefits performance as this increases the diffusivity of the reactant gases, enabling mass transport to the electrodes [9]. Air stoichiometry has close relation with temperature and pressure; too high stoichiometry causes membrane drying, while too low stoichiometry indicates low partial pressure that initiates mass transport losses.

Finally, the cell voltage of the system can play a key role in its exergy cost; in the specified cell voltage range of PEMFC (0.7 to 0.9 V) the lower the cell voltage, the greater the mass flow rates required for reactants and products operating the system to produce the desired power output. Power increase without adding more cells to the stack or extra energy storage reduces cost and improve reliability and commercialisation. Power demand is continuously increasing as the technology advances.

This PhD project expects to provide a unique scientific contribution to PEMFC technology through a better understanding of temperature, pressure, air stoichiometry, cell voltage and

humidity effect and suggesting ways to optimise operation to improve performance, efficiency, power production, reliability, and reduce cost.

1.4 Organisation of this work

Chapter two covers the literature review of PEMFC, including PEMFC challenges and breakthroughs, modelling of PEMFC, fuel cell applications, and hydrogen as an alternative clean fuel. Chapter three highlights the relevant fundamentals to this work, including concepts of PEMFC, exergy and exergy cost of PEMFC, and electrical circuit of PEMFC. Chapter four shows the methodology applied, including the experimental setup of the H-500XP PEMFC and Nexa™ 1.2kW PEMFC systems, the simulations of H-500XP and Nexa 1.2kW fuel cells using MATLAB/Simulink, and the development of the exergoeconomic model using MATLAB M.script. Chapter five covers the result and discussion while Chapter six presents the summary, conclusion and recommendations for future work.

In summary this introduction chapter covered a four subsection, a background of fuel cells which shows that the most used type of fuel cells in automotive is the PEM fuel cell which required a hydrogen and oxygen to operate. The aim and objectives subsections highlighted that to improve performance, efficiency, reliability, voltage and reduce cost a three MATLAB/Simulink models must be built, validated, and implemented. Although there has been an increasing interest in prototype of PEM fuel cell automotive, research show that more work needs to be done before full commercialisation. Research gap shows that more work in atomic level need to be done to achieve the aim and objectives. The last subsection outlined the structure of the thesis which showed that the thesis includes six chapters in addition to the appendices and references.

2 Literature Review

This chapter covers the challenges and breakthroughs of PEM fuel cells and the progress of ongoing research on the topic. Besides, it covers how research has been conducted through mathematical modelling or experiments. It also includes some applications of PEM fuel cells in addition to hydrogen as an alternative clean fuel.

2.1 Proton Exchange Membrane Fuel Cells (PEMFC)

PEMFC, also identified as, Polymer electrolyte membrane (PEM) fuel cells, use a proton-conducting polymer membrane as the electrolyte. A polymer electrolyte is a material that allows hydrogen ions to travel across the membrane layer. These cells typically operate at relatively low temperatures (< 90 ◦C) and can swiftly adjust their output to meet altering power requirements. Nevertheless, due to their low operating temperature, they cannot directly use fossil fuels, such as natural gas, liquid natural gas, or ethanol. These fuels must be transformed into hydrogen in a fuel reformer to be utilized by a PEM fuel cell [23]. The low functioning temperature permits them to be started rapidly (low warm-up time), resulting in less wear on system components, thus increasing the cell stability.

Nevertheless, a noble-metal catalyst (typically platinum) is required to start the electrochemical activity at low temperatures. This fuel cell is supplied with hydrogen, which is oxidised at the anode, and oxygen, which is reduced at the cathode. The protons released during hydrogen oxidation are directed across the polymer electrolyte membrane to the cathode. The electrons liberated from the hydrogen travel along the external electrical load provided. Since the membrane is not electronically conductive, it generates an electrical current. This technology has drawn the most interest because of its simplicity, viability, and quick start-up (due to the low running temperature), and it has been demonstrated as a good solution for generating static and mobile electrical power. PEMFC systems are specifically well-suitable for vehicle applications since they do not require hazardous fluids and have high power densities and low operating temperatures. Nevertheless, cold start problems should be enhanced for a cost-effective vehicle application of PEM fuel cells.

Figure redacted

Figure 6. Proton Exchange Membrane Fuel cell diagram [40]

Like all fuel cell types, PEMFC comprises three essential parts, as shown in Figure 6: anode, cathode, and membrane. These parts are manufactured from separate sheets. The electrolyte layer electrodes are then merged by a hot-pressing process to create a “membrane electrode assembly” (MEA) [41–43]. The MEA comprises two gas diffusion layers (GDL), a proton exchange membrane and two catalyst layers. Typically, these components are fabricated individually and then pressed together at moderate temperatures and pressures.

Although many various types of membranes are used, the most common is Nafion (DuPont), a sulphonated polymer along with a polytetrafluoroethylene (PFTE) backbone [44]. The Nafion is created by adding sulphuric acid classes hooked on the dimension of a polymer matrix of Teflon, and its layer holds a thickness in the range of 50-175 μm. The thinner Nafion membrane permits a higher conductivity of the cell but introduces more challenging water management; a bulkier membrane reduces the conductivity. The purpose of this formation is to behave as an electrolyte (ionic conduction) and a barrier between oxygen and hydrogen. Other types of membranes being researched are polymer-zeolite nanocomposite PEM, sulfonated polyphosphazene-based membranes, and phosphoric acid-doped poly (bisbenzoxazole) high-temperature ion-conducting membranes [45]. Still, the Nafion membrane is so commonly used (due to its high chemical steadiness) that it is regarded as an industry standard, and all other new membranes are compared to it. The main characteristics

of the membrane are 1) high water uptake; 2) good proton (H^+) conductor if well hydrated but does not allow the conveyance of electrons which are restricted to follow an outside path, thus generating an electrical current; 3) does not permit the intermixing of hydrogen and oxygen, thus maintaining the two gases separated; 4) high chemical and mechanical resistance owed to the properties of Teflon backbone.

The catalyst layer, also stated to as the effective layer, interacts directly with the membrane and the gas diffusion layer. Together with the anode and cathode, the catalyst layer is the position of the half-cell reaction in a proton exchange membrane fuel cell. The catalyst layer is applied to the membrane or the gas diffusion layer. In any case, the purpose of the catalyst layer is to put catalyst nanoparticles (commonly 5-15 nm platinum or platinum alloys, similar to Pt_xRu_y) within the vicinity of the membrane [41]. The aim is to produce a gas/solid/membrane triple contact to allow electrochemical reactions. The permeable gas diffusion layer in PEM fuel cells guarantees that reactants efficiently diffuse to the catalyst layer. Furthermore, the electrical conductor is the gas diffusion layer that transfers electrons in the catalyst layer. The tasks of the supporting layer are to (1) act as a gas diffuser, (2) deliver mechanical support, (3) deliver an electrical route for electrons, and (4) channel creation of water away from the electrodes.

The gas diffusion layers are built from porous carbon composition, or carbon cloth, with a thickness of 100–300 μm and coated with a microporous carbon powder/PTFE layer. The purpose of PTFE is to prevent water from “merging” within the pore volume of the backing layer so gases quickly make contact with the catalyst sites. Furthermore, it simplifies product water elimination on the cathode as it produces a non-wetting exterior within the tracks of the backing material. The gas diffusion layer also supports water management by permitting a proper quantity of water to reach and be kept at the membrane for hydration. Furthermore, gas diffusion layers are normally wet proof with a PTFE (Teflon) dispersion coating to guarantee that the holes of the layer do not come to be congested with liquid water [17] . Those parts and their characteristics permit the standard fuel cell process. Hydrogen at the anode divides into electrons and protons. The membrane lets the passage of only protons; the electrons travel outside, thus generating an electrical current.

In the meantime, protons pass through the ionic conductive membrane to the cathode. The H^+ protons then reach the cathode, generating water across their mixture with oxygen. Since elevated temperatures are not needed to hydrate the membrane, the PEM can be operated at shallow temperatures, in general, at 80 °C or lower. A typical fuel cell delivers a voltage between 0.5 and 0.9 V under normal operation condition, so to provide greater voltage and power various cells are arranged in series making a cell stack. Within a cell stack, each MEA constructed is positioned between two bipolar plates apart from the first and the last cell (Figure 7). Numerous different materials can be used for the realisation of a traditional bipolar plate; nevertheless, some necessities must always be guaranteed: 1) functionality of the electrical connection between two consecutive cells, 2) a continual and homogeneous source of hydrogen and oxygen to the electrodes of the diverse cells, 3) an effective thermal dissipation, and 4) the subtraction of the water formed by the reactions.

Figure 7. The way PEMFC stacked [40]

The advantages of the PEMFC are as follows [38]: 1) The power density of the cell stack is significantly elevated, especially in pressurised systems, 2) the operative pressure variation between the anode and the cathode can be huge due to the mechanical characteristics of the solid polymer electrolyte, therefore, operating with a pressurized system is relatively easy, and 3) A wide variety of cell component materials can be adopted because of its low operating temperature (80 °C). Using low-cost carbon materials may reduce the cell stack cost.

In contrast, the PEMFC technology shows the disadvantages listed as follows [18]. 1) PEMFC catalysts are vulnerable to CO poisoning owing to their low running temperature. Therefore, CO concentration must be decreased to less than 0.52 ppm with CO elimination if the reformate from hydrocarbons or alcohols is utilised as fuel for the PEMFC [46]. 2) The temperature of reclaimed waste heat is lesser than that of other fuel cells. As a result, retrieved heat can be utilized just as hot water. 3) The water management of the membrane electrolyte is essential for cell performance because it secures the proper amount of water to show its adequate ionic conductivity. Because of these features, PEMFC development for electric vehicles (EVs) and portable power applications still requires more time. The PEMFC technology also has the potential for residential cogeneration systems if combined with small-scale natural gas fuel processors.

PEM fuel cells have reached a partial commercialisation phase due to many initiatives issued worldwide (USA, Japan, Europe) by the more significant car constructors and governments. The initiatives mainly focus on further advancement of the cells for many demonstration purposes, which are simultaneously used to deepen the knowledge of the life cycle of PEMFC. However, each application of PEMFC has its issues. Two central problems are shared among all applications: the requirement to provide a stable quantity of pure hydrogen and reduce the costs of producing the cells.

The first issue refers to the difficulty to provide highly efficient hydrogen storage for long periods. In addition, there is lack of a detailed norm to provide operational and security standards for developing hydrogen distribution networks. The second issue concerns the use of platinum as a catalyst. The minimum Pt load in the electrodes is 0.2 mg Pt/cm^2. This low amount still increases the cost of fuel cell manufacture, whereas, at the same time, the performance is diminished. This is addressed by using electrodes with higher Pt content, thus increasing the costs even further.

Decreasing the quantity of Pt has been one of the foremost concerns throughout the past decade; one of the efforts has centred on the rise of consumption efficiency of the catalyst. To fully utilise the catalyst, all the Pt nanoparticles must have immediate contact with the gas,

the electron-conducting medium, and the proton-conducting medium. This condition is attained via an appropriate blending of Pt-supporting carbon elements and Nafion in the catalyst layer prepared by the conventional ink process. However, a significant portion of Pt is still isolated from the external circuit, resulting in low utilization. Even with the best-developed conventional electrodes, Pt utilization in commercial prototype fuel cells stays very low (20–30%). Nanomaterials can hold new viewpoints in solving the abovementioned problems. Nanostructured materials have very high specific surface and are essential for enhanced catalytic action.

An additional concern regards the actual high costs of producing hydrogen. There are various studies and ideas of methods (mainly electrolysis) to produce hydrogen; however, none has found a way to produce hydrogen with comparable costs to fossil fuels. The costs of generating electricity from PEMFC range between 3,000- 5,000 €/kW, and nearly 80% of those come from the membranes, catalyst, bipolar plates and the electrodes used (usually platinum), and hydrogen production [41,42,47]. These costs are far too high to allow the technology to be competitive with those based on fossil fuels, which cost for power generation range from 300 – 500 €/kW. In conclusion, further development focused on reducing cell prices (like discovering new catalysts and building materials) is yet needed for a mass introduction of PEMFC on the market. Water electrolysis is the best way to create high-purity hydrogen without using fossil fuels but, unfortunately, it requires high consumption of electrical power.

2.2 PEMFC Challenges and Breakthroughs

Although FCEVs were introduced decades ago, a remarkable market breakthrough has not yet been reached. A recent techno-economic and environmental study of the fuel cell was conducted using life cycle and value chain analysis [48]. The study identified the formal barriers in fuel cell commercialisation and the main end-user acceptance criteria: function, cost, and reliability. It concludes that green energy delivered with fuel cells is the business ideal of the prospect. The study recommended more alteration of public funds and the implementation of policy advantages that inspire more sustainable industrial investments.

The high expense and technical matters are the distinct significant obstruction to fuel cell commercialisation [49]. There have been several successfully specialised applications of fuel cells in the last decades, such as unmanned aerial vehicles (UAVs) [50], space shuttles [51] and submarines [52]. Fuel cells show advantages over ICEs and boilers regarding operation cost, but they have disadvantages in manufacturing cost and quality. Their expensive reparation and preservation costs, up to 60% of the overall system cost, outweighs their thermal efficiency advantages. Therefore, high quality and reliability are key factors for end-user approval and commercialisation of fuel cells [48].

A recent study [53] has conducted an in-depth review of fuel cell reliability, durability and performance. Fuel cell components, individual cells, and stack have each been subdivided into three operation ranges. Ranges of temperature and relative humidity (RH) have been associated with components such as membranes. Cells have been linked to parameters like pressure drop and channel velocity. At the same time, the stacks were connected to a tighter operational area than cells due to load variation and disproportionate flow circulation. The study suggested a solution for fuel cell scaling-up through connection building among components, cells, stack, process and system control.

Another study [54] states that the challenge of making cheap and robust fuel cells that can compete with other alternative energy sources comes from the lack of understanding of fuel cell operation at the atomic level. The study showed that out of the $22 billion in fuel cell research and development (R&D) globally, only a little had been spent on basic scientific research. Most venture has gone to subsidisations and product growth to create profitmaking markets for explicit fuel cell rehearsals.

Recent studies on an 80 kW PEMFC system presented by Argonne National Laboratory (ANL) [55] showed that the stack costs around 30 $/kW. Electrodes (51%), bipolar plate (24%) and seals (7%) are the most expensive parts of the stack (Figure 8). It was also found that the entire PEMFC system costs 59 $/kW at mass production volume, out of which 50% goes to stack (Figure 9). The research concluded that the stack and the management of air, fuel and thermal are the most affluent parts of the system.

Figure redacted

Figure 8. ANL PEMFC stack cost share [55].

Figure redacted

Figure 9. ANL PEMFC system cost [55].

Many investigations have covered the individual parts of the PEMFC system to enhance the resilience and dependability of the whole system [12,56,57]. To address the issues of fuel cell maturity level, a recent study [48] adopted the Technology Readiness Levels (TRLs) method (Figure 10) from previous applications [58,59] and used it to fuel cells. It was concluded that fuel cells, contrasting other products, have no strong TRLs. There are overlapping on all levels from TRL 1 until TRL 9. Many deployments have been reported (TRL 9) [54,60], while there is still essential investigation (TRL 1) going on subjects like platinum catalyst and multiphase

flow in a channel [61–63]. Wang et al. [48] showed that identifying the primary aspect of stumpy readiness and extraordinary overheads of fuel cells should be based on the development and authentication of the tools.

Figure redacted

Figure 10. TRLs of Fuel Cells [48].

Nevertheless, many stakeholders believe in fuel cell development and have invested heavily in promoting it. In Japan alone, company patents increased by 23-fold between 2000 and 2010 [64]. There is strong trust from many governments, investors and companies around the globe, arguing that a breakthrough could be realised with limited resources and time [65]. The European Union (EU) invested 2.8 billion euros in fuel cells and hydrogen economy in a framework program between 2014 and 2020 [49]. According to the European Hydrogen and Fuel Cell Association, 10.7 billion euros is invested by Hydrogen Council from 2019 to 2024

and, in 2019, there were 11200 fuel cell vehicles on the road. In Germany only, 350 million euros were invested in hydrogen station deployment. In 2018, there were 381 Hydrogen fuelling stations worldwide [66]. In 2014, the UK announced £11m as initial network funding to establish 15 hydrogen refilling stations by the end of 2015 out of 65 stations to be established in the following years.

Durability is one of the critical factors for automotive applications, as the US Department of Energy (DOE) target was 5000 h by 2025 and 8000 h beyond 2030 [19,67]. Reliability and availability appeared more critical for end-users [65]. All factors together require many investigations in materials, catalysts, cells and stack to eliminate or minimise deprivation as a result of the flow of water and temperature distribution obstacles [12,68–70].

2.3 Modelling and Simulation of PEM Fuel Cells

The electrochemical conversion in a PEMFC needs a battery for a start-up, air and hydrogen source, heat removal, and exhaust. The difficulties of the reaction and energy interaction between the elements and the environment and the high expenses of experimental studies stimulate the development of simulation models [71]. In addition, the fuel cell stack optimisation is challenging, and controlling the many accessories during operation is difficult as they affect the system's efficiency and performance.

Mathematical modelling of fuel cell structures is an appropriate approach to decrease investigation time and costs while providing in-depth analysis of various parameters that affect fuel cell performance and efficiencies, such as stack temperature, pressure, reactant moisture and air stoichiometry. A study applying a one-dimensional (1D) mathematical model for a completely hydrated and isothermal PEMFC concluded that the greater the cell current density, the greater the threshold of oxygen or air bleeding [71]. Simulink modelling was effectively applied to develop a temperature controller for the cooling system of an urban bus PEMFC stack, maintaining the target temperature in the range of ±0.5°C [72]. A bench test study applying a mathematical model to simulate the ability of the battery-PEMFC hybrid control system has proven its efficiency in managing the energy supply of an EV [18]. An

energy management system was designed using a neural network to control the power flux from a fuel cell-battery hybrid vehicle, showing its suitability for real-time vehicle controllers [73]. Modelling and simulation of fuel cells have also been used to study fuel-air flow patterns [74] and to perform an exergetic analysis [75].

Modelling of PEM fuel cell to examine its static and dynamic activities have been done in different ways, each one depending on the model aim. Some investigations highlight the mechanical and chemical occurrence in the stack, analysing performance of membranes, electrodes, and mass transfer [76–78]. These type of models, known as mechanistic models, tolerates the evaluation of durability, assessing optimal performing conditions or operating materials. This category of models has the disadvantages of requiring large number of parameters, making the simulation complex and not easy to implement. Models that include empirical and semi-empirical equations are more suitable for electric output evaluation [79–82]. Particle Swarm Optimisation (PSO) is a method originally found by Kennedy and Eberhart [83] that researchers have recently been using as an approach to solve optimisation problems.

The large number of internal and external parameters to be controlled simultaneously – gas flow, operating temperature, humidification membranes and others – makes PEM fuel cells a complex system to model. Modelling and simulation play an integral part in the development of fuel cells as they facilitate a better understanding of the physicochemical phenomena and parameters affecting the performance of fuel cell systems. The building of a model usually depends on its intended use, and a model can be used to design, understand, or management. The management of fuel cell systems is complex because of the many internal physical parameters, such as the current required by the load, the temperature of the stack, pressures and flow rates. All the used approaches for physical modelling are accompanied by a long and challenging experimental stage, including domain applications such as electrical engineering. Those parameters can be expressed by nonlinear relationships, but they are difficult to model because of their interdependency [84]. A study utilizing a 1D mathematical model for an entirely hydrated and isothermal PEMFC concluded that the greater the cell current density, the larger the threshold of oxygen or air bleeding [71]. Simulink modelling was successfully

applied to manage the temperature of a PEMFC stack and maintain it in a small variety near the target value [72].

A new methodology to determine the complex impedance parameters for a PEMFC was described [84]. The impedance modelling was based on electrical components such as resistors, inductors and capacitors. The MATLAB/Simulink model considered the parameters of the mathematical equations derived from the experimental test bench results and algorithm identification based on the least squares method. The simulation results are presented in the Nyquist diagrams, allowing to identify the transport phenomena inside the PEMFC. These results could be used to obtain a generalised model for on-board diagnostics of PEMFC vehicles.

A model for parameter identification of an equivalent circuit-based proton-exchange membrane fuel cell has been presented [85]. This model is represented by two electrical circuits, of which one reproduces the fuel cell output voltage and the other its thermal characteristics. The output voltage model includes activation, concentration, and ohmic losses as the static properties, while the double-layer charging effect, which delays fuel and oxygen supplies, and other effects provide the dynamic properties. In addition, a novel thermal model included the effects of the stack fan, which significantly improve the model accuracy. The parameters of both the electrical and thermal equivalent circuits were estimated based on experimental data from a Ballard Nexa™ 1.2kW fuel cell using an evolution strategy. The model was proven to be suitable for use in real-time fuel cell emulators.

A study was conducted on several DC-DC converter topologies to form a segment of a bus microgrid, concluding that unidirectional isolated current-fed DC-DC converters are desired for fuel cells while bidirectional converters are the selected option for ultracapacitors [86]. A bench test employing a mathematical model to simulate the capability of a battery-PEMFC hybrid control system demonstrated its efficiency in energy management of an EV [18]. An investigation on PEMFC energy management control for hybrid vehicles used mathematical modelling to reduce the cost and time of investigation activity [73]. A comparison study

between 1D and three-dimensional (3D) simulation models of PEMFC using the commercial code FLUENT-PEMFC module shows that the 3D model is helpful for more detailed predictions [87]. Nevertheless, 1D model is more likely to be utilised in instantaneous PEMFC simulations.

Another study investigated a PEMFC using a 3D model on COMSOL Multiphysics [88]. The model shows the significant effects of temperature and pressure on current density, in agreement with experimental data. Meiling et al. [89] reviewed the existing energy management approaches for FCEVs, intending to study the option of enhancing a health-conscious energy management strategy that improves the robustness of FCEVs by excellent prediction of deprivation. A recent study [90] investigated the deficiency of PEMFC and the driving forms influencing the lifecycle valuation of FCEVs. The study concluded that unfavourable operating conditions due to the starts/stops, speeding up/slowing down, membrane humidity discrepancy and high engine heap up influenced the truck average fuel economy by about 23%. The PEMFC system cost is relatively high to use in the experimental research field, therefore, simulation modelling is advantageous to emulate it.

A straightforward mathematical equation for steady-state and thermodynamic modelling was developed for the equivalent electrical circuit of a PEMFC [91]. MATLAB/Simulink was used for the simulation based on the experimental parameters of a Horizon H-500 fuel cell stack. Comparative parameter effects on the performance of the PEMFC was investigated. The study concluded that the ambient temperature and input gas pressure affected the performance of the PEMFC power delivery.

A review of the challenges and opportunities for modelling proton exchange membrane fuel cells has been presented [92]. Water management is regarded as the hot research area for PEMFC development for the last two decades. To maintain good proton conductivity of the electrolyte membrane (e.g., Nafion), it is critical to hydrate the membrane entirely, and external humidification is usually needed. On the other hand, the relatively low working temperature of PEMFC (about 80°C) causes the produced water to condense on the cathode side. The condensed water can flood the electrode pore regions, preventing the reactant gas from reaching the reaction sites and reducing fuel cell performance. Even worse, the electro-

osmotic drag effect causing water stream from the anode to the cathode is more significant at high current density, leading to dehydration of the electrolyte membrane (thus a lower proton conductivity) on the anode side and more significant flooding in the cathode. Thus, it is critical yet challenging to thoroughly hydrate the electrolyte membrane while efficiently removing the produced water from the cell.

The critical components of a PEMFC include the membrane, catalyst and gas diffusion layers, and bipolar plates [92]. The bipolar plate (BPP) is a vital element of PEM fuel cells because it supplies fuel and oxidant to the reactive sites, eliminates reaction products, collects the produced current, and provides mechanical support for the cells in the stack. Bipolar plates employ various patterns of grooves or flow field channels to feed reactant gases to the electrode of PEM fuel cells.

Blockage in the flow field channel of a PEM fuel cell can enhance the mass shift of reactant gas from the channel into the catalyst layer and improve cell performance [93]. The consequences of in-line and staggered blockage configurations within a parallel flow field and their fuel cell performance were numerically investigated using a 3D, multiphase, non-isothermal arithmetic simulation for this purpose. The results were contrasted with those of a baseline parallel flow field, not including blockages, showing that the staggered configuration enhances maximum net power by up to 11% over the baseline case and by 7% equated to the in-line case. The existence of over-rib-convection in the staggered configuration reduces the pressure drop by 70% compared to the in-line case, which only experiences over-block-convection.

A three-dimensional, multi-phase numerical model was established to analyse the optimal slope angle of the wave structure and the specific differences between the 3D wave flow field and a conventional serpentine flow field [94]. The simulation results show that waved flow channels are overall better than conventional flow channels. The wave flow can promote oxygen transport and remove the liquid water accumulated in micropores. The periodic waved structure leads to a cyclical variant of local flow direction, local flow velocity and local pressure to enhance forced convection, which improves oxygen transport rate in porous

electrode structure and, thus, the cell performance. Experimental verification proved that the waved serpent flow channel had a lower pressure decrease over the entire current density range and enabled a higher cell performance than conventional flow channels. The net maximum power density of the waved serpent flow channel was 17.8% higher than the conventional serpent flow channel.

An investigational test cell with an interdigitated flow field run under several aspect ratios, where the aspect ratio is the channel length-to-width ratio, improved net power densities with diminishing aspect ratios after accounting for parasitic pump losses [95]. In-situ neutron radiography found more water in great aspect ratio flow field patterns than in low aspect ratio patterns. It was also discovered more water in the 1.5/2 stoichiometry states than in the 2/4 stoichiometry conditions, indicating that liquid water is a likely cause of performance changes. A single-phase model applied to determine the variance in power from the changing distribution of cross flow found that decreasing aspect ratio resulted in higher overall performance. Experiments produced significantly more deficiencies in power density with a growing aspect ratio, suggesting that liquid water subtraction was the foremost contributor to the development in net power density rather than the dissemination of cross flow.

Convective heat transfer improvement of PEMFCs has been investigated numerically [96]. As the elevated heat transfer surfaces lead to elevated heat transfer levels, a flat plate porous layer is employed in the gas flow network. This improvement in heat transfer stems from the comparable alteration in the temperature and velocity profiles. The motivating parameters on these profiles are the stiffness, permeability, and porosity of the gas flow channel porous layer. The results indicate that convective heat transfer directly correlates with the gas flow channel porous layer thickness and permeability. Lower values of porosity conducted to higher Nusselt numbers and thicker microporous layer led to elevated heat transfer levels. The dimensions the total size of the microporous layer and gas diffusion layer have insignificant effects on heat transfer. The simulated values were utilized for training an artificial neural network model with high precision to produce more sensitivity analysis data and present respective 3D diagrams of the influencing parameters on heat transfer.

The plant system of a 9.5-kWe Nedstack P9.5-75 low-temperature proton exchange membrane fuel cell stack was tested up to the power of 2 kWe [97]. The system has been designed as a range extender for a series of hybrid EVs driven under urban duty cycles. Vehicle simulations have estimated that an average gross power requirement of 4 kWe is needed from the fuel cell, whilst simulations of the fuel cell stack and balance of plant components have allowed for the characterisation of transient behaviour and performance degradation.

Water distribution is one of the most significant handicaps and disadvantages for adequate operation of the polymer membrane of a PEMFC energy system. A mathematical model for defining the static and dynamic characteristics of energy behaviour (voltage, electricity, and relative humidity) for various input operating parameters (hydrogen, oxygen, water flow rates, temperature and current) [98]. This behaviour was designed to deduce and recommend an energy management plan for the PEMFC system that considers the various states of flooding and drought and contributes to an optimal humidity level for the system implementation. The study concluded that, to operate correctly, the relative humidity must be about 100% for the device to be effective.

The unbalanced direct current (DC) power produced from fuel cell stacks has to be controlled by power management subsystems to gratify load demands in terms of voltage, current and power quality [99]. Most of the control strategies can be implemented by using MATLAB/Simulink, one of those is the feedback and feed-forward control using proportional integral derivative control (PID). This has been used widely to improve the performance of PEMFCs [100–102]. In feedback control, the control variable is calculated and equated with its anticipated value or set point. The error is fed back into the system via the action of the deployed variable that is commonly known as downstream variable, which is proportional to the error, the totality of the current errors and the rate of variation of the error [103]. A self-tuning PID feedback control can be used to handle the non-linear dynamics by continuously retuning the control constants to adapt to the varying dynamic parameters [101]. To improve the work of self-tuning PID a close-loop least square parameter identification algorithm and assignment of closed-loop poles in real-time can be applied [104]. An optimisation-based approach to identify parameters is a promising solution [105,106]; one of those approaches

is the Particle Swarm Optimisation (PSO) method, which is has been applied in various engineering purposes and successful achieved satisfactory outcomes.

2.4 Exergy and Exergoeconomic Analysis of PEM Fuel Cells

The importance of using clean fuels is acknowledged by the need to reduce emissions caused by fossil fuels. The current geopolitics in Europe and the energy crisis related to it made the demand for renewable energy even more appealing. In this respect, hydrogen-fed energy systems such as proton-exchange membrane (PEM) fuel cells can positively affect the future of the energy sector [107]. PEM fuel cells is a promising renewable power generation system that solves some of the existing and future energy shortages [108].

Two primary performance analyses are here applied: energy-based analysis and exergy-based analysis. Several authors [4,5,109] emphasise that the energy-based analysis can be misleading because it does not identify deviations from ideal situations. In contrast, the exergy of an energy form or substance is a measure of its usefulness, quality, or potential to cause change. However, a better understanding of exergy and the insights it can provide into the efficiency, environmental impact and sustainability of energy systems are required for researchers working in energy systems and the environment. Furthermore, as energy policies play an increasingly important role in addressing sustainability issues and a broad range of local, regional and global environmental concerns, policymakers must also appreciate the exergy concept and its ties to these concerns.

During the past decade, the need to understand the connections between exergy and energy, sustainable development and environmental impact has become increasingly significant. Indeed, the universe energy content is constant, just as its mass content. On the other hand, exergy is not conserved; once the exergy is wasted, it can never be recovered. When energy is used for heating homes or public places, it is not destroyed but merely converted to a less proper form, a form of less exergy. The exergy of a system can be defined as its work potential compared to an exergy reference environment. The work potential is intimately related to the maximum work obtainable when the analysed system interacts with the reference

environment and simultaneously reaches equilibrium. The term exergy is also related to the thermodynamic availability of a system [110]. The exergy analysis complements the energy analysis and allows including the effect of the temperature level at which the analysis is being carried out [111].

The concept of exergy has also been explored in the area of fuel cells [108]. A thermodynamic and exergoeconomic assessment of a PEM fuel cell system was conducted at steady-state operation conditions [112]. The study found that, by increasing the current density, power density, exergy destruction rate, hydrogen consumption and the cost rate of power generation increases. An exergy analysis was carried out on a hybrid system consisting of 64 photovoltaic modules, a 5.5 kW fuel cell and an electrolyser [113]. The study concluded that the average annual exergy efficiency of the fuel cell is 32.8%.

Energy and exergy analyses were performed for a 1.2 kW Nexa PEM Fuel Cell unit in a solar-based hydrogen production system [114]. The study used a model and experimental setup of the system with different operating conditions and found that the increase in current density reduces the energy and exergy efficiencies by 14%. Varying pressure, temperature and anode stoichiometry, the research concluded that the energy and exergy efficiencies respectively increased by 23% and 15% when the pressure was increased, and by 17% and 14% while increasing the anode stoichiometry. Unlike pressure and anode stoichiometry, increasing the temperature has not affected the efficiency level.

Exergy analyses were conducted on 10 kW [115] and 1.2 kW [116] PEM fuel cells, respectively, to observe the effect of the operating temperature, cell voltage, air stoichiometry and pressure on the efficiency. The study concluded that the air stoichiometry should be less than 4, otherwise the membrane will dry out at a high temperature and the relative humidity level in the product air will not be maintained.
The economics of producing electricity from a PEM fuel cell was examined under various conditions [117], investigating the possibility of using a fuel cell vehicle to generate power while parking outside houses or offices. The study found that, for California, USA, net savings

could be reached if the fuel cell costs are about $6000 for a 5 kW home system ($1200/kW) with favourable natural gas costs of $6/GJ at residences.

Cogeneration using PEM and other potential fuel cell types was investigated, using both exergy and energy analyses [118]. The research found that exergy analysis is more rational and meaningful as it considers the equivalent work potentials of the thermal and electrical energy products. The study added that energy analyses often present misleadingly optimistic views of performance. The feasibility of fuel cells in cogeneration applications was studied concentrating on both engineering and economic viewpoints [38], using an optimisation approach through a numerical study. The investigation concluded that, in terms of plant capacity, economics, and energy savings, fuel cell cogeneration is better than conventional gas engine cogeneration.

A model was developed from an experimentally investigation of the operation of a PEMFC by applying an open cathodic plate fuel cell to improve the performance and efficiency [119]. The PEMFC efficiency was measured according to the operating pressure and voltage. The energy and exergy efficiencies of the PEMFC were found to be 47.6% and 50.4%, respectively.

A mathematical model of a PEMFC was developed to examine the causes of operating parameters such as temperature, anode and cathode pressures, gases flow rates, membrane thickness, and humidity [120]. The developed model comprised electrochemical, heat energy and exergy elements. Model simulation for the voltage yield of the cells displayed decent agreement with the investigational results sourced from the literature and exposed that the functioning flow rate of the reactants, temperature and pressure positively affect the presentation and efficiencies (energy and exergy) of the cell. The findings also suggested that high membrane thickness beyond 150 μm is disadvantageous to both the cell energy and exergy efficiencies and the fuel cell performance but the membrane humidity can positively favour both the energy and exergy efficiencies, which are also affected by the operational pressure, temperature, fuel and oxidant flow rates.

An exergoeconomic analysis conducted on a vehicular PEMFC including the stack, compressor, humidifiers and cooling systems concluded that the increase in temperature and pressure and the reduction of membrane thickness led to a decline in cost and an upsurge in system efficiency [121]. An exergoeconomic assessment of a heat recovery system for power generation using a PEMFC showed that high current density with a low operating temperature raises the total cost [122]. A thermodynamic and exergoeconomic evaluation of a PEMFC system at steady-state operation conditions investigated the feasibility of integrating a PEM electrolyser to supply the required fuel [112]. The results demonstrated that increasing the current density raises the exergy devastation rate of each component, hydrogen creation and consumption rates in the cycles, electrolyser output voltage, price rate of power production and power cost of the PEMFC. Moreover, increasing the PEMFC output voltage diminishes energy and exergy efficiencies but raising its outlet temperature boosts the power, power density rates, exergy and energy efficiencies of the system. Amplifying the outlet and operating temperature of the electrolyser improves the power consumption rate and lowers the energy and exergy efficiencies. The highest energy efficiency of the PEMFC was 54%, and the corresponding maximum exergy efficiency was 36.7%; the cost rate of power production was between 7.96×10^{-4} and 1.33×10^{-3} US$/s, and the equivalent rate of the exergy unit cost range was 115.6–132.2 US$/GJ.

Cost analyses developed for fuel cells were reviewed, focusing mainly on PEMFC technology since the solid polymer membrane electrolyte is strong and operates under conditions needed for most critical applications, especially in the automotive sector [123]. The cost of electrodes and membranes substantially impacts the total PEMFC cost, driving research to diminish the costs of these components. The most significant cost objective for the PEMFC of US$ 30/kW is obtained when the MEA price is lowered by 45%, which relates to a forecasted cost drop of catalyst fee by US$ 6.41/kW and membrane by US$ 1.44/kW. If these costs were met, PEMFC vehicles would reach a cost-competitive price to ICE vehicles.

In conclustion, the literature review showed that there is an interst in PEM fuel cell for automotive but part of the challenges is the reseach gap on the atomic level. Some of the techniqes used is the modelling and experimentals. Some of the gaps in research are the

parameter control and improve of performace, effecieny, reliability and reduction of cost which will be addressed in the projcet.

3 Fundamentals

This chapter covers the fundamentals of this research. It consists of four sections: Principles of PEM fuel cells, exergy and exergoeconomic analyses, the electrical circuit of PEM Fuel Cells and summary and conclusion. The first section is divided into five sub-sections on PEMFC: 1) Operations and Design; 2) Ideal PEMFC performance; 3) The PEMFC efficiency; 4) The effect of losses on the actual performance of PEMFC; and 5) The operating variables of PEMFC. The second section is divided into two sub-sections: 1) The energetic efficiency and the set of equations needed to calculate; and 2) the energetic cost analysis, which is based on the exergy analysis. The third section includes two main sections: 1) The electrical circuit of the PEMFC load model; and 2) The boost converter and the external load model. The chapter concluded with a summary and conclusion section.

3.1 Principles of PEM fuel cells

Fuel cells are energy conversion devices that alter the chemical energy of hydrogen into electrical power. The conversion necessitates a battery for start-up, air and fuel supply, heat removal, and exhaust. The main difference from conventional ICE is that fuel cells are zero-emission devices which exhaust is primarily water vapour [124]. Both fuel cells and batteries stimulate electrochemical conversion and are customarily assembled into stacks. Nevertheless, unlike batteries, fuel cells do not involve recharging and can continuously operate fed with hydrogen and oxygen or air. On the other hand, fuel cells align a wider group of ancillaries, and controlling them during operation is difficult as they affect performance and efficiency. Scaling up the stacks does not require a significant effort, but the difficulty in upgrading the ancillaries entails complete change.

A fuel cell comprises a negative electrode (anode) and a positive electrode (cathode) packed around an electrolyte. A reactant, such as a hydrogen, is fed to the anode and air is supplied to the cathode. A catalyst divides hydrogen atoms into protons and electrons in a polymer electrolyte membrane fuel cell (PEMFC), which gets distinct paths to the cathode. The

electrons go via an external circuit, generating a flow of electricity. The protons transfer across the electrolyte to the cathode, and they reunify with oxygen and electrons to generate water and heat. Although the fundamental processes of all fuel cells are the same, unique variations have been established to take advantage of numerous electrolytes and serve various application needs. The fuel and the charged species travelling through the electrolyte may differ, but the principle is the same. Oxidation ensues at the anode, while a reduction happens at the cathode. The two reactions are linked by a charged species that migrate via the electrolyte and electrons flowing via the external circuit.

Fuel cells can transform the chemical energy of fuels and oxidants into electrical power via electrochemical reactions in an efficient, quiet, and clean manner. In addition to electricity, fuel cells generate heat, which can fulfil heating needs involving hot water and room heating. Fuel cells which combine heat and power are essential for powering homes and buildings, where overall efficiency as high as 90% is attainable. This high-efficiency operation conserves money and energy and decreases GHG emissions. The essential operation of the hydrogen fuel cell is effortless [22].

The first presentation of a fuel cell made by William Grove employed an experiment similar to that shown in Figure 11. In water electrolysis (a), Water is separated into hydrogen and oxygen by the passage of an electric current. The flow of a small current (b) results from the combination of hydrogen and oxygen. The leading causes for the small current are the low contact area between the electrolyte, the gas and the electrode – just a tiny ring where the electrode emerges from the electrolyte – and the long distance between the electrodes causes the electrolyte to resist the flow of electric current.

To overcome these problems, the electrodes used in fuel cells are typically flat with a thin electrolyte layer, as in Figure 12. The electrode formation is permeable, allowing the infiltration of the electrolyte and the gas from different sides; this offers the highest potential contact between the electrode, the electrolyte, and the gas. However, the separate reactions at each electrode need to be considered to realize how the reaction between hydrogen and oxygen generates an electric current and how the electrons are generated. These critical

details vary for different types of fuel cells but starting with a cell-based around an acid electrolyte, as utilised by Grove, provides an understanding of the most common type.

Figure redacted

Figure 11. (a) Water is separated into hydrogen and oxygen by the passage of an electric current. (b) Flow of a small current from the combination of hydrogen and oxygen [22].

Figure redacted

Figure 12. The construction of a fuel cell's basic cathode-electrolyte-anode [22].

In the overall fuel cell reaction, hydrogen fuel is oxidised and water is generated [22]:

$$2H_2 + O_2 \rightarrow 2H_2O \quad (3.1)$$

At the anode side, electrons and hydrogen protons are released from hydrogen fuel as follows [22]:

$$2H_2 \rightarrow 4H^+ + 4e^- \quad (3.2)$$

At the cathode side, water is produced from the combination of oxygen with electrons transferred from the electrode and H^+ ions from the electrolyte [22]:

$$O_2 + 4e^- + 4H^+ \rightarrow 2H_2O \quad (3.3)$$

Electrons created at the anode must pass across an electrical circuit to the cathode for both these reactions to proceed continuously. Also, H^+ ions must pass across the electrolyte. An acid is a liquid with free H^+ ions, and so serve up this purpose. Specific polymers can also be prepared to contain mobile H^+ ions. These materials are called proton exchange membranes (PEM) as an H^+ion is also a proton. Equations (3-1) to (3-3) show that two hydrogen molecules will be required for each oxygen molecule if the system is balanced, also depicted in Figure 13. It is observable that the electrolyte must only allow H^+ions to cross over it, and not electrons, which should go around the external circuit.

Figure redacted

Figure 13 . An acid electrolyte fuel cell's electrode reactions and charge [22].

The overall reaction is the same in an alkaline electrolyte fuel cell (Figure 13), but the reactions at each electrode are different. In an alkali, hydroxyl (OH^-) ions are existing and movable. At the anode, these react with hydrogen, discharging energy and electrons and producing water [22]:

$$2H_2 + 4OH^- \rightarrow 4H_2O + 4e^- \quad (3.4)$$

Electrons removed from the electrode react with oxygen at the cathode, and water in the electrolyte, creating OH^- ions [22]:

$$O_2 + 4e^- + 2H_2O \rightarrow 4OH^- \quad (3.5)$$

For these reactions to proceed continuously, the OH^- ions must be able to cross over the electrolyte, and there must be an external electrical circuit for the electrons to travel from the anode to the cathode (Figure 14). Water is created twice as fast at the anode as it is consumed at the cathode. Hydrogen reacts releasing energy at the anode, but this reaction does not continue at an infinite rate. Although energy is liberated, the activation energy must be provided to get over the energy hill (Figure 15). There are three ways to make reaction proceed fast: 1) increasing the electrode area, 2) raising the temperature, and 3) using catalysts. The first two can be utilized in any chemical reaction but the third is solution is the mot adequate to fuel cells.

Figure redacted

Figure 14. Alkaline electrolyte fuel cell electrode reactions and charge flow [22].

Figure redacted

Figure 15. A simple exothermic chemical reaction classical energy diagram [22].

The bringing together of reactants, electrolyte and electrode is a fundamental aspect in fuel cell design. The rate at which the reaction comes about will be proportional to the electrode area, which is such a vital issue that the functioning of a fuel cell design is repeatedly quoted in terms of the current per cm^2. However, the specific area (length $\times$ width) is not the only problem. As it has already been stated, the electrode is extremely porous, significantly expanding the functional surface area. Advanced fuel cell electrodes have a microstructure providing huge surface areas that can be multiple times their basic length $\times$ width. The microstructural design, creation, and fabrication of a fuel cell electrode is thus a crucial matter for practical fuel cells. In addition to these surface area factors the electrodes may have to contain a catalyst and endure high temperatures in a corrosive environment.

The voltage of a fuel cell is relatively small, about 0.7 V when drawing an adequate current. Various cells must be connected in series to produce a suitable voltage. Such an assemblage can exist of tens or hundreds of cells, and the formal name of it is stack. A much better cell interconnection method is a bipolar plate. It covers the whole area of the cathode from one side, and the other side connects to the anode of the following cell. Simultaneously, the bipolar plate operates as a way of supplying oxygen to the cathode and hydrogen gas to the anode.

Although an excellent external circuit must be there to allow the electrons to move from the anode to the cathode while the two reactions must be apart, connecting a single PEM fuel cell covers the electrode surfaces while simultaneously supplying hydrogen and oxygen to the cell. Figure 16 shows the parts where the hydrogen and the oxygen enter the cell. Hydrogen enters through small channels from the anode side while the oxygen enters the cell through similar channels but on the cathode side. The plate serves as a gas channel to the whole electrode and takes current from all over the face to the electrodes. Conversely, grooved plates are created from a decent conductor such as stainless steel or graphite. To connect numerous cells in series, bipolar plates are prepared. The channels on the plates help the reactants to stream through over the face of the electrodes. At the same time, they are prepared in such a way that they make great electrical contact with the exterior of each alternate electrode.

Though design, manufacture and cost of the system are very significant, the two ultimate technical complications with fuel cells are the sluggish reaction rate, leading to small currents and power, and that hydrogen is not a readily available fuel. As mentioned earlier, several diverse fuel cell categories have been tried to resolve the difficulties. The numerous fuel cell types are usually distinguished by the electrolyte used, despite other significant differences exist. Now, six classes of fuel cells have developed as workable systems for the current time and near future. Basic information about these systems is provided in Table 1.

Figure redacted

Figure 16. A Single PEMFC cell [22].

Table 1. Different types of cell data [22].

Table redacted

Whenever two distinct materials are connected, there is an accumulation of charge on the surfaces, or a charge moves from one to the other. For illustration, in semiconducting materials, there is a dissemination of holes and electrons crossway junctions between (negative) n-type and (positive) p-type materials. This forms a phenomenon called double charge layer at the connexion of electrons in the p-type area and holes in the n-type, which

strongly impacts semiconductor devices behaviour. In electrochemical systems, the charge double layer forms primarily due to diffusion effects (as in semiconductors), secondly due to reactions among the ions in the electrolyte and the electrons in the electrodes, and thirdly as result of applied voltages.

As an example, Figure 17 depicts a situation that may occur at the cathode of an acid electrolyte fuel cell, where electrons accumulate at the outside of the electrode and H^+ions are drawn to the electrolyte surface. The electrons and H^+ions, together with O_2 provided to the cathode, take part in the cathode reaction. The probability of the reaction taking place depends on the density of charges of electrons and ions on the electrode and electrolyte surfaces. The more the charge, the higher the current. Any gathering of charge of electrons and H^+ions at the electrode/electrolyte interface produces an electrical voltage that, in this instance, is the activation overvoltage.

Figure redacted

Figure 17. The charge double layer phenomenon at the surface of a fuel cell cathode [22].

The activation overvoltage indicates that a charge double layer needs to exist for a reaction to occur, the extra charge is necessary if the current is higher, and the overvoltage is higher if the current is more significant. It also demonstrates that the catalytic effect of the electrode is essential, as an efficient catalyst will also enhance the likelihood of a reaction so that a higher current can stream without such an accumulation of charge. The charge layer on or near the electrode-electrolyte edge is a store of electrical charge and power and acts much

like an electrical capacitor. If the current alternates, it will need a specific time for this charge (and its accompanying voltage) to disperse (if the current decreases) or to increase (if there is a current increase).

Therefore, the activation overvoltage does not instantly follow the current as the ohmic voltage drop does. If the current unpredictably shifts, the operating voltage immediately alters due to the internal resistance but goes reasonably sluggishly to its ultimate equilibrium amount. One way of modelling this is by utilizing an equivalent circuit, with the charge double layer exemplified by an electrical capacitor. The capacitance C (F) of a capacitor is given by [22]:

$$C = \varepsilon \frac{A}{d} \tag{3.6}$$

where ε is the electric permittivity (F/m), *A* is the outer region (m^2), and *d* is the plate separation (m).
The exterior part of the electrode *A* is various thousand times greater than its length x width. Also, the separation *d* is minimal, typically only a few nanometres. The effect is that, in some fuel cell types, the capacitance amount is of the order of a few Farads, which is high regarding normal capacitance of electrical circuits (typically in the order of μF).

As shown in Figure 18, the correlation between this capacitance, its stored charge, and the resulting activation overvoltage leads to an equivalent circuit. The resistor Rr models the ohmic losses. A variation in current gives an instant change in the voltage drop across this resistor. The resistor Ra models the activation overvoltage and the capacitor smooths any voltage drops across this resistor. If the concentration overvoltage is included, it would also be incorporated into this resistor. This capacitance from the charge double layer gives the fuel cell a perfect transient performance in which the voltage goes gently and smoothly to a new amount in the reaction from a change in current demand. It also permits a simple and effective way to distinguish between the main types of voltage drop and analyse the performance of a fuel cell.

Figure redacted

Figure 18. Equivalent circuit model of PEMFC [22].

One of the methods used by researchers to understand the electrical characteristics of fuel cells is electrical impedance spectroscopy. Adjustable frequency oscillating current is driven across the cell, the voltage is evaluated, and the impedance is determined. At greater frequencies, the capacitors in the circuits will have less impedance. Plotting impedance graphs against frequency makes it conceivable to find the standards of the equivalent circuit of Figure 18. It is sometimes even more likely to differentiate between the damages at the cathode and the anode and between mass transport and activation-type losses. However, special signal generators and measurement systems are needed because the capacitances are large and the impedances small. Frequencies as low as 10 mHz may be utilized, so the experiments are often relatively slow [125].

The current break technique is an option that can use standard low-cost electronic equipment to give accurate quantitative results and fast qualitative signals [126]. Suppose a cell provides a current at which the intensity (or mass transport) overvoltage is negligible. In this case, the ohmic losses and the activation overvoltage will produce the voltage drop. If the current is unexpectedly cut off, the charge double layer will take some time to disappear, and so will the accompanying overvoltage. Nevertheless, the ohmic losses will immediately decrease to zero and the voltage will change as in Figure 19 if the load is abruptly disjointed from the cell.

Figure redacted

Figure 19. A fuel cell voltage against a time curve using a current interrupt method [127].

The simple circuit required to perform this current disconnect test is shown in Figure 20. The button is closed, and the load resistor is adjusted until the desired test current flows. The storage oscilloscope is set to a proper time base, and the load current is turned off. The oscilloscope initiating will require to be set so that the oscilloscope turns into 'hold' mode. However, with some cells, the system is so sluggish that this can be accomplished by hand. The two voltages, the immediate increase in voltage Vr and the slow final rise to OCV Va are then read off the screen.

Figure redacted

Figure 20. A circuit for a current interrupt test performing [127].

Current interrupts, alongside electrical impedance spectroscopy, is another powerful methods to find the causes of fuel cell irreversibility. While the method is straightforward, when achieving quantitative solutions care must be taken as it is likely to overestimate missing the point where the vertical transition ends [128]. The oscilloscope time base setting will change for different fuel cell types, subject to the capacitance, as in the three examples of interrupt tests shown in Figure 21 to 23. These three cases are displayed because of the clear qualitative signal and the different types of voltage drop. Since oscilloscopes do not appear as vertical lines, the appearance is slightly different from Figure 19, as no vertical line corresponds to Vr. The current interrupt test is elementary to operate with single and small fuel cell stacks. With more giant cells, switching the high currents can be problematic.

The tests were done on three distinct fuel cell categories: PEMFC (Figure 21), direct methanol fuel cell (DMFC, Figure 22), and solid oxide fuel cell (SOFC, Figure 23). In each example, the total voltage decrease was almost the same, though the current density was not. These three examples give a decent summary of the reasons for voltage losses in fuel cells. Concentration or mass transport losses are essential only at more significant currents. In a well-constructed system, with excellent fuel and oxygen supply, they should be minimal at rated currents.

Figure redacted

Figure 21. PEMFC current interrupt test at standard temperature and pressure. (Time scale $(Time\ scale\ 0.2\frac{s}{div^{-1}}\ , i = 100\ mA\ cm^{-2})$ [127].

Figure redacted

Figure 22. DMFC current interrupt test ($Time\ scale\ 0.2\frac{s}{div}$, $i = 10\ mA\ cm^{-2}$) [127].

Figure redacted

Figure 23. SOFC current interrupt test ($Time\ scale\ 0.02\frac{s}{div^{-1}}$, $i = 100\ mA\ cm^{-2}$) [127].

In hydrogen fuel cells with low temperature, the activation overvoltage at the cathode is essential, particularly at low currents. However, the ohmic losses play a crucial part too, and the activation and ohmic losses are similar (Figure 21). In fuel cells utilizing fuels such as methanol, there is a significant overvoltage at both the anode and cathode, so the activation overvoltage always dominates (Figure 22). In high-temperature cells (the temperature of SOFC in this test was 700◦C), the activation overvoltage becomes much less essential, and ohmic losses are the main problem (Figure 23).

After covering sufficient detail of the principles of fuel cell operation, the functional features of different fuel cell systems will be described in the following sections. There are several fuel cell types with different electrolytes. The specifics of the anode and cathode responses are

unique in each case. Typical fuel cells include PEMFC, DMFC, direct alcohol fuel cells, alkaline fuel cells, phosphoric acid fuel cells, molten carbonate fuel cells, and SOFC [127,129]. In addition, PEMFC could be reversed to produce hydrogen and oxygen from water; this type is called electrolyser or reversible fuel cell.

3.1.1 Fuel Cell Operation and Design

Table 2 shows the benefits and disadvantages of PEMFC [134–136].

Table 2. Advantages and disadvantages of PEMFC [134–138].

ADVANTAGES	DISADVANTAGES

Table redacted

As was noted earlier, PEMFC has no combustion, unlike an ICE. Electrochemical reactios occurring instantaneously on the anode and cathode sides convert the chemical energy of hydrogen into electrical energy [134]. The equations and critical responses of the hydrogen oxidation reaction is summarised in Table 3. The energy input is calculated with the hydrogen higher heating value, while the output is the electrical power which resembles Gibbs free energy.

Table 3. Thermodynamics of PEMFC [134].

EQUATIONS	COMMENTS
Table redacted	

PEMFC is an energy conversion device where the energy moves from hydrogen through the electrons forming the electric current. For the electric current to increase, the interfacial area between anode, cathode and electrolyte should be increased. To get a large area, PEM fuel cells are generally made of thin, planar structures (Figure 24). This assembly allows making the most of surface-to-volume ratios. In addition to the structure, the anode and cathode increase the reaction surface area by their porous shape, guaranteeing decent gas admittance (Figure 25).

The electrolyte layer in the middle guarantee the separations of the electrochemical reaction to occur in two halves. The fuel reaction in the anode electrode (see Table 3) is the oxidation reaction where the electrons are detached from a species and the oxidant reaction in the cathode electrode (see Table 3) is the reduction where the electrons are added to a type.

(a) (b)

Figure redacted

Figure 24. The planar structure of PEM fuel cell in closed view (a) and exploded view (b) [139].

Figure redacted

Figure 25. Zoomed view of a PEM fell cell components [140].

Using Figure *26* as guidance, the four steps of fuel cell operation are explained [139]:

- (1) Reactant passage. PEM fuel cell is an open thermodynamic system functioning at steady state as long as the reactant is recurrently provided. This mission can be reasonably intricate when PEM fuel cells function at high currents. If the reactants are not provided speedily enough, the fuel cell will starve, and if the product is not extracted correctly, it will cause some areas to be flooded with liquid water. To avoid starvation or flooding, a flow of field plates is utilised. As Figure *27* shows, the three measure flow patterns are: (a) parallel flow, where reactants follow in the same or opposite direction, (b,c) serpentine flow, where reactants follow in a zig-zag, and (d) interdigitated flow, which causes reactants to follow through the gas diffusion layer. Not using the right design decreases the output current and impacts the fuel cell performance.
- (2) Electrochemical reaction. The current output is proportional to the speed of the reaction. A Higher current means a higher reaction. To maintain the reaction speed, a well-chosen catalyst must be combined with an adequate design of the reaction areas. An excessive restraint to PEMFC performance is the reaction kinetics.
- (3): Proton and electron transference. As mentioned, electrons and protons are produced and consumed at the cathode. For this to happen, both must be transported. The transportation of electrons is simple if there is an external circuit, but protons must travel through the cell and need an electrolyte as a passage where big resistance loss occurs lowering the PEMFC efficiency.
- (4): Water subtraction. The water produced must be removed; otherwise, the cell will be flooded. Again, the performance and efficiency of the PEM fuel cell will drop.

Figure redacted

Figure 26. Electrochemical reaction diagram showing PEMFC operation: (1) reactant passage, (2) electrochemical reaction, (3) protons and electrons transference, (4) Product amputation [139].

Figure redacted

Figure 27. The main flow channel designs: (a) parallel, (b) serpentine, (c) parallel serpentine, (d) interdigitated [139].

3.1.2 Ideal PEM Fuel Cell Performance

To evaluate the performance of a PEM Fuel cell, the chemical and thermodynamic processes need to be connected to the operating conditions. Variable quantities such as gas constituents, temperature, and pressure influence PEM fuel cell performance [140]. The Gibbs free energy ΔG (kJ) is used to determine the possible maximum electrical work $W_{e,\max}$ (kJ) from the PEM fuel cell:

$$W_{e,max} = \Delta G = -nFE \tag{3.7}$$

where n is the number of electrons that contribute to the reaction, F is Faraday constant, and E is the ideal potential of the cell (V).

The Faraday constant is defined as [83]:

$$F = N_a \cdot e \tag{3.8}$$

where $\mathrm{N_a} = 6.022 \times 10^{23}$ is Avogadro's number and $\mathrm{e} = 1.602 \times 10^{-19}\ C$ is the charge on one electron. Therefore, $\mathrm{F} = 96485\ C = 96485\ A.s$ per mole of electrons.

The Gibbs free energy can be expressed as follows:

$$\Delta G = \Delta H - T\Delta S \tag{3.9}$$

where $\Delta\mathrm{H}$ is the variation of enthalpy (kJ), $\Delta\mathrm{S}$ is the variation of entropy (kJ/K), and T is temperature (K). The product $\mathrm{T}\Delta\mathrm{S}$ represents the heat loss from the system. Reactions such as hydrogen oxidation have negative entropy variation as they produce heat.

The following equation represents the general cell reactions:

$$\alpha A + \beta B \rightarrow \gamma C + \delta D \tag{3.10}$$

The variation of Gibbs free energy at normal state (298 K, 1 atm) Δg is given by:

$$\Delta \bar{g}^{\circ} = \gamma \bar{g}_C^{\circ} + \delta \bar{g}_D^{\circ} - \alpha \bar{g}_A^{\circ} - \beta \bar{g}_B^{\circ} \tag{3.11}$$

where $\bar{\mathrm{g}}_\mathrm{i}^{\circ}$ is the partial molar Gibbs free energy of species i and α, β, γ and δ are the molar fractions of species A, B, C and D, respectively (kJ/kmol).

The enthalpy and entropy can be calculated from the heat capacities of each species $\bar{c}_{p\mathrm{i}}$ (kJ/kmol.K):

$$\bar{c}_{pi} = a + bT + cT^2 \tag{3.12}$$

where a, b, and c are empirical constants.

The specific enthalpy $\bar{h}_I$ (kJ/kmol) and specific entropy $\bar{s}_I$ (kJ/kmol.K) on molar basis of each component i are given by:

$$\bar{h}_i = \bar{h}_i^\circ + \int_{298}^{T} \bar{c}_{pi}\, dT \tag{3.13}$$

$$\bar{s}_i = \bar{s}_i^\circ + \int_{298}^{T} \frac{\bar{c}_{pi}}{T} dT \tag{3.14}$$

Once the specific enthalpies and entropies of each species are known, the total variation in enthalpy and entropy can be calculated as:

$$\Delta H = \left(\sum_i n_i \bar{h}_i\right)_{out} - \left(\sum_i n_i \bar{h}_i\right)_{in} \tag{3.15}$$

$$\Delta S = \left(\sum_i n_i \bar{s}_i\right)_{out} - \left(\sum_i n_i \bar{s}_i\right)_{in} \tag{3.16}$$

where n_i is the number of moles of component i (kmol). The values of a, b, c, $\bar{h}_i^\circ$, and $\bar{s}_i^\circ$ can be taken from reference tables. $\Delta\bar{g}$ and E can be calculated by:

$$\Delta\bar{g} = \Delta\bar{g}^\circ + \bar{R}T ln \frac{f_C^\gamma f_D^\delta}{f_A^\alpha f_B^\beta} \tag{3.17}$$

$$E = E^\circ + \frac{\bar{R}T}{nF} ln \frac{f_C^\gamma f_D^\delta}{f_A^\alpha f_B^\beta} \tag{3.18}$$

where $\bar{R} = 8.314$ kJ.kmol.K is the universal gas constant and f_i is the fugacity of species i. Equation (3-18)is also known as Nernst equation.

3.1.3 PEM Fuel Cell Efficiency

In an ideal PEM fuel cell the Gibbs free energy (ΔG) provides the useful electric energy, therefore the PEMFC efficiency can be calculated as:

$$\eta_{ideal} = \frac{\Delta G}{\Delta H} \tag{3.19}$$

To calculate the terms of the PEM fuel cell efficiency, the overall hydrogen oxidation reaction described in Eq. (3-1) and summarised in Tab. 3 must be considered. Thus, following Eq. (3.12):

$$\Delta G^{\circ} = \bar{G}^{\circ}_{H_2O} - \bar{G}^{\circ}_{H_2} - \frac{1}{2}\bar{G}^{\circ}_{O_2} \tag{3.20}$$

If the product of Eq. (3-1) is liquid water the ideal potential (E°) at 298 K, 1 atm is 1.229 V and, if it is water vapour, the value becomes 1.18 V [140]. As the reaction occurs at the standard condition, the product water is in liquid phase and the calculation of ΔG from Eq. (3-17) results in 237.1 kJ/mole. Since the enthalpy of reaction (ΔH) is 285.8 kJ/mole, then, using Eq. (3.14):

$$\eta_{ideal} = \frac{237.1}{285.8} = 0.83 = 83\%$$

The fuel cell efficiency can be expressed as a function of the single cell voltage V_{FC} as follows:

$$\eta_{FC} = \frac{W_e}{\Delta H} = \frac{V_{FC} \cdot I}{\frac{E \cdot I}{0.83}} = \frac{0.83 V_{FC}}{E} = \frac{0.83 V_{FC}}{1.229} = 0.675 V_{FC} \tag{3.21}$$

Equation (3-21) assumes that hydrogen is entirely consumed in the reaction.

3.1.4 Effect of Voltage Losses on the Actual Performance of PEM Fuel Cell

PEM fuel cells have three significant losses, known as polarisation overvoltage losses. These losses minimise the fuel cell ideal potential, as shown in Figure 28.

Figure redacted

Figure 28. The effect of losses on the PEM fuel cell performance [140]

- Activation losses (V_{act})

These losses are related to the electrochemical reactions at the electrodes, but they are connected with the electro-catalyst material and microstructure, the state of the current density and the reactant actions. The leading cause of these losses is the slow electrode kinetics. Although it is tedious to quantify it in the case of a PEM fuel cell where the loss is less or equal to 50-100 mV, it is valued by a semi-empirical equation termed the Tafel equation [141]:

$$V_{act} = \frac{RT}{\alpha\, n\, F} ln \frac{I}{I_{\circ}} \qquad (3.22)$$

Where α is the electron transfer coefficient of the reactions, whether at the cathode or the anode, and $I_\circ$ is the exchange current density (mA/cm^2). Figure 29 shows that the exchange current density can be found by extrapolated intercept at negligible polarisation and transfer coefficient.

Figure redacted

V (mV)

Figure 29. Activation polarization of PEM fuel cell using Tafel Plot [141]

From the Tafel Plot, the curve can be represented by a logarithm equation in the following form:

$$V_{act} = a + b\, ln\, I \qquad (3.23)$$

In equation (3-23), a is (-RT/ αnF), and b is (RT/ αnF), which is the Tafel slope and is attained from the slope of a plot as a function of ln i. A low slope of reactions, which can be obtained by fostering appropriate electro-catalysts, results in a current density upsurge with an insignificant rise in activation polarization. Although many other factors contribute to the increase of activation polarisation, such as the crossing of electrons through the fuel cell, absorption of reactant species and the kind of electrode surface, only the slower electrode kinetics has here been considered.

- Ohmic losses (V_{ohm})

These are the only losses that happen due to resistance to the flow, whether of the electrons through the electrode or proton flow through the electrolyte. The resistance could be minimised by reducing the electrode split-up and enriching the electrolyte ionic conductivity. The following equation can represent the ohmic losses:

$$V_{ohm} = IR \tag{3.24}$$

where i is the current flowing through the PEM fuel cell and R is the sum of all ionic, electronic and interaction resistance.

- Concentration losses (V_{conc})

The concentration losses are also known as the mass transport losses. While in use the reactant is often mitigated by the reaction products, and this happens due to the restriction of new supply and removal of products by determinate mass transport valuates. The effect of this phenomenon is the formation of a concentration gradient that drives mass transport. In a PEM fuel cell, the concentration losses have a substantial effect as the flow is multi-phase compared with other high-temperature fuel cells. Due to the difference in the diffusivities of hydrogen and water or vapour, the effect is more noticeable at the cathode under applied situations such as low reactant concentrations and high current densities. Using total polarization, the losses can be summed as follow:

$$V_{ano} = V_{act,ano} + V_{conc,ano} \tag{3.25}$$

$$V_{cat} = V_{act,cat} + V_{conc,cat} \tag{3.26}$$

where ano denotes the anode and cat refers to the cathode.

The potential of the electrode ($\mathrm{E_{electrode}}$) has been altered to a fresh quantity through the outcome of polarization, as shown by:

$$V_{electrode} = E_{electrode} \pm |V_e| \tag{3.27}$$

Furthermore, in equation(3-27) and (3-28), this value has been split into a value for the anode and a value for the cathode, respectively:

$$V_{anode} = E_{anode} + |V_{ano}| \quad (3.28)$$

$$V_{cathode} = E_{cathode} - |V_{cat}| \quad (3.29)$$

The reduction in the cell voltage occurs by the net result of current flow, which is the product of the upsurge of the anode potential and the decline of the cathode potential (Figure 30):

$$V_c = V_{cathode} - V_{anode} - IR \quad (3.30)$$

Combining Eq. (3-31) with Eqs. (3-29) and (3-30) yelds:

$$\begin{aligned} V_c &= E_{cathode} - |V_{cat}| - (E_{anode} + |V_{ano}|) - IR \\ &= \Delta E_e - |V_{cat}| - |V_{ano}| - IR \end{aligned} \quad (3.31)$$

Figure redacted

Figure 30. The two half cells and their contribution to polarisation [140]

From Eq. (3-31), the decrease of losses on the electrode and ohmic polarization will result in cell voltage approaching the electrode potential. There are different ways to minimise those losses, for example, by PEM fuel cell design amendments such as extra conductive electrolytes, narrower cell apparatuses, improved electrocatalysts and perfection of the electrode assembly. Alternatively, by modifying the operating conditions, such as change the gas composition to decrease the gas impurity concentration, increase the gas pressure and temperature. However, the achievement of higher performance should not be at the expense of the stability and durability of the PEM fuel cell components.

3.1.5 The Operating Variables of the PEM Fuel Cell

Operating variables of PEM fuel cells, such as current density, pressure, temperature, gas constituents and reactant exploitation, are among the influences that impact the ideal cell potential and the scale of the voltage shortages. While the current density deviates, activation, ohmic, and concentration losses occur. Figure 31 illustrates how cell voltage-current properties are being distressed by the losses. The cell voltage decreases during the start of the current due to the activation losses. At the same time, the performance falls sharply at higher current densities due to reactant shortage, which has to do with the diffusivity problem (concentration losses).

Figure redacted

Figure 31. Power and Voltage association [140].

As equation (3-24) shows, the ohmic loss is iR, where i is the current and R is the sum of all internal resistances within the cell. This shows that current (which is the current density multiplied by the cell area) relates to the ohmic losses and voltage alteration. From Figure 31, it can be assumed that the best operations point is at the right where power and current densities are high, but that means running at low cell voltage or lower cell efficiency. On the other hand, the control will be unstable if the cell run around the peak power density as the system will tend to fluctuate about the peak between the advanced and minor current densities. This fluctuation due to the deficits which have been mentioned earlier, at the lower current density side the activiation losses instigate reduction in cell voltage and at high current density, there is a failure to disperse enough reactants to the reactions positions (concentration lesses). The ideal way is to operate the cell at low process cost, which means high cell efficiency at high voltage/low current density and at a low capital cost which occurs when there is less cell area related to low voltage/high current density.
Using Gibbs free energy, the outcome of temperature and pressure on the ideal potential (E) can be evaluated:

$$\left(\frac{\partial E}{\partial T}\right)_P = \frac{\Delta S}{nF} \tag{3.32}$$

$$\left(\frac{\partial E}{\partial P}\right)_T = -\frac{\Delta V}{nF} \tag{3.33}$$

where ΔS (entropy change) is negative for the hydrogen and oxygen reaction. The reversible potential of the hydrogen and oxygen declines with temperature by 0.84 mV/ °C in case the reaction product is water. It can be said the same with the increase of pressure, which lets the potential grow while the volume change is negative. It can be assumed that pressure is equal on both electrodes.

The higher the partial pressures of hydrogen and oxygen, the higher the efficiency, as the Nernst equation shows:

$$U_f = \frac{H_{2,in} - H_{2,out}}{H_{2,in}} = \frac{H_{2,consumed}}{H_{2,in}} \quad (3.34)$$

where $\mathrm{U_f}$, $\mathrm{H_{2\ in}}$ and $\mathrm{H_{2\ out}}$ are utilisation, inlet and outlet hydrogen flows, respectively. The same calculation could be used for oxygen.

Hydrogen can be consumed in various ways, not only on the electrochemical reaction (loss by outflow or reaction with oxygen). Gas composition variations between inlet and outlet diminish cell voltages as the cell voltage alters to the lowest electrode potential specified by the Nernst equation for several gas compositions at the departure of the anode and cathode compartments [140].

3.2 Exergy and Exergoeconomic Analysis of PEM Fuel Cell

Unlike energy analysis, exergy evaluation deals with the quantity and quality of energy [142]. Figure 32 shows a flow schematic of a PEM fuel cell where an exergy analysis is applied. The exergy efficiency is defined as the ratio between the actual power output and the possible work output. By adding the cost, capital investment, operations, and maintenance cost, the exergy analysis becomes exergoeconomic analysis. The exergoeconomic efficiency is defined as the ratio of the cost of electrical power output to the difference between the exegetic cost rate (cost per unit time) of the streams entering and exiting the PEM fuel cell plus the capital investment, operation, and maintenance costs.

Each exergy inflowing and departing the PEM Fuel cell system has a cost. Performing an exergoeconomic analysis can help to scrutinise several operating settings and their consequences on performance [115].

$$P_e$$

Figure redacted

Figure 32. Flow schematics of a PEM fuel cell.

3.2.1 Exergy Analysis

Application of exergy analysis to a PEM fuel cell can determine the exergetic efficiency, which reflects the actual cell performance. The exergetic efficiency η_{ex} is calculated by the ratio of the electrical power output of the whole fuel cell stack P_e (W) to the total exergy difference between reactants and the products, as follows [115]:

$$\eta_{ex} = \frac{Output\ electrical\ power}{(Total\ exergy)_R - (Total\ exergy)_P} = \frac{P_e}{\left(\dot{E}x_{air,R} + \dot{E}x_{H_2,R}\right) - \left(\dot{E}x_{air,P} + \dot{E}x_{H_2O,P}\right)} \quad (3.35)$$

where subscript *R*, *P* refer to reactants and products, respectively, and $\dot{E}x$ is the total exergy of the corresponding component (W). It is assumed that there is no kinetic and potential energy effect on the reactions.

The electrical power output of a single cell P_e (W) is calculated as:

$$P_e = I \cdot V_{FC} = P_{aux} + P_{ext} \quad (3.36)$$

where I is the fuel cell stack electric current (A), V_c is the voltage of each cell in the stack (V), the auxiliary load power P_{aux} (W) and the external load power P_{ext} (W):

The external load power is the product of the measured current (I_{ext}) and voltage (V_{ext}):

$$P_{ext} = I_{ext} \cdot V_{ext} \tag{3.37}$$

The fuel cell current I (A) can be calculated by:

$$I = \frac{n \cdot F \cdot \dot{m}_{H_2}}{M_{H_2}} \tag{3.38}$$

where $n = 2$ is the number of electrons released per mol of hydrogen fuel (see Eq. (3.4)) (mol^{-1}), $\dot{m}_{H_2}$ is hydrogen mass flow rate (kg/s), and $M_{H_2} = 2.02 \frac{kg}{kmol}$ is the molar mass of hydrogen. It is here assumed that all hydrogen is fully reacted.

Since the auxiliary power is not available individually, it can be determined from Eq. (3.36) as the difference between $\mathrm{P_e}$ and P_{ext}. The total exergy transfer per unit mass ex (kJ/kg) includes both specific chemical exergy ex_{CH} (kJ/kg) and specific physical exergy ex_{PH} (kJ/kg) [110]:

$$ex = ex_{CH} + ex_{PH} \tag{3.39}$$

The physical exergy combines the pressure and temperature of both reactants and products. It can be distinguished as the maximum beneficial work attained by passing the unit of mass of an element from the generic state (T, P) to the environmental state $(\mathrm{T_0}, \mathrm{P_0})$. The general expression of the physical exergy is:

$$ex_{PH} = (h - h_0) - T_0(s - S_0) \tag{3.40}$$

where $\mathrm{h_o}$ and $\mathrm{s_o}$ are the specific enthalpy and entropy at T_o = 298 K, p_o = 1 atm = 1.013 bar.

The physical exergy of an ideal gas can be calculated using the constant pressure specific heat $\mathrm{c_p}$ (kJ/kg.K) and specific heat ratio κ as:

$$ex_{PH} = c_p T_0 \left[\frac{T}{T_0} - 1 - ln\left(\frac{T}{T_0}\right) + ln\left(\frac{p}{p_0}\right)^{\frac{\kappa-1}{\kappa}}\right] \quad (3.41)$$

The chemical exergy represents the attainment of a maximum quantity of valuable work by assigning a system in equilibrium with the environment using T_0 and P_0, calculated as follows [115]:

$$ex_{CH} = \sum y_n ex_{CH,n} + (\bar{R}/M_n)T_0 \sum y_n \, ln \, y_n \quad (3.42)$$

where y_n, $ex_{CH,n}$ and M_n are the mass fraction, chemical exergy (kJ/kg) and molar mass (kg/kmol) of each component (n) under consideration, respectively.

The chemical exergy considers the properties based on the standard temperature and pressure (Table 4) [115]. Table 5 shows the standard chemical exergies and reactant mass fraction of the components involved in the fuel cell reactions [114]. The total exergies of reactants and products are calculated as [187]:

$$\dot{E}x_{H_2,R} = \dot{m}_{H_2,R} ex_{H_2,R} = \dot{m}_{H_2,R}(ex_{CH} + ex_{PH})_{H_2,R} \quad (3.43)$$

$$\dot{E}x_{air,R} = \dot{m}_{air,R} ex_{airR} = \dot{m}_{air,R}(ex_{CH} + ex_{PH})_{air,R} \quad (3.44)$$

$$\dot{E}x_{H_2O,P} = \dot{m}_{H_2O,P} ex_{H_2OP} = \dot{m}_{H_2O,P}\,(ex_{CH} + ex_{PH})_{H_2O,P} \quad (3.45)$$

$$\dot{E}x_{air,P} = \dot{m}_{air,P} ex_{airP} = \dot{m}_{air,P}(ex_{CH} + ex_{PH})_{air,P} \quad (3.46)$$

where $\dot{m}_{H_2}$, $\dot{m}_{air}$ and $\dot{m}_{H_2O}$ are the mass flow rates of hydrogen, air and water, respectively (kg/s).

Table 4. Properties at the standard condition [187].

PROPERTY	VALUE

Table redacted

Table 5. PEM Fuel cell standard mass fraction and chemical exergy of reactants [190].

Table redacted

The mass flow rates of both reactants and products can be found using the following equations [127]. From the combination of Eqs. (3.36) and (3.38):

$$\dot{m}_{H_2,R} = \frac{M_{H_2} \cdot P_e}{n \cdot F \cdot V_c} \tag{3.47}$$

Similarly, for water production:

$$\dot{m}_{H_2O,P} = \frac{M_{H_2O} \cdot P_e}{n \cdot F \cdot V_c} \tag{3.48}$$

where $n = 2$ since one mole of water is produced for every two electrons (see Eq. (3.3)) (mol^{-1}) and $M_{H_2O} = 18.02 \frac{kg}{kmol}$ is the molar mass of water.

The intake air flow rate is calculated as [127]:

$$\dot{m}_{air,R} = \frac{\lambda \cdot M_{air} \cdot P_e}{x_{O_2} \cdot n \cdot F \cdot V_c} \tag{3.49}$$

where λ is the air/fuel mixture equivalence ratio, $\mathrm{M_{air}} = 28.97 \times 10^{-3}\ \frac{kg}{mol}$ is the molar mass of air, $x_{O_2} = 0.21$ is the molar fraction of oxygen in air, and $n = 4$ is the number of electrons transferred for each mol of oxygen (see Eq. (3.5)) (mol^{-1}).

The fuel/air misture equivalence ratio is defined as:

$$\lambda = \frac{A/F}{(A/F)_s} = \frac{\dot{m}_{air,\mathrm{R}}/\dot{m}_{H_2,R}}{\left(\dot{m}_{air}/\dot{m}_{H_2}\right)_s} = \frac{\dot{m}_{air,\mathrm{R}}/\dot{m}_{H_2,R}}{\frac{n_{air} \cdot \left(M_{O_2} + \frac{79}{21}M_{N_2}\right)}{n_{H_2} \cdot M_{H_2}}} \tag{3.50}$$

where $n_{air} = \frac{1}{2} kmol$ is the number of moles of air per mole of hydrogen in the stoichiometric reaction, $M_{O_2} = 32.0 \frac{kg}{kmol}$ is the molar mass of oxygen molecule, $M_{N_2} = 28.0 \frac{kg}{kmol}$ is the molar mass of nitrogen molecule, $n_{H_2} = 1\ kmol$ is the number of moles of hydrogen in the stoichiometric reaction. The stoichiometric air/fuel ratio $(A/F)_s$ of the hydrogen oxidation reaction is 34.3.

Calculation of the mass flow rate of product air needs to consider oxygen consumption in the fuel cell reaction. Thus:

$$\dot{m}_{air,P} = \frac{\lambda \cdot M_{air} \cdot P_e}{x_{O_2} \cdot n \cdot F \cdot V_c} - \frac{M_{O_2} \cdot P_e}{n \cdot F \cdot V_c} \tag{3.51}$$

3.2.2 Exergoeconomic Analysis

The exergy costs of the PEM fuel cell streams added to the exergy analysis shown in the previous section provide the exergoeconomic analysis. Based on Figure *32*, the cost balance of the PEM fuel cell is [76-87]:

$$c_{H_2O}\dot{E}x_{H_2O,P} + c_{air}\dot{E}x_{air,P} + c_{P_e}P_e = c_{air}\dot{E}x_{air,R} + c_{H_2}\dot{E}x_{H_2,R} + \dot{C}_{FC} \quad (3.52)$$

where c_{H_2O}, c_{air} and c_{H_2} are the costs per unit of exergy of water, air and hydrogen streams entering or leaving the fuel cell, respectively (US$/kJ per year); c_{P_e} is the cost of exergy the electrical power produced (US$/kJ per year); and $\dot{C}_{FC}$ is the annualised investment cost of the equipment (US$/s).

Rearranging Eq. (3.52) for the exergy cost of the electrical power produced c_{P_e} [128,186]:

$$c_{P_e} = \frac{c_{air}\dot{E}x_{air,P} + c_{H_2}\dot{E}x_{H_2,R} - c_{H_2O}\dot{E}x_{H_2O,P} - c_{air}\dot{E}x_{air,P} + \dot{C}_{FC}}{P_e} \quad (3.53)$$

The total annualised fuel cell investment cost is found by summation of the annualised capital investment cost $\dot{C}_{CI}$ (US$/s) and the cost rate of operation and maintenance $\dot{C}_{OM}$ (US$/s) [128,186]:

$$\dot{C}_{FC} = \dot{C}_{CI} + \dot{C}_{OM} \quad (3.54)$$

The annualised capital investment cost can be calculated in terms of the power output, capacity factor (CF) and the annual capital cost (ACC) [128,186]:

$$\dot{C}_{CI} = \frac{ACC \cdot P_e}{CF} \cdot \frac{1}{8760(h/year) \cdot 3600(s/h)} \quad (3.55)$$

Considering the fuel cell operational rate as 90%, i.e. $CF = 0.9$, ACC can be calculated in terms of the fuel cell capital cost C_{FC} and the capital recovery factor (CRF), which is based on the equivalent annual fuel cost over a number of years $(\mathrm{n_y})$ at an annual interest rate i [143]:

$$ACC = C_{FC} \cdot CRF \tag{3.56}$$

$$CRF = \frac{i(1+i)^{n_y}}{(1+i)^{n_y} - 1} \tag{3.57}$$

Assuming $\mathrm{i} = 10\%$ and taking n_y as five years [143], CRF is calculated as 0.244 per year. C_{FC} is adopted as 2500 $/kW of power output, based on the annual average cost for mass production [144]. The cost rate of operation and maintenance is calculated as follows [128,186]:

$$\dot{C}_{OM} = \frac{C_{OM} \cdot P_e}{8760(h/year) \cdot 3600(s/h)} \tag{3.58}$$

where C_{OM} is the annual operation and maintenance cost, here taken as 300 US$/kW per year [117]193].

The values of the PEM fuel cell parameters considered in the exergoeconomic analysis are shown in Table 6 [117,142,145–147].

Table 6. Properties of PEM fuel cell at standard condition

PARAMETER	VALUE
Standard temperature, T_o	298 K
Standard pressure, p_0	1 atm
Electrical power output, P_e	1.2 kW
Air/fuel mixture equivalence ratio, λ	3
Hydrogen cost	10 US$/kg

Water cost	1 US$/$m^3$
Air cost (O_2)	0.011 $/kg
Fuel cell capital cost	2500 $/kW
Fuel cell capacity factor	0.9
Fuel cell lifetime	5 years
Average annual interest rate	10%
Annual operation and maintenance (O&M) cost	300 US$/kW

In conclusion, the fundamentals chapter covered the principles of PEM fuel cell which show the equations of operation and design, ideal performance, efficiency, effect of voltage losses on performance and the exergoeconomic analysis. These equations have been referred to in the next chapter to avoid repetition.

4 Materials and Methods

A steady-state mathematical model was developed using MATLAB/Simulink based on experiments performed in a H-500XP PEM fuel cell at Aston University laboratories. The model was redeveloped to simulate a Nexa™ 1.2 kW PEM fuel cell operating at transient conditions and optimised using a PID tool. The simulations aimed to increase the power production from the fuel cell by using an equivalent electrical circuit instead of adding more cells to the stack. Finally, an exergoeconomic model was developed using MATLAB M-script to further analyse the performance and efficiencies of the Nexa™ 1.2 kW PEM fuel cell. A flowchart of the methodology applied in this research is provided by Figure 33.

Figure redacted

Figure 33. The experimental setup and model flowchart.

4.1 Experimental Setup

4.1.1 H-500XP PEM Fuel cell

The H-500XP model PEM fuel cell stack employed in this project has 30 cells with rated power of 600W [148]. The DC voltage varies from 15 V to 28.8 V and the rated current is 33.5 A at 18 V. The stack is self-moistened and driven with high-purity hydrogen (99.99 % dry H_2) and air for the reaction. Two axial fans provide cooling. Figure 34 illustrates the fuel cell system components, including the boost converter and the external load. Besides the stack, the main features of the H-500XP system are the fuel source, system controller, purging valves and pipe, battery, and super-capacitor bank. The hydrogen tank was set to deliver the fuel at 1.5 bar absolute pressure.

Figure redacted

Figure 34. H-500XP PEM Fuel Cell system and auxiliaries

The H-500XP stack system comprises hydrogen storage, DC boost converter, and external resistive loads, which offer adjustable power demand. The boost converter provides 48 V voltage through the load system, and the power is dispersed to the resistance as heat by the Joule effect. Figure 35 illustrates the PEMFC system in a purpose-built casing (1), bank of electric resistances (2), and load controller (3). The fuel cell battery works for start-up, and the super-capacitor supplies power during a short circuit or when the stack output power required is over 500 W [148]. The regulated system parameters are stack temperature – through variation of the fan velocity – fuel purging valve, and fuel supply. The regulator also monitors the stack voltage, current and temperature to avoid over current, low voltage and high temperature. The PEMFC system was supervised using dedicated software supplied by the manufacturer.

Figure redacted

Figure 35. H-500XP PEMFC test set: 1. stack, 2. load bank, 3. load bank control.

The system was tested by increasing the load, starting from the open-circuit condition and steadily reducing to the lowest external load resistance of 4.63 Ω. For every load change, 1 min could achieve the steady-state condition before making the measurement readings. Then, the data were recorded for 5 min at a given load. A digital flowmeter marked the hydrogen flow rate sandwiched between the stack inlet and tank. The instantly acquired data to be processed by the software were: stack voltage (V), stack current (I), stack output power (W), stack temperature (°C), ambient temperature (°C), and battery voltage (V). An schematics of the H-5000XP PEMFC test apparatus is shown by Figure 36.

4.1.2 Nexa™ 1.2kW PEM Fuel cell

The Nexa™ power module unregulated DC output can reach around 1.2 kW, and the voltage levels are 43 V at no load and 26 V at full load [199]. Such as the H-500XP PEMFC system, the Nexa power system was connected through a DC/DC converter to a load bank which acts as an external load. By variation of the load, the variation of the current density was observed and recorded in real-time. The DC/DC converter with its independent data logging software (NexaMon OEM) was provided by ISLE. The stack has 47 cells connected in series with 120 cm^2 geometric area. The stack temperature is around 65°C at full load. Figure 37 shows the Nexa™ 1.2kW system schematic diagram, illustrating oxidant air, cooling air and hydrogen as the system inputs and exhaust air, product water and coolant exhaust as the system outputs.

Figure redacted

Figure 36. Schematics of H-500XP experimental apparatus

Figure redacted

Figure 37. Nexa™ 1.2 kW power module's schematic [116]

Unlike the H-500XP PEMFC system, the Nexa™ power system has a built-in humidity exchanger to humidify the inlet air by transporting product water and heat from the wet cathode outlet to the dry inlet air with the pressure maintained at 0.1 bar by the control system. Any excess product water is discharged from the system as liquid and vapour. The

primary purpose of the humidity exchanger is to extend the life of the membrane by preserving membrane saturation. Like H-500XP PEMFC, the fuel is 99.99% un-moistened hydrogen and oxygen is drawn from ambient air. The air compressor is adjusted to match the required oxidant air depending on the power demand. Like the oxidant air, the cooling air also uses a fan to draw ambient air. The control system is equipped with many sensors to maintain the hydrogen pressure at 0.3 bar, regulate the cooling air to cool the stack and keep the temperature in the stated range, and monitor the fuel cell performance. The fuel cell also incorporates an operational safety system for indoor operation [116].

The humidity exchanger uses the fuel cell product water and the heat from the wet cathode outlet to humidify the oxidant air. The cooling air supplied through a small cooling fan pulls air from the ambient environment. The user sets the regulators on the external cylinder supplying hydrogen, but the control system regulates the pressurised hydrogen entering the fuel cell. One of the system problems is that some products, water and nitrogen migrate through the membrane and accumulate in the anode. To minimise the effect of this accumulation in the anode, which decreases the performance, a purge valve at the stack outlet opened periodically to flush out inert residents in the anode and reinstate performance. The amount of hydrogen in the residents is less than 1%, diffusing into the cooling air stream and diluting to a lower level than the minimum flammability limit. There is a leak detector in the cooling air exhaust for safety reasons. The fuel cell control system receives many input signals from the onboard sensors, including hydrogen pressure, fuel cell stack current, air mass flow, stack temperature and stack voltage.

Figure 38 shows the experimental setup of the Nexa™ system connected to the load bank and a PC [149]. Two 12 V batteries connected in series (1) are needed for start-up and during load changes. A fuse (2) serves as a safety to protect the batteries from the backflow of the current. A wire wound panel mount resistor with a ceramic core (3) to sustain the load is illustrated, as well as the load bank cover (4) to protect users from the high temperature of the resistors. The ISLE DC/DC converter (5) stabilises the DC output at 24 V, and the display unit of the DC/DC converter (6) is used in case the system is not connected to a PC. The battery isolator (7) switches on only at starting and during changing of load. A relay (8) connects the

test rig circuit with the batteries. The terminal blocks/busbar (9) serves as a bridge between the DC/DC converter, the resistors, and its switch box.

The hydrogen leak sensor (10) monitors any escaping fuel from the hydrogen cylinder (11) supplying pressurised hydrogen to the Nexa™ system (Fig. 41). The hydrogen cylinder regulator (12) sets the output pressure from the Nexa™ system and the other regulator serve as indicators of the hydrogen level in the cylinder. The figure also depicts a PC monitor with the NexamonOEM data logging software (13), hydrogen cylinder housing units and brackets (14,15) for safety purposes, extension cable from the grid to power the PC and monitor (16), and the bank load switch boxes (17). The excess water tank (18) collects and measures the remaining product water. Finally, the Nexa™ fuel cell stack is also displayed (19).

Figure redacted

Figure 38. The Nexa™ system experimental setup [149].

4.1.3 Load cell setup

For both H-500XP and Nexa™ 1.2 kW fuel cell systems the load cell bank setup (Figure *39*) is similar except for the series of input loads, which is 48 VDC output for the former and 24 VDC for the latter. As a result, there are 15 power input combinations for the H-500XP system and 26 combinations for the Nexa™ 1.2kW system. The load bank consisted of panel mount resistors connected directly onto switches (A), which combinations interconnected the resistors in series and parallel arrangements. Although there are 26 combinations of power inputs for the Nexa™ 1.2 kW system, it was noticed in the experiments that only 22 combinations seemed stable and presented with negligible losses. Single pole single throw (SPST) switches were used to control the resistance input, and single pole double throw (SPDT) switches were used to control the series to parallel arrangement of the resistors.

Terminal blocks/busbar (B) allowed the resistors to be connected to either the DC/DC converter or the relay (Figure 39). Every output configuration from the switch box is connected to one of the two busbars. The relay connects the primary test rig circuit with the two batteries independently connected in series. As previously stated, the batteries are needed for start-up and load change during operation since the fuel cell cannot empower the auxiliaries during these states. The panel mount resistors (C) are also shown in the schematics.

Figure redacted

Figure 39. The load bank schematic of both experimental setups.

4.2 Simulation of PEM fuel Cell using MATLAB/Simulink

4.2.1 Fuel cell stack model

Fuel cells are generally developed with the current as an independent variable to calculate the stack voltage. In the presented model, as Figure 40 illustrates, the exterior load resistance is the independent parameter to influence current and voltage [35]. The fuel cell stack has been developed with a DC voltage source monitored by equations that relate the fuel cell stack current and temperature with its voltage. The stack current flows from the voltage supply to the circuit. The voltage source provides energy to an electrical circuit created by a DC boost converter and variable quantity load. The converter is manipulated by a voltage Proportional-Integral (PI) controller with pulse-width modulation (PWM) signal control. The regulated current source demonstrates the power utilisation of auxiliary components. The model is established with MATLAB Simulink, incorporating its package Simscape, to resolve the electrical circuit.

Figure redacted

Figure 40. Schematics of the PEMFC system equivalent electrical circuit [150].

The stack was developed as unidimensional and isothermal, and steady-state operating conditions were assumed. The partial pressure of the reactants was considered steady, while the increase of pressure owing to the blower and pressure decline of the fuel flow in the pipe was overlooked. The humidity of the membrane was assumed as constant at saturated situations. Power consumption of the auxiliary elements was also taken as constant. As the model does not consider the transient conditions during start-up, the battery and super-capacitor are omitted. The maximum power demand was considered 600 W. Figure *36* shows a schematic diagram of the PEMFC setup.

Oxygen reaction with H_2 in a single cell with liquid water as the product is represented by Eq. (3.1). Based on equation (3.7), the reversible open-circuit voltage at the standard specification (298.15 K, 1.013 bar), E^0, is given by [197]:

$$E^0 = \frac{-\Delta \bar{g}_f}{2F} = 1.229\ V \tag{4.1}$$

where $\Delta \bar{g}_f$ (kJ/kmol) is the variation in the specific Gibbs free energy of formation and F is the Faraday constant.

Applying Nernst's equation, the reversible open-circuit voltage $E^{T,P}$ (V) can be assessed at different conditions [197]:

$$E^{T,P} = \frac{-\Delta \bar{g}_f}{2F} + \frac{\bar{R}T_s}{2F} ln\left(\frac{p_{H_2} \cdot {p_{O_2}}^{\frac{1}{2}}}{p_{H_2O}}\right) - \frac{\Delta \bar{s}}{2F}(T_s - 298.15) \tag{4.2}$$

where T_s is the stack temperature (K), $\bar{R}$ is the universal gas constant (8.314 kJ/kmol.K), p is the partial pressure of reactant hydrogen and oxygen and product water (bar), and $\Delta \bar{s}$ is the specific entropy variation (kJ/kmol.K).

When load is applied to the fuel cell, an external current I_{ext} (A) streams causing the voltage to drop [36]. During fuel cell operation, a small amount of hydrogen can disperse across the membrane from the anode to the cathode where it reacts without generating current and several electrons may cross over the membranes rather than the external load. Those consequences are equivalent and taken into account by adding a current loss I_{loss} (A) to the entire fuel cell current I (A) as shown by [197]:

$$I = I_{ext} + I_{loss} \tag{4.3}$$

The voltage required to maintain the electrochemical reactions in the cathode and anode represents the activation voltage losses, ΔV_{act} (V), which can be calculated as [197]:

$$\Delta V_{act} = \xi_1 + \xi_2 T_s + \xi_3 T_s \, ln\left(C_{O_2}\right) + \xi_4 T_s \, ln(I) \tag{4.4}$$

The constant parameters $\xi_1 \ldots \xi_4$ are displayed in Table 7.

Table 7. PEMFC model parameters.

Parameter	Value	Parameter	Value	Parameter	Value
$p_{H_2}\ (atm)$	1.0÷1.5	ξ_1	1.00	$\tau_m(\mu m)$	25
$p_{O_2}\ (atm)$	$\simeq 0.21$	ξ_2	-3.4×10^{-3}	λ_m	7
$p_{H_2O}\ (atm)$	1	ξ_3	-7.80×10^{-5}	$A(\mathrm{cm}^2)$	76
$I_{loss}(A)$	0.3	ξ_4	1.85×10^{-4}	$I_{L,c}(A)$	47

In Eq. (3.62), C_{O_2} is the concentration of dispersed oxygen (mol/cm^3) at the liquid interface as defined by Henry's law [197].

$$C_{O_2} = \frac{p_{O_2}}{5.08 \cdot 10^6 \, exp\left(-\frac{498}{T_s}\right)} \tag{4.5}$$

Furthermore, the equivalent activation resistance is given by:

$$R_{act} = \frac{n_{cell}\Delta V_{act}}{I} \tag{4.6}$$

where n_{cell} the number of cells connected in series.

The ohmic voltage losses, ΔV_{ohm} (V), are described by [197]:

$$\Delta V_{ohm} = R_{ion}I + (R_{ele} + R_{con})I_{ext} \tag{4.7}$$

where R_{ion} (Ω) is the resistance to the stream of ions in the membrane, R_{ele} (Ω) is the electronic resistance to the stream of electrons in the conductive material, and R_{con} (Ω) is the contact resistance of the electrodes. Only R_{ion} is here regarded and, for a Nafion-based membrane, it is given by [197]:

$$R_{ion} = \frac{\tau_m r_m}{A} = \frac{\tau_m}{A} \cdot \frac{181{,}6\left(1 + 0{,}03\frac{I}{A} + 0{,}062\left(\frac{T_s}{303}\right)^2\left(\frac{I}{A}\right)^{2.5}\right.}{\left(\lambda_m - 0{,}634 - 3\frac{I}{A}\right) \cdot e^{4{,}18\left(\frac{T_s - 303}{303}\right)}} \tag{4.8}$$

where r_m is the ionic conductivity of the membrane (Ω/cm), τ_m is the membrane thickness (cm^2), and A is the single-cell active area (cm^2). λ_m is the average amount of water in the membrane and is a function of the water movement a, both dimensionless parameters [197]:

$$\lambda_m = \begin{cases} 0.043 + 17.81a - 39.85a^2 + 36.0a^3 & for\ 0 < a \leq 1 \\ 14 + 1.4(a - 1) & for\ 1 < a \leq 3 \end{cases} \tag{4.9}$$

Then the stack membrane is a composite Nafion/PTFE (poly-tetrafluoroethylene) type [41] with an active area of 76 cm^2 and thickness of 25 µm. Concentration voltage losses ΔV_{con} (V) are proposed to consider the effect on Nernst voltage and activation voltage losses owing to the pressure fall in the gas diffusion layer. These deficiencies occur at the high current caused by a reduction in gas intensity at the electrode surface and are given by [197]:

$$\Delta V_{con} = \left(1 + \frac{I}{\alpha}\right)\frac{RT}{nF} ln \frac{I_L}{I_L - I} \tag{4.10}$$

where I_L (A) is the limit current of the electrode, which transpires when the partial pressure of the reactants drops to zero, and n is the number of electrons engaged in the electrode reactions. Since anode concentration losses are considered negligible, n = 4 and I_L is also the cathode limit current.

The equivalent concentration resistance R_{con} (Ω) is given by [197]:

$$R_{con} = \frac{n_{cell}\Delta V_{con}}{I} \tag{4.11}$$

The activation and concentration resistances with a capacitance in parallel replicate the double-layer charge transient effect. The equivalent double-layer stack capacitance C_{dl} has been calculated starting from a single-cell capacitance per area equal to 0.01974 F/cm^2. This indicates a single-cell double-layer capacitance of 1.5 F and $C_{dl} = 0.05\ F$. The steady state polarization curve of the fuel cell stack is described by [197]:

$$\begin{aligned} V_{stk}(I) &= n_{cell}V_{cell}(I) = n_{cell}(E - \Delta V_{act} - V_{ohm} - \Delta V_{con}) \\ &= n_{cell}\Big\{E - \left[\xi_1 + \xi_2 T_s + \xi_3 T_s\, ln\left(C_{O_2}\right) + \xi_4 T_s\, ln(I)\right] - R_{ion}I \\ &- \left(1 + \frac{I}{\alpha}\right)\frac{RT}{4F}\, ln\frac{I_L}{I_L - I}\Big\} \end{aligned} \tag{4.12}$$

The number of cells attached in series, $\mathrm{n_{cell}}$, is 30. The stack output power is given by [197]:

$$P_{stk} = V_{stk}I_{ext} \tag{4.13}$$

Airstreams inside the cathode flow channels are pulled out (blown/pushed) by two axial fans at the end of the flow channels. Since the pressure drop is insignificant, the pressure within the channels is atmospheric (p_{atm}). The partial pressure of oxygen within the cathode flow channels is given by [197]:

$$p_{O_2} = x_{O_2}p_{atm} \tag{4.14}$$

The partial pressure of oxygen can be found by contemplating the reactant air flow oxygen content. The reacted oxygen creates water and water membrane flow from the anode to the cathode. Thanks to the solid stoichiometric usage of air, the oxygen molar fraction x_{O_2} at steady state is that of the atmospheric inlet air, 0.21. Hydrogen is supplied at 1.5 bar, and the flow rate is self-regulated, a function of the pressure variation between the inlet and the anode flow channels. Inlet hydrogen equals the reacted hydrogen at steady-state operation, and the purge valve is closed. Thus, hydrogen is neither stored nor depleted. The pressure difference ΔP_{H_2} is merely owing to the frictional effects in the provided valves and pipeline. No water or air is considered inside the anode flow channels but only hydrogen. Thus [197]:

$$P_{H_2} = P_{H_{2,in}} - \Delta P_{H_2} \tag{4.15}$$

The pressure inside the flow channels must always be more significant than atmospheric pressure. When the purge valve is started, the gas must flow outside the stack, not vice versa. Hydrogen pressure drop can be articulated as a function of the squared hydrogen flow rate, $\dot{V}_{H_2}^2$ (m^3/s) [197]:

$$\Delta P_{H_2} = k_f \dot{V}_{H_2}^2 \tag{4.16}$$

where k_f is 2.22×10^{-3} atm·min^2/nL^2. The atmospheric pressure is supposed to be achieved with the highest flow rate of the supply system, equivalent to 15 nL/min. The parameters considered by the PEMFC model are shown by Table 7.

4.2.2 Boost converter and external load model

The use of a PEM fuel cell in a hybrid system involves a DC boost converter. A schematics of a basic DC boost converter are shown in Figure 41 [197]. The PWM signal commands the beginning and end of a switcher with a secured switching frequency FSW (Hz). The corresponding period of switching ($\mathrm{t_{SW}}$) is the sum of ON ($\mathrm{t_{ON}}$) and OFF ($\mathrm{t_{OFF}}$) times [197]:

$$t_{SW} = \frac{1}{F_{SW}} = t_{ON} + t_{OFF} \tag{4.17}$$

The duty cycle (d) is described as the portion of time when the switcher is 'ON state', as [197]:

Figure redacted

Figure 41. Schematics of a primary DC boost converter circuit [150]

$$d = \frac{t_{ON}}{t_{ON} + t_{OFF}} \tag{4.18}$$

Assuming the switcher, the diode, the inductor (L) and the capacitor (C) are ideal, the equations that connect the duty cycle, the converter input voltage (V_i) and current (I_i) and the output voltage (V_0) and current (I_0) are given by [197]:

$$\frac{V_O}{V_I} = \frac{1}{1-d} \tag{4.19}$$

$$\frac{I_O}{I_I} = 1 - d \tag{4.20}$$

Employing Ohm's law on external load resistance (R_{ld}), one can obtain [197]:

$$R_{ld} = \frac{V_O}{I_O} = \frac{\frac{V_I}{(1-d)}}{I_I(1-d)} \tag{4.21}$$

The equivalent resistance to the fuel cell is given by [197]:

$$R_{eq} = \frac{V_I}{I_I} = R_{load}(1-d)^2 \tag{4.22}$$

Equation (4-22) displays the impact of the duty cycle on the fuel cell running point. The highest duty cycle value leads to the minor equivalent resistances detected through the fuel cell and, consequently, to the highest current and power demand. The PI controller commands the quantity of the duty cycle, safeguarding 48 V for every external load. The amount of the reactive components of the boost converter is selected to restrict the input current ripple (fuel cell current ripple) and the output voltage ripple. Restricting the fuel cell current ripple is essential to guarantee an extended lifespan of the fuel cell. Sudden alterations in the fuel cell current should be limited to prevent starvation challenges and degradation of a catalyst layer. This is usually done by regulating the fuel cell current with the boost converter [28].

In the simulation, a PI voltage controller instructs the boost converter to ensure an output voltage of 48 V, but it does not consider the fuel cell current variation. Table 8 exhibits the highest current and voltage ripple permitted, and the parameters applied for the DC boost converter and PI controller.

Table 8. DC boost converter and PI controller parameters.

DC boost converter	Value	PI Controller	Value
Switching frequency (kHz)	50	k_P	0.0001
Maximum input current ripple (%)	4	k_I	0.5
Maximum output voltage ripple (%)	2	Duty cycle range	$0.2 - 0.7$
Inductance (mH)	1.37		
Capacitance (mF)	1.80		

Figure 42 reveals a controlled DC voltage source V_{stk} (I) attached to the PEMFC equivalent electrical circuit. The stack output current is used to update the value of the output voltage. The fuel cell stack output voltage is enhanced to 48 V at the resistance load bank by the DC boost converter. A PWM signal manipulated by a PI controller is employed to alter the boost

converter duty cycle. After the stack, a regulated current source is used to simulate the fan power consumption variation with temperature from 36.5 W at 296.15 K to 52 W at 338.15 K.

Figure redacted

Figure 42. Fuel cell electrical circuit [150].

4.2.3 Performance parameters calculation

For a specific external load resistance ($\mathrm{R_{load}}$), the theoretic power demand ($\mathrm{P_{req}}$) from the stack is calculated by [197]:

$$P_{req} = \frac{48^2}{R_{load}} \tag{4.23}$$

The boost converter efficiency (η_{con}) is given by its output power over its input power. Consequently, dividing the power provided to the load ($\mathrm{P_{load}}$) by the output power of the stack minus power consumption by auxiliary components, the efficiency of the boost converter can be calculated as follows [197]:

$$\eta_{con} = \frac{P_{out}}{P_{in}} = \frac{P_{load}}{P_e - P_{aux}} = \frac{\frac{V_{load}^2}{R_{load}}}{V_{FC} I - P_{aux}} \quad (4.24)$$

The fuel cell stack efficiency η_{FC} is calculated by [197]:

$$\eta_{FC} = \frac{P_{ext} + P_{aux}}{P_{H_2}} = \frac{V_{ext} I_{ext} + P_{aux}}{\rho_{H_2} \dot{V}_{H_2} HHV_{H_2}} \quad (4.25)$$

where $\mathrm{P}_{\mathrm{H}_2}$ is the hydrogen power input (W), which is given by the product of its flow rate $\dot{V}_{H_2}$ (m^3/s), density ρ_{H_2} (kg/m^3) and higher heating value $\mathrm{HHV}_{\mathrm{H}_2}$ (kJ/kg). The number of moles of hydrogen consumed by the stack for the reactions and losses due to internal fuel crossover, $\dot{\mathrm{N}}_{\mathrm{H}_2}$ (mol/s), is obtained by [151]:

$$\dot{N}_{H_2} = \frac{n_{cells} I}{2F} \quad (4.26)$$

which is necessarily equivalent to the moles of fuel because hydrogen with a purity degree of 99.99% has been utilised. If one assumes the fuel utilisation factor (η_{fu}) equals to 1 and hydrogen behaves as an ideal gas, then the actual volumetric fuel flow rate is calculated as:

$$\dot{V}_{H_2} = \dot{N}_{H_2} \cdot \bar{v}_{H_2} \cdot \frac{1}{\eta_{fu}} = \dot{N}_{H_2} \frac{\bar{R} T_n}{p_n} \quad (4.27)$$

where T_n and p_n are respectively the fuel temperature and pressure at normal conditions ($273.15\ \mathrm{K}$, $101.325\ \mathrm{kP_a}$) and $\bar{\mathrm{v}}_{\mathrm{H}_2}$ is the specific volume of hydrogen on molar basis ($\mathrm{m}^3/\mathrm{kmol}$).

The overall fuel cell system efficiency η_0 is given by the product of the DC boost converter efficiency η_{con} and the stack efficiency η_{stk}:

$$\eta_0 = \eta_{FC}\eta_{con} = \frac{P_{load}}{P_{H_2}} = \frac{\frac{{V_{load}}^2}{R_{load}}}{\rho_{H_2} \cdot \dot{V}_{H_2} \cdot HHV_{H_2}} \quad (4.28)$$

4.2.4 Improved power electronics interface (PEI) model to optimise voltage, current and power signals.

The PEM fuel cell model described in the previous section was initially developed based on the H-500XP fuel cell then adjusted with the details of the Nexa 1.2 kW fuel cell, as shown by Table 9, to optimise its operation. The maximum operating point has been extended to reach the aim of 2 kW power through the model. The voltage value of 22 V is still in the Nexa 1.2 kW range, and the current was calculated using Eqs (4-13). This model gives a better understanding of the possibility of enhancing the power output using an improved power electronics interface. In addition, it helps to examine and optimise voltage, current and power signals using a PID controller.

Table 9. Nexa 1.2kW PEMFC parameters

PARAMETER	VALUE
Voltage @ 0 A	42 V
Voltage @ 1 A	35 V
Nominal operating point	46 A, 26 V
Maximum operating point	91 A, 22 V
Number of cells	47
Nominal stack efficiency	44 (%)
Operating temperature	65°C
Nominal air flow rate	2400 L/min
Nominal fuel supply pressure	0.3 bar
Nominal air supply pressure	0.1 bar
Nominal H_2 composition (%)	99.95%
Nominal O_2 composition in air	21%
Nominal H_2O composition	1%

Figure 43 shows a simplified schematics of the Simulink model of the Nexa 1.2kW stack. The simulated I-V characteristic curve has been extended to reach 2 kW, as shown by Figure 44. This linearisation allows the evaluation of power optimisation using an improved DC/DC boost converter together with PID control system to optimise the voltage signal. Alternatively, the stack cells could be increased to operate safely within the linear part of the carve from 22 V to 36 V but that would increase the stack cost.

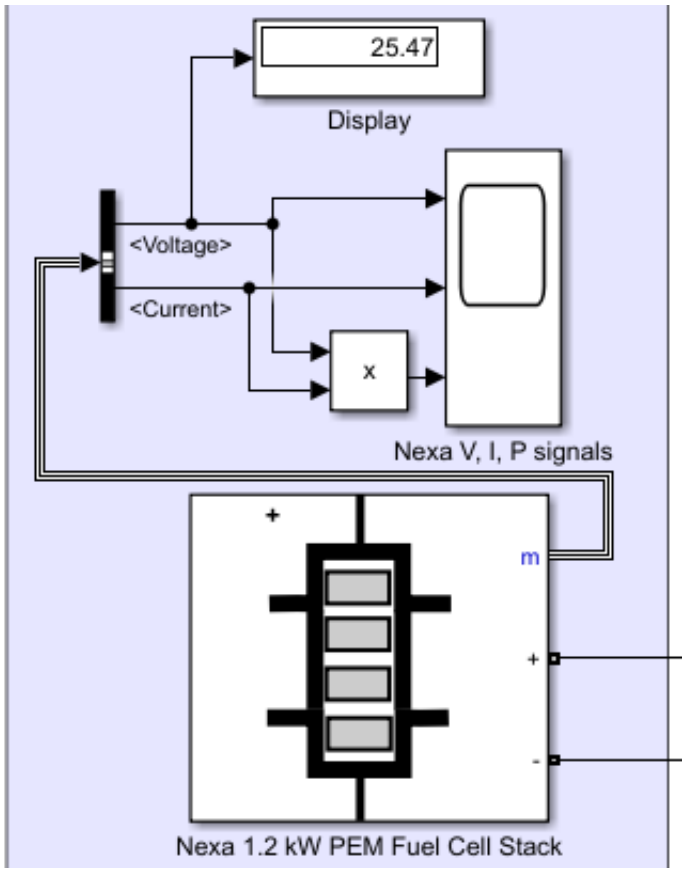

Figure 43. Simplified schematics of the Nexa 1.2kW PEM fuel cell model.

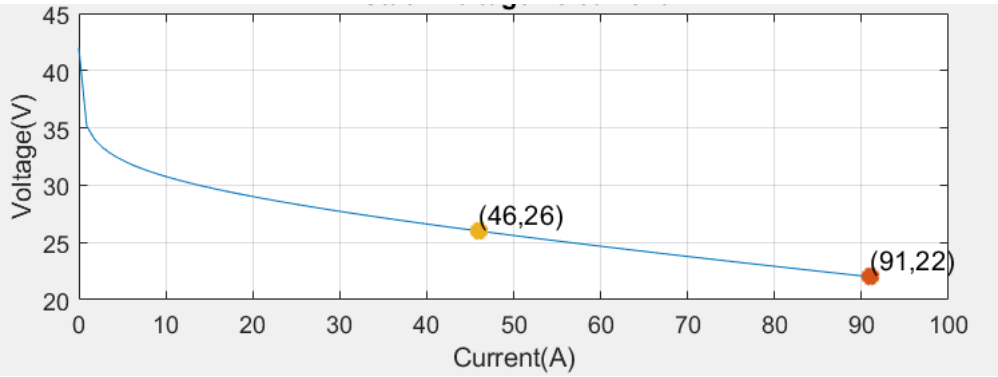

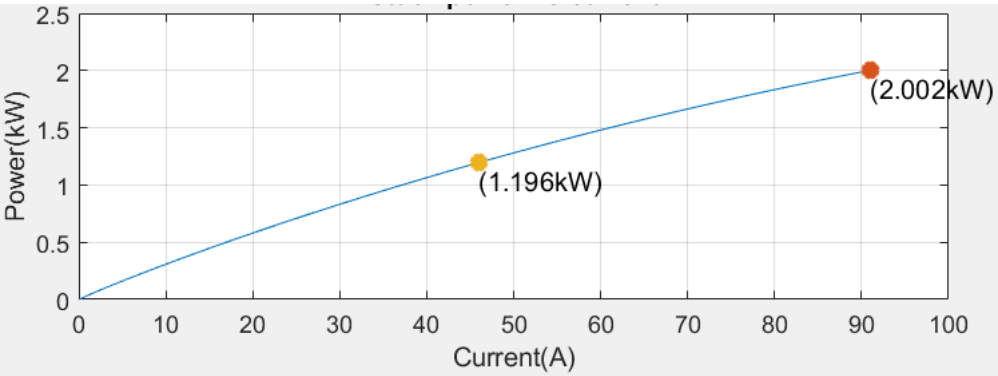

Figure 44. The PEM fuel cell I-V characteristics curve.

4.2.5 Improved DC/DC boost converter

The higher efficiency, its ability to convert the unregulated voltage into needed regulated voltages and the less parts count is some of the pros of using DC/DC boost converter [152]. Only the linear region has been considered as the bending part of the curve cannot be specifically interfaced to the DC bus. The linear part was from 26 V to 36 V but through the model it is extended to 22 V which is the limit of the DC/DC boost converter in the laboratory settings. Moreover, if the power generated by the fuel cell is not enough, there is a need for energy storage devices such as battery. As the Nexa 1.2 kW fuel cell shows, the use of batteries required additional control circuit to regulate the power flow during charging and discharging conditions [153].

Figure 45, shows the basic DC/DC Boost converter which have been used as part of the Nexa™ 1.2kW PEMFC settings, which have been explained in the previous section. An improved DC/DC Boost converter (Figure 46) was modelled using Eqs. (4.17) to (4.22). The calculation of the inductance, two capacitors and resistance were based on the values shown in Table 10. Some of the advantages of using power electronics interface for Nexa 1.2 kW PEM fuel cell are:

1) the possibility of getting a higher gain of the input to output voltage ratio that can let the DC/DC converter boost the output voltage to a required level.
2) evaluation of the voltage and current ripples (variation around the mean or median values) to attain lower ripples values, which reflect on efficient and constant output voltage.

3) provide a higher power value for the Nexa 1.2 kW PEM fuel cell that can allow to get a higher output voltage from a lower input voltage [32].

In addition to the above advantages, the system is not complicated to design and build, and it is easy to operate comparing with the physical system. Evaluating and investigating the system through modelling makes it more affordable and economical. The DC/DC converter consist of an inductance that helps with current losses by reducing the equivalent series resistance and other losses (Figure 46). The capacitors work as energy storage and the reason of choosing two is that one work as input filter and the other work as an output filter. The diode selected has a good reverse recovery time and higher current rating. The IGBT/Diode (insulated gate bipolar transistor) switch is selected instead of the MOSFET (metal oxide semiconductor field effect transistor) in the basic DC/DC converter. The advantages of IGBT/Diode comparing with MOSFET are its hybrid device structure, current control capability that conducts charges through both electrons and holes, higher forward voltage drop (2V), higher power and voltage handling capacity, handle of higher transient currents and voltages, and suitability for higher power applications. Some of its disadvantages are more expensive, slower switching speed, and longer turn off time [154–158].

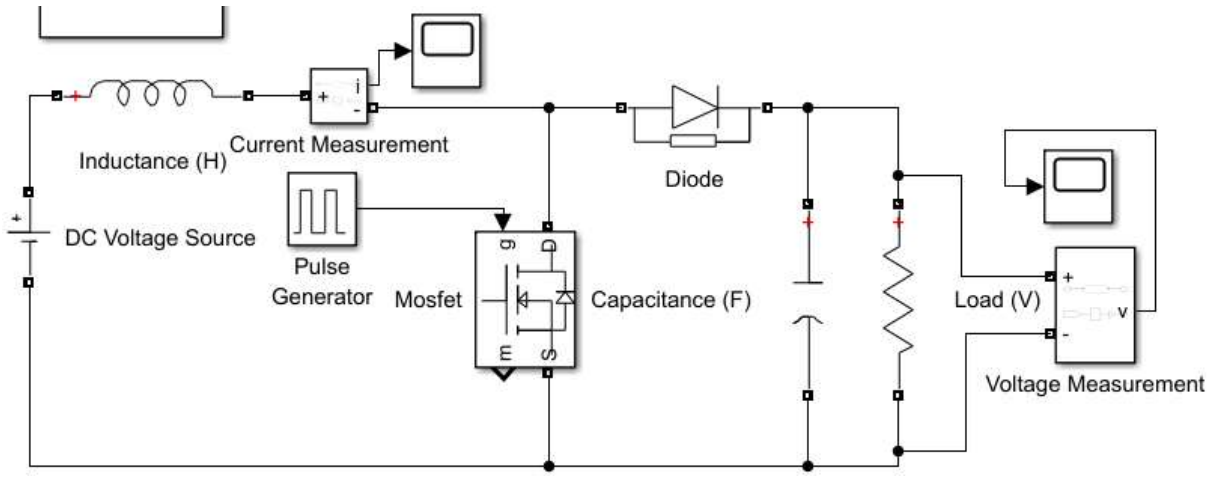

Figure 45. Basic DC/DC Boost Converter

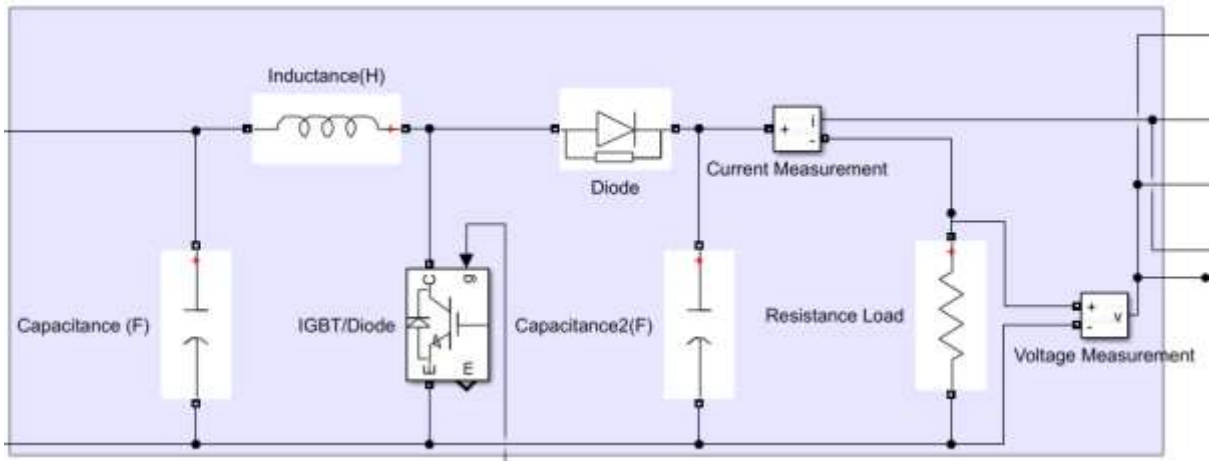

Figure 46. Improved DC/DC Boost Converter

Table 10. Improved DC/DC Boost Converter parameters

PARAMETER	VALUE
Switching Frequency (kHz)	10
Output voltage (V)	48
Maximum Power (kW)	2
Input Voltage (V)	22
Inductance (mH)	1.3
Capacitance (mF)	4.7
Resistance load (Ω)	1.9264

4.2.6 PID (Proportional Integral Derivative) Controller

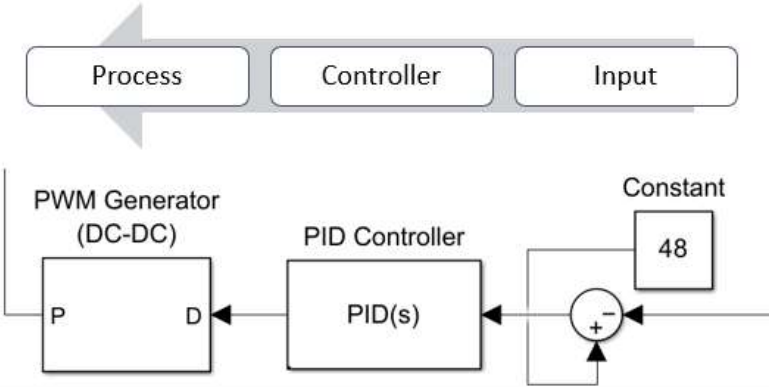

Figure 47. The PID Controller

As Figure 47 shows, the main three blocks of the control system are the input, which includes the setpoint and the fixed voltage of 48 V, PID controller, and pulse-width modulation (PWM) generator. The PID controller continuously modulates the system by adjusting the duty cycle. The PID looks for the proportional gain (Kp) value of the current error, the past value of the error to integrate it over time and find the integral gain (Ki), and the derivative gain (Kd), which is the value proportional to the rate of change of the error. All three values are given in the PID text box after the running of the PID controller is finished. The self-tunning option let the operator find the most optimum values by using sliders or typing values in the boxes. To find the best values of gains is challenging but in general the best value of Kp should let the system respond rapidly to variations in the setpoint, while the best value of Ki should eradicate the steady state error and the best value of Kd should help the system to be satisfactorily restrained. Based on experience, all three values should not be elevated as this will make the system uneven and vacillate [157–162]. Table 11, shows the parameters of the PID control system.

Table 11. PID Controller values

PARAMETER	VALUE
Maximum output current ripple (%)	11
Duty Cycle (s)	0.5
Switching period (ms)	5
Kp	0
Ki	0.1667
Kd	0

The control system is a closed loop process and the method used to tun the PID is the Ziegler-Nichols, which is one of the heuristic methods. It works by increasing the Kp gain while keeping Ki and Kd on zero until the system alternate at steady amplitude then the found gains value and the period are used to calculate the three gains using a set of equations. The expression that represents a PID is [163]

$$P + I\frac{1}{S} + D\frac{N}{1 + N\frac{1}{S}}$$

In the above representation, P is the proportional term that adjusts the output based on the error between the desired value and the actual value of the system. P is multiplied by the error to provide an immediate response. The term I is the integral of the error over time to eliminate any steady-state errors that may persist even after the proportional term has adjusted the system. It helps in accumulating the error and continuously adjusting the output to reach the desired value. 1/S is the Laplace variable that amounts to the complex frequency domain representation of the system. The third term is D, which is the derivative term calculating the rate of change of the error and adjusts the output based on the rate at which the error is changing. It helps in providing a damping effect and reducing overshoot and oscillations in the system. The factor N scales the contribution of the derivative term to further fine-tune the controller response while 1/S in this part represents the rate of change of the error [160].

The PWM is controlling the output voltage to ensure a stable level that reflects in a regular power output. On the other hand, it controls the input voltage by rapidly switching it on and off at high frequency. The width of the on-time pulse, known as the duty cycle, determines the average power delivered to the load. The PWM keeps monitoring the output voltage and compares it to the desired reference voltage by adjusting the duty cycle of the switching signal. Some of the advantages of using PWM are the allowance of smooth regulation of power flow, reduction of power losses, ability of handling a wide range of input and output voltages, high efficiency, and precise control [164].

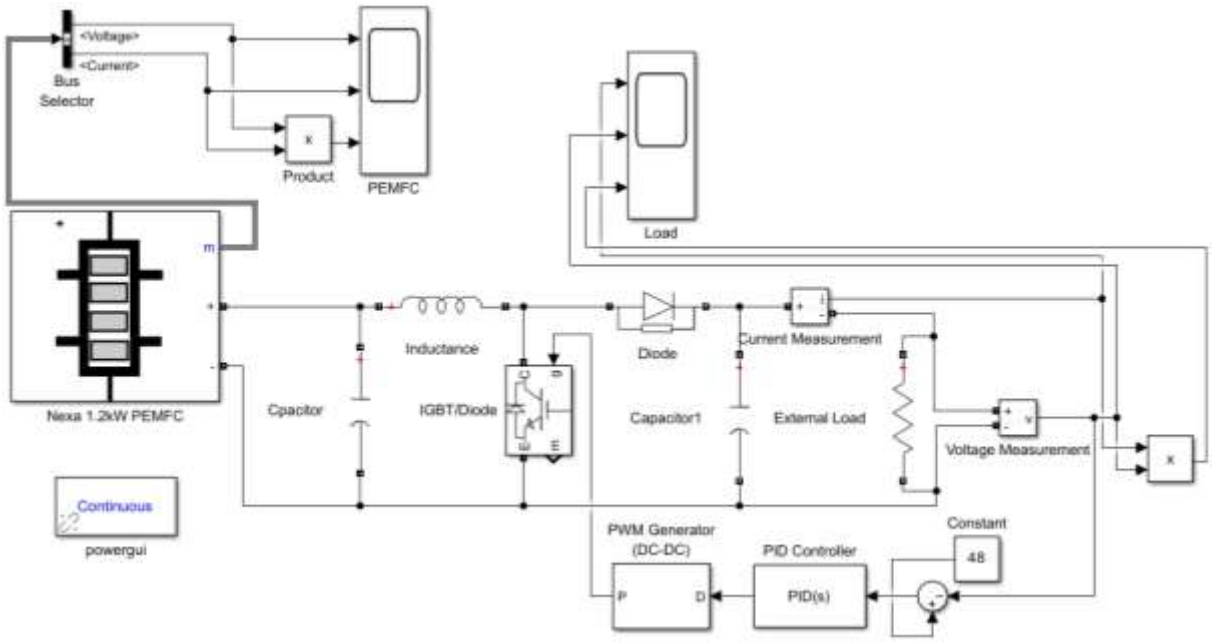

Figure 48. The Nexa™ 1.2kW PEMFC model with the improved power electronic interface.

Figure 48 shows the complete system diagram of the Nexa 1.2 kW PEMFC model with the improved power electronics interface consisting of three main parts: fuel cell model, improved DC/DC converter, and control system. One of the challenges of PID controller is how operators should set the coefficients to achieve the best controlling state [165]. The method used in this study is an online system feed that decides the values of the coefficients of the PID. The PID controller can be further optimised using Particle Swarm Optimisation (PSO) algorithm [158,166]. An initial development of this technique is shown in Appendix A.6, but its application is left as suggestion for future work.

4.3 Development of the exergoeconomic model of Nexa™ 1.2kW system using M. Script

The exergoeconomic model was developed using MATLAB M. Script and validated using experimental data from the Nexa™ 1.2 kW system [167]. The model considers the exergy cost of all reactants and the products of the electrochemical process at several operating conditions, such as cell voltage, inlet air stoichiometry, temperature, and pressure (Table 12).

Table 12. 1.2 kW PEM fuel cell specifications.

Next Performance	Rated power	1.2 kW
	Dissipated heat at rated power	1.6 kW
	Voltage at rated power	43 V / 26 V DC
	idle/full	22 V to 50 V
	Input voltage allowable	18 V to 30 V
	Current at rated power	46 A DC
	Number of cells	47
	Lifetime	1,500 h
Reactant Data	Hydrogen (dry)	99.99%,
	Pressure range of hydrogen	0.7 to 17 bar
	Hydrogen consumption	<18.5 L/min
	Process Air	≤ 90 L/min
	Air pressure	1.013 bar
	Air stoichiometry (λ)	3
Operating Environment	Ambient temperature	(3°C to 40°C)
	Maximum stack temperature	65°C
	Humidity	5% to 95%
Product Data	Pure water (vapour and liquid)	0.870 L/h
Physical Data	L x W x H	56 cm x 25 cm x 33 cm
	System mass	13 kg

4.3.1 Exergy analysis

The following algorithm was applied to the model calculations for the exergy analysis [142]:

- Calculate the exergetic efficiency using Eqs. (3-35) and the external load (P_{ext}) using Eqs. (3-37)
- Calculate the current I using equation (3-38)

- The auxiliary power is calculated as the difference between the electrical power output P_e and the calculated power from the reactant consumption P_{ext} using Eq. (3.36)
- Calculate the physical exergy of the stream components using Eqs (3-41) the chemical exergy using Eq.(3-43), and the total exergy transfer per unit mass using Eq. (3-40)
- Calculate the mass flow rates of reactants (R) and products (P) using Eqs. (3-44) to (3-48)
- Calculate the total exergy of hydrogen, air and water using Eqs. (3-49) to (3-50).

4.3.2 Exergy cost analysis

After calculating the parameters of the exergy analysis, the exergy cost are calculated according to the following algorithm [142]:

- Calculate the capital investment cost $\dot{C}_{CI}$ using Eq. (3-55)
- Calculate the cost rate of annual operations and maintenance costs $\dot{C}_{OM}$ using Eq. (3-58)
- The total investment cost $\dot{C}_{FC}$ is found by summation of $\dot{C}_{CI}$ and $\dot{C}_{OM}$ using Eq. (3-54)
- Calculate the exergy cost of the electrical power produced c_{P_e} using Eq. (3-53).

4.3.3 MATLAB™ M. Script exergoeconomic model

A flowchart of the exergoeconomic model built using MATLAB M. Script is shown by Figure *49*. A model characteristic is the following:

1. A database of parameters for calculation of the thermal properties of the fluids of interest was built. The equations used for the exergy and exergoeconomic analyses

were supported by parameter values available at standard tables of thermodynamic properties.

2. The traditional approach of conducting the exergoeconomic analysis was improved by using a value of new primary power value, which was extracted from the model based on the experimental data. The traditional approach depends on the manufacturing data sheet regarding the primary power, which in this case is 1196 W
3. The model used the current as the independent variable to find the voltage value. The reduction of maximum stack voltage by 1.4% could increase the power by around 2%
4. The model can analyse different PEM fuel cells by altering the input values to reflect the system under investigation.

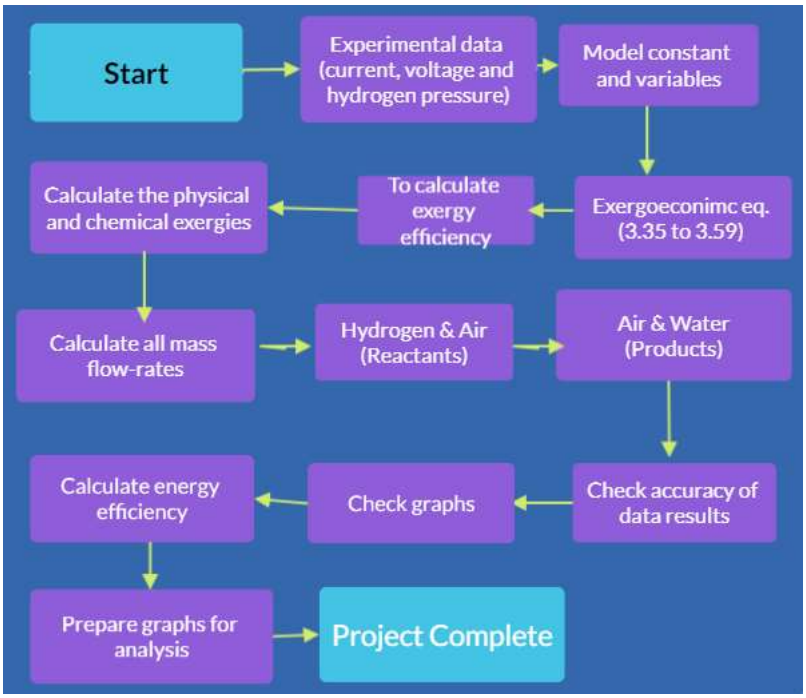

Figure 49. Flowchart of exergoeconomic model of Nexa™ 1.2 kW PEM fuel cell system development.

To summarise, this chapter includes three main subsections, the experimental setup which includes a 0.5 kW PEM fuel cell which used for the steady state MATLAB/Simulink model and the 1.2 kW which used for the exergoeconomic analysis and the Power electronic interface. As the exergoeconomic model had been built in M. Script more details have been given here.

5 Results and Discussion

The results from steady-state model simulation of the H-500XP PEM fuel cell stack are presented and compared with experiments. The model is then applied to the Nexa™ 1.2 kW PEM fuel cell to provide the data to conduct exergy and exergoeconomic analyses, which results are also shown and discussed. Finally, the results from the PEI model to improve current, voltage and output power from the fuel cell are also displayed.

5.1 Simulation of PEM Fuel Cell using MATLAB/Simulink

The H-500XP PEMFC stack polarisation curve at steady-state operation is represented in Figure 50 (a). The model polarisation curve was close to the experimental values, with a maximum discrepancy of 3.1%. The lowest external load resistance tested was 4.63 Ω, corresponding to the maximum electric current of 29.2 A at 19.67 V, thus providing 574.4 W. Similar comparison of the polarisation curve has been applied elsewhere to certify that the model adequately follows the fuel cell characteristics [168–170]. The polarization curve is sometimes preferred to be represented in terms of electric current density per unit area (A/cm^2) instead of electric current (A) [18,171,172].

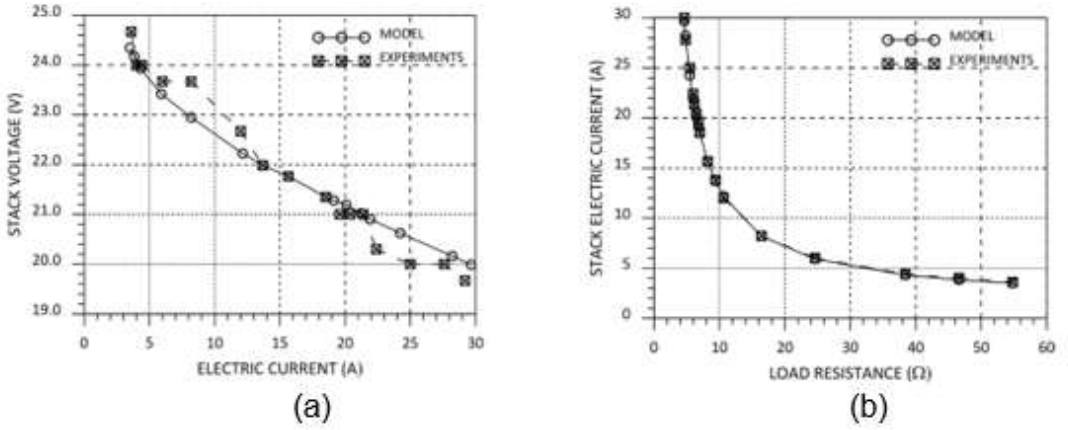

Figure 50. (a) H-500XP PEMFC stack model polarisation curve (b) Variation of H-500XP PEMFC stack current with external load

Both experiments and model agreed that higher PEMFC stack current is attained with decreasing external load resistance, as Figure *50* (b) shows. The maximum discrepancy between model and experimental data was 4.2%. Lower external load resistance means higher power demand from the PEMFC stack. Following the dependence of stack voltage with external current shown in Figure 50 (a), the increase of external load resistance increases the stack output voltage (Figure 51 (a)). The maximum discrepancy between the model and experiments for these results was 3.1%.

- The external load decrease shows increased stack output power (Figure 51 (b)). Both models and experiments show similar trends, with a maximum discrepancy of 5.7%. Fuel cell current is increased with the power output, as Figure 52 (a) shows [173]; therefore, when a decrease in the external load resistance occurs, the stack raises its output current (see Figure 50 (b)) and, consequently, demands a higher fuel flow rate, as Figure 52 (b) shows. Experiments and model show a linear dependence of hydrogen consumption with stack current. The maximum discrepancy was 8.7%. When plotted against the output power, the hydrogen flow rate also displays increasing values though the linearity is lost (Figure 53 (a)). A similar trend is reported by other authors [174].

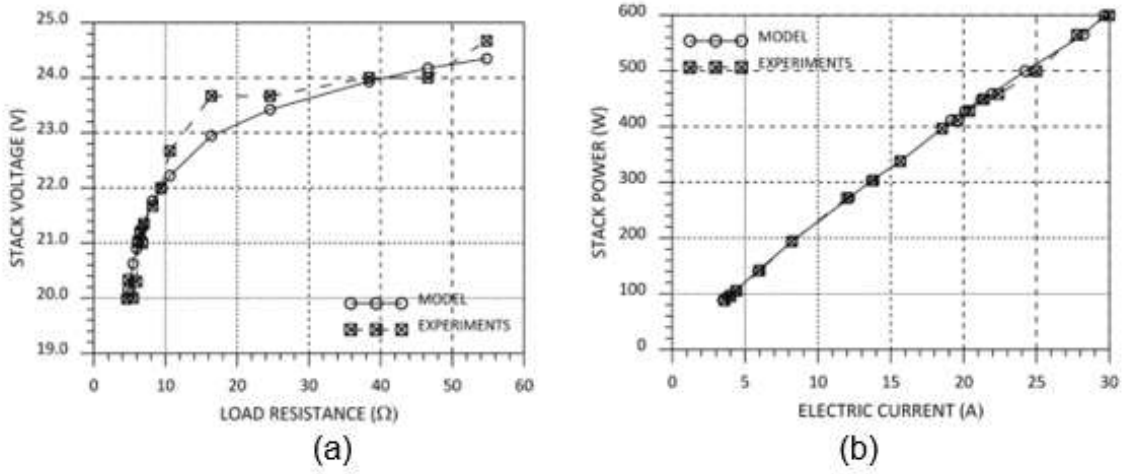

Figure 51. (a) Variation of H-500XP PEMFC stack voltage with external load (b) Variation of H-500XP PEMFC stack output power with external load

Figure 53 (b) shows the overall system efficiency predicted by the model and calculated from the experiments. The peak efficiencies were 47.6% (model) and 48.6% (experiments), attained at around 50% of the rated power. These values are below those reported by other authors, where peak efficiencies of around 54% have been obtained [168][175]. The maximum discrepancy between model and experiments was 4.6%. These results indicate a gap for fuel cell performance improvement, which is expected to be further explored using the current model in future works.

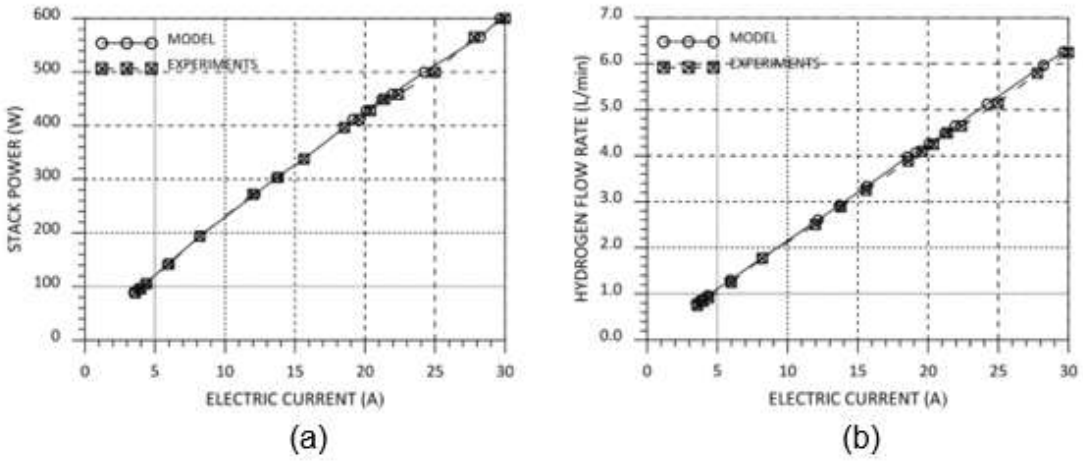

Figure 52. (a) Variation of H-500XP PEMFC stack output power with electric current (b) Variation of H-500XP PEMFC stack hydrogen flow rate with electric current.

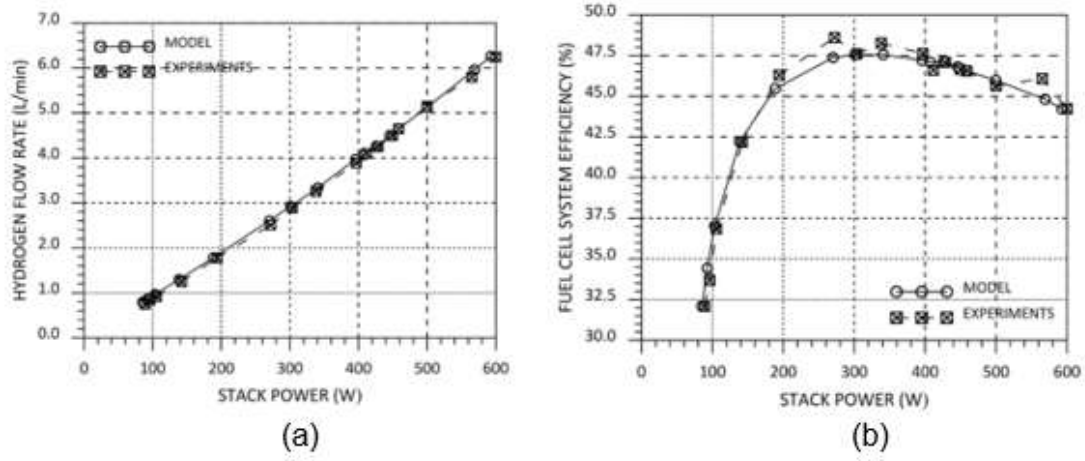

Figure 53. (a) Variation of H-500XP PEMFC stack hydrogen flow rate with output power (b) Variation of H-500XP PEMFC stack overall system efficiency with output power.

The main advantages of using a simplified, one-dimensional fuel cell model like the one presented here are the possibility of reducing development costs from experiments and providing relatively accurate results without long processing time. A previous study has shown that a one-dimensional model produced a tight polarisation curve to a three-dimensional model but with a processing period nearly 300 times higher [87]. The model here introduced can predict PEMFC performance by assessing various operating parameters, such as optimisation of stack temperature. The fuel cell performance can be improved with high operating temperatures, but it will require more fan power, increasing the operation cost. This exemplifies how a compromise can be reached with the aid of this type of model.

5.2 Exergy and Exergoeconomic Analysis of PEM Fuel Cell

The MATLAB exergy and exergoeconomic model is based on experimental data collected from the Nexa™ 1.2 kW PEM Fuel Cell system installed at Aston University laboratories. According to the manufacturer data sheet, the module can provide 1.2 kW of unregulated DC output and the voltage level can vary from 26 V at full load to 43 V with no load. The current density output data was taken in real time by increasing the load. The stack operating temperature was 65°C. The number of cells is 47, connected in series in the stack.

5.2.1 Nexa™ 1.2 kW PEM fuel cell electrical parameters

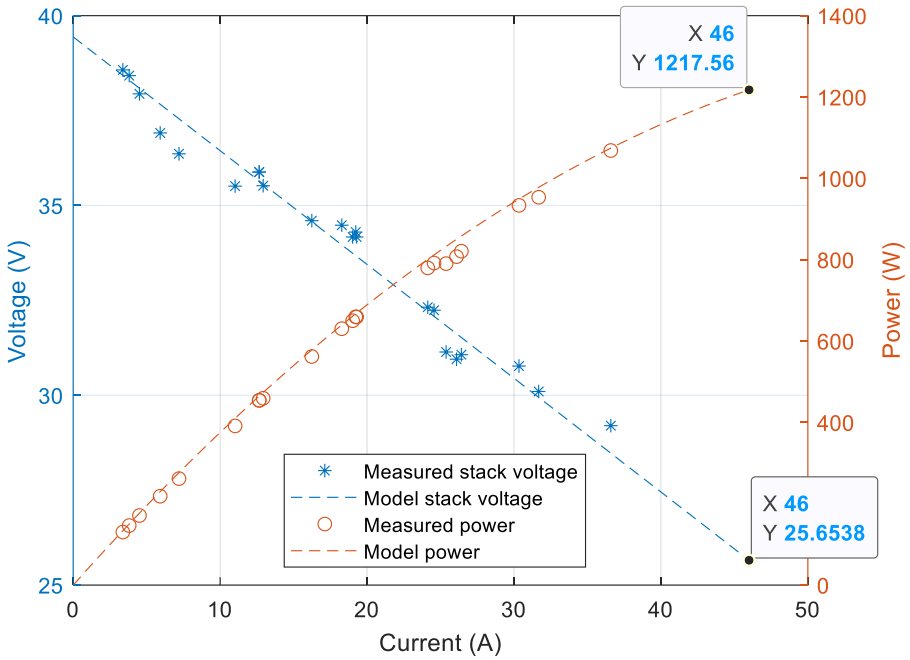

Figure 54. Measured voltage and power curves of Nexa™ 1.2 kW PEM fuel cell.

Figure 54 shows the measured voltage and power curves with varying electric current. The curves have similar behaviour as the H-500XP PEMFC shown by Figure 50 (a) and Figure 52 in the activation losses, ohmic losses and mass transport losses regions. Figure 55 show the polarisation curve of the fuel cell. The specified current at the rated power is 46 A (see Tab. 12), for which an extrapolation of the curves provides estimated values of 25.65 V for maximum voltage and 1217.56 W for maximum power. These values were used throughout all the exergy and exergoeconomic analyses.

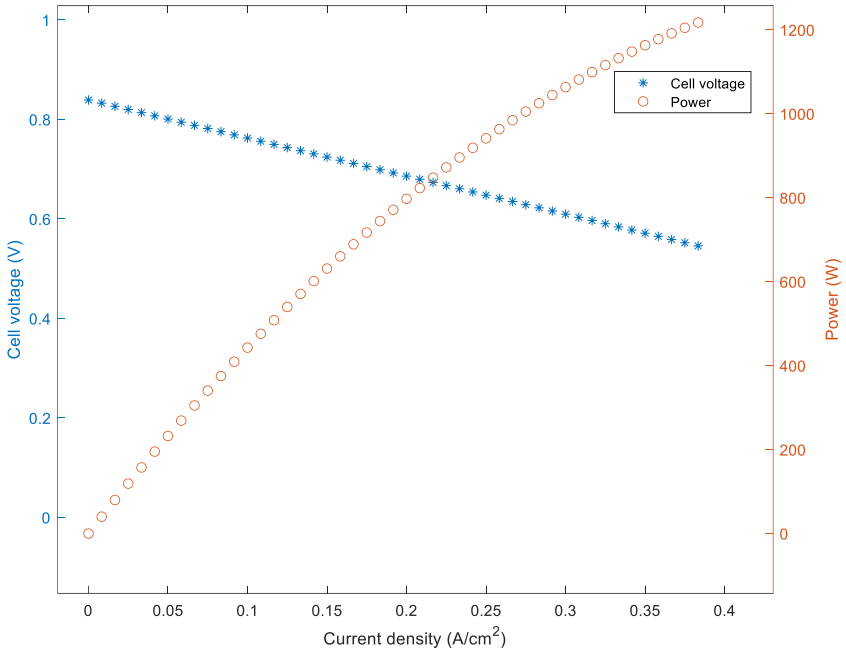

Figure 55. Polarisation curves of Nexa™ 1.2 kW PEM fuel cell.

To optimise the voltage, the irreversible losses must be reduced. For example, to decrease the activation losses that happen due to the energy barriers that obstruct the kinetics of reaction to the electrode, the following steps can be adopted [43,176]:

- Raise the cell operating temperature.
- Employ a catalyst that improves the reaction kinetics.
- Increase the electrode roughness to increase the catalyst surface on the electrode and thus increase the reaction sites.
- Increase the concentration of the reagents as the density of the current exchange increase.

To minimise the losses due to the crossing of the electric charges in the conductor materials of the ions and electrons, the electrical resistance of these materials has to be minimised in the following ways [177]:

- Use electrodes with the highest conductivity.
- Optimisation of design and choice of materials for bipolar plates
- Make the membrane as thin as possible.
- Increase the membrane humidity.

5.2.2 Exergy analysis of PEM fuel cell

The results presented in this section were obtained considering fuel cell operation along 5 years (Table 6) without the need of replacement, corresponding to 39,420 h of operation according to Eq. (3-58). This is based on a previous report that the polymer membrane of a PEM fuel cell can exceed 40,000 h of operation at harsh conditions [22]. Thus, the manufacturer declaration of 1,500 h lifetime (Table 4) and the need of capital reinvestment each time this limit was reached along the evaluation period have not been part of the calculation. In an energy analysis, the loss of quality of energy is not considered as it is based on the first law of thermodynamics, where all forms of energy are equivalent. In comparison, exergy analysis is based on both the first and second laws of thermodynamics, showing the process shortcomings in materials and energy quality losses.

In other words, exergy analysis shows the degree of irreversibility of a process due to the increase of entropy. Since the process of PEM fuel cell involves temperature and pressure changes, it involves exergy destruction. This destruction is proportional to the entropy growth of the system together with its surrounding. The exergy analysis is performed on cell operation from 0.55 V to 0.85 V. The air stoichiometry ranged between 2 to 4 to see the effects on the efficiency. The rest of the calculations – such as mass flow rates, physical and chemical exergy and exergy efficiency – are conducted at a pressure ratio p/p_0 in the range from 7.4 to 4.88 and T/T_0 from 0.99 and 1.2.

Figure 56 illustrates the variation of hydrogen pressure and the inlet air mass flow rate with the current density. Hydrogen and reaction air mass flow rates were calculated using equations (3-47) and (3-49), respectively. Hydrogen pressure was taken from the experimental data. With increasing current density, the hydrogen pressure decreases and the intake air mass flow rate increases. The correct set of the following parameters can improve the supply of reactants to enhance the cell performance [177]:

- The speed with which the reactant gases are supplied.
- The geometry of the reactant delivery channels.
- The diffusive characteristics of gas diffusion layers and electrodes

– The air circulation in the cathode to avoid the accumulation of water produced by the reaction. This point has been solved in the Nexa™ 1.2 kW PEMFC system by using this product water to humidify the reactant air, as explained later.

However, it is necessary to operate with sufficient knowledge of the facts and to have an overall vision of the system when variation of the operating parameters is used since improving some aspects can lead to the worsening of others.

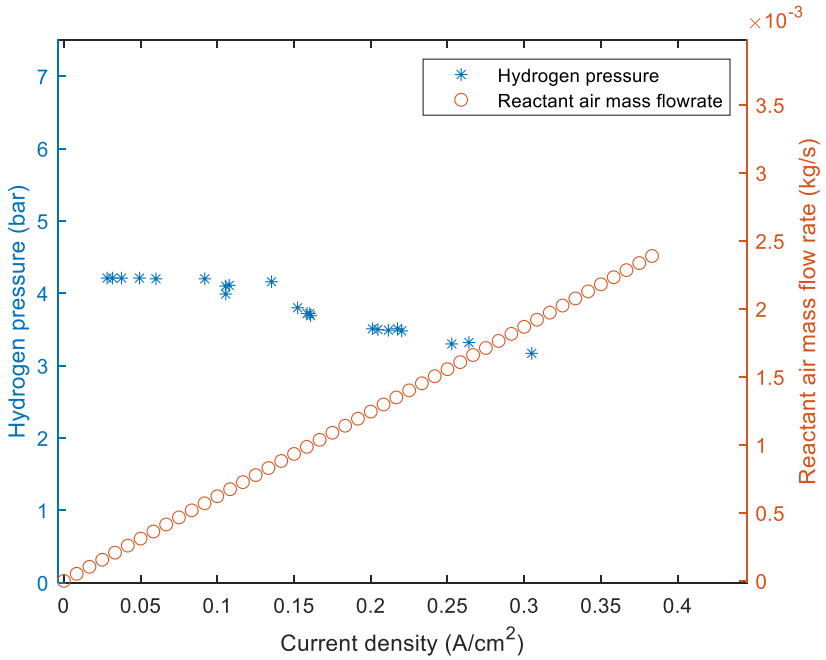

Figure 56. Variation of hydrogen pressure and reactant air mass flowrate with current density of Nexa™ 1.2 kW PEMFC.

The reactant air mass flow rate was calculated as 0.00062 kg/s at low current density using the measured air stoichiometry (λ) of around 3. Figure 57 shows the effects on the mass flow rates of the reactant air and hydrogen when the air/fuel mixture equivalence ratio λ was varied. The fact that Nexa™ 1.2KW PEMFC is self-humidified makes the control of the mass flow rate of reactant air and hydrogen crucial as they significantly impact performance. As the humidity exchanger used product water to humidify the inlet air, the decrease of reactant air flow rate if λ is lowered to 2 will dehydrate the membrane. When increasing λ to 4, the reactant mass flow rate is increase and, consequently, it leads to higher power output. However, at the same time, the air carries away more water produced at the cathode, limiting

the amount that can be used for humidifying the membrane. So, it is imperative to find a compromise in the air flow that can increase performance while maintaining the right level of membrane hydration [178]. Furthermore, air stoichiometry has close relation with temperature and pressure: too high λ causes membrane drying, an too low λ leads to low partial pressure that causes mass transport losses.

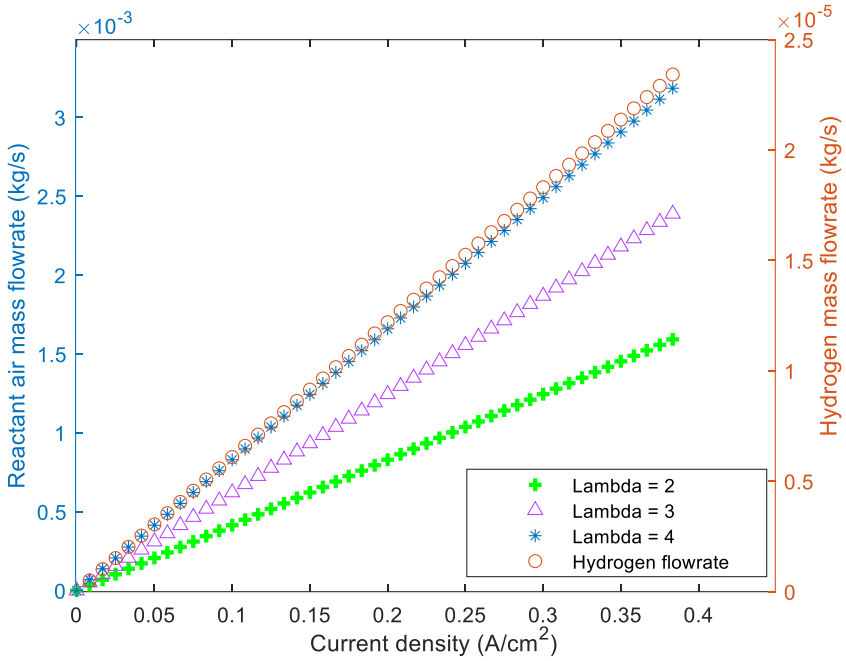

Figure 57. Variation of reactant air and hydrogen mass flow rates with current density and air stoichiometry of Nexa™ 1.2 kW PEMFC.

Figure 58 shows that product air mass flow rate, defined as the variation between the amount of oxygen in the electrochemical reaction and the amount of oxygen consumed by reacting with hydrogen to produce water. The product air and water were calculated using equations (3-51) and (3-48), respectively. It can be observed that the product air and water increase with the increase of current density, while the amount of water is less than the amount of product air. The humidity exchanger transfers the product water and heat from the wet cathode outlet to the dry incoming air. The excess product water is discharged from the system as liquid and vapour in the exhaust. The oxidant and cooling air were drawn from the ambient through a compressor and fan. They are both regulated by the control system.

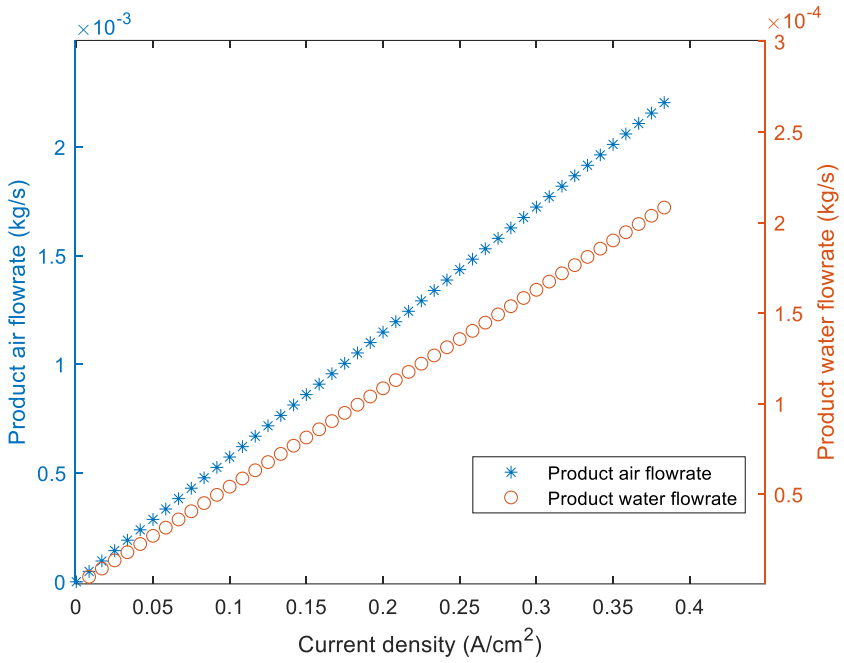

Figure 58. Variation of Product air and water mass flow rates with current density of Nexa™ 1.2 kW PEMFC.

Figure 59 illustrates the energy and exergy efficiencies of the PEMFC system. The energy efficiency is calculated by Eq. (4.28) and the exergy efficiency is computed by Eq. (3.35). It can be observed that both the energy and exergy efficiencies decrease with increasing current density. In the current density range from 0.02 – 0.37 A/cm^2, the energy efficiency varies from 56% to 37% while the exergy efficiency drops from 39% to 26%. The decrease in fuel cell efficiency is a consequence of the increasing hydrogen mass flow rate with increasing current density (see Figure 57). The improvements on the fuel cell operation provided by the model increase the rated energy efficiency of the Nexa™ 1.2 kW fuel cell by 8% compared with the declared data sheet value of 48%. The maximum exergy efficiency here found is only 3% lower than suggested by other studies [116], thus showing a good agreement.

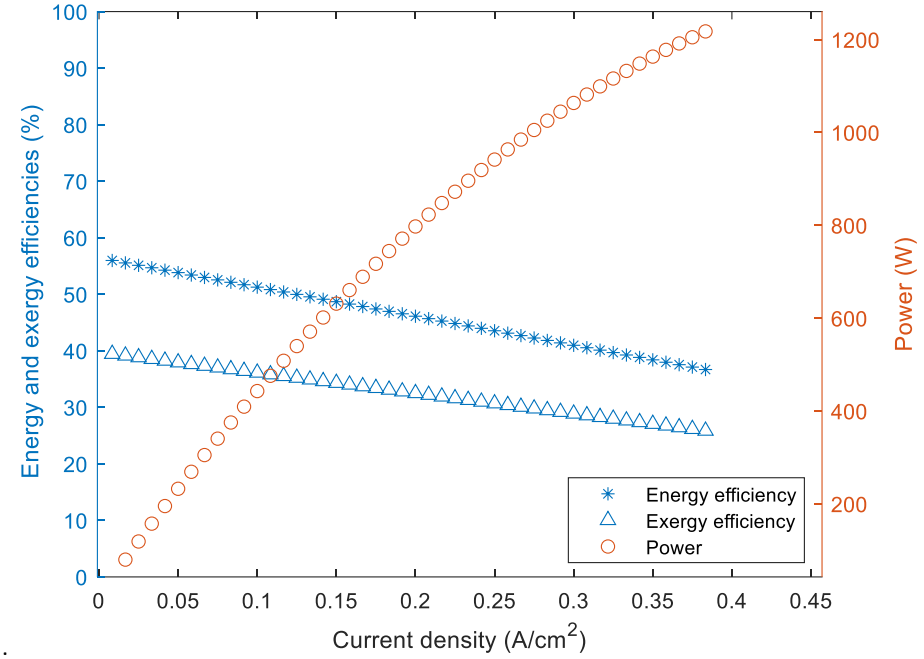

Figure 59. Variation of energy and exergy efficiencies with current density of Nexa™ 1.2 kW PEMFC.

Physical exergy, also known as thermomechanical exergy, is the work obtainable by taking the substance through a reversible process from its initial state (T, P) to the state of the environment (T_0, P_0) which are 298.15k and 1 bar respectively. Figure 60 shows that the physical exergy is consistently increased with increasing temperature ratio and spiral growth rates at higher temperatures. Although higher temperatures increase the diffusivity of the reactants and improve ionic conduction of the membrane, they also lead to higher evaporation of water and, therefore, drying of the membrane, which loses its conductivity [179]. As Nexa™ 1.2kW system has a humidity exchanger, water vapour in the reactant gases balances the drying effect of the temperature, favouring the fuel cell operation at higher temperatures to increase the physical exergy.

Figure 61 shows that increasing the pressure ratio increases the physical exergy but, unlike the temperature variation (see Figure 60), the growth rate decreases at higher pressures. Increasing pressure benefits performance as it increases the diffusivity of the reactant gases, facilitating mass transport to the electrodes. At a first view of Figure 60 and Figure 61, it can be inferred that the physical exergy will be more favoured by small increases of pressure and only large increase of temperature will provide similar effect. However, one must consider

that, at high temperatures, the reaction kinetics is occurs at faster speed while pressurisation primarily increases the reactant concentration to achieve better performance. On the other hand, at low temperatures, the reaction kinetics is slow and higher reactant concentration from high pressure operation does not yield a proportional increase in the cell potential due to the significant cell potential loss associated with the slow kinetics [180]. Therefore, the physical exergy can be improved by a balanced increase of both pressure and temperature.

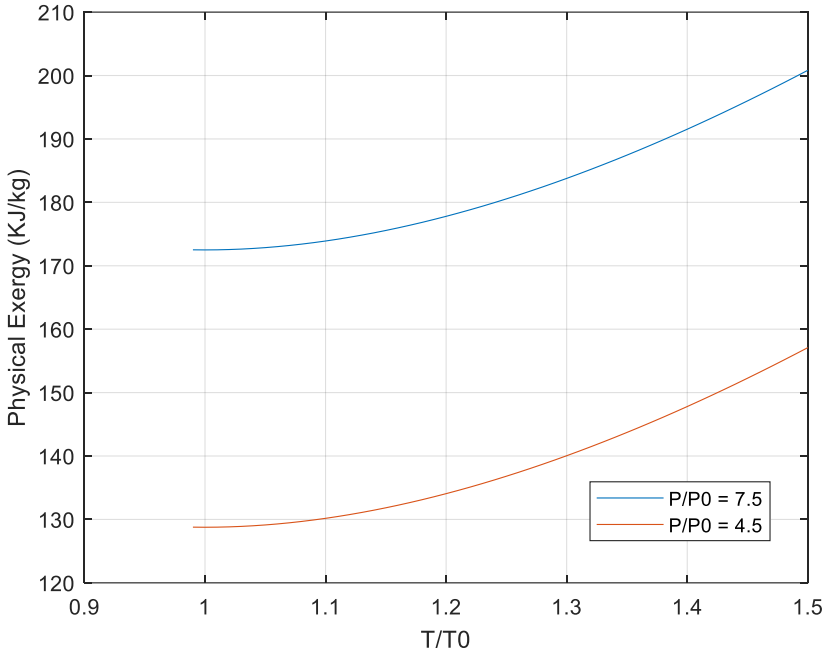

Figure 60. Variation of physical exergy with temperature ratio of Nexa™ 1.2 kW PEMFC (T_0 =298.15 k, P_0 = 1 bar)

The physical exergy of product water, calculated by Equation (3-45) and shown by Figure 62 and Figure 63, increase with both temperature and pressure increase in similar patterns as the total fuel cell physical exergy (see Figure 60 and Figure 61). As the Nexa™ 1.2 kW fuel cell has an internal humidifier, the increase of product water is beneficial to the system. The heated air from the compressor evaporates the water used by the humidifier and, as a result, the air reaches an ideal temperature without the need to operate at low pressure. The absence of an internal humidifier would require cell operation at lower temperatures thus decreasing the available exergy (see Figure 60). Therefore, the balanced increase of operating pressure and temperature brings the fuel cell double benefit on its overall exergy and the

product water exergy. A previous study approved that an operating pressure ratio for a low-temperature PEMFC system should be between 4.5 and 5.0 [181].

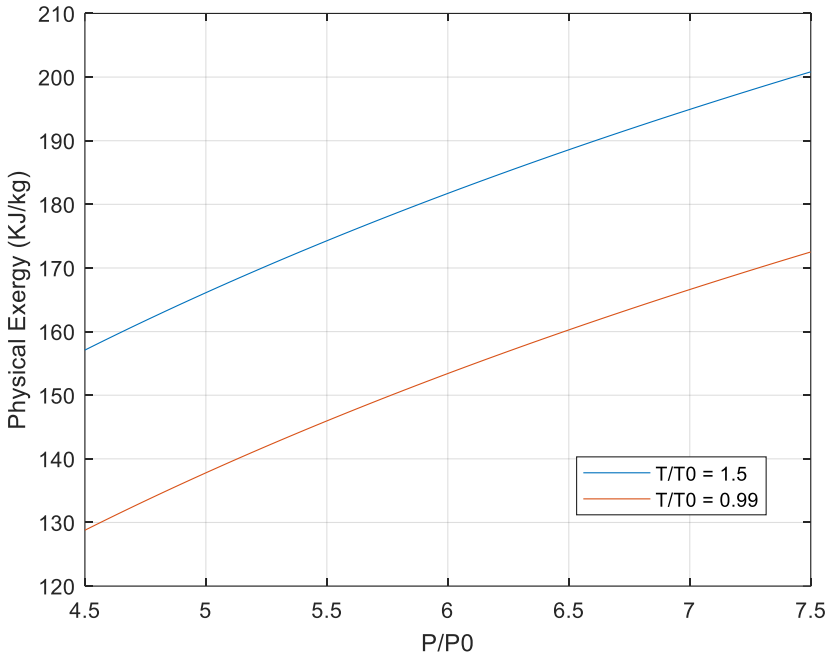

Figure 61. Variation of physical exergy with pressure ratio of Nexa™ 1.2 kW PEMFC (T_0 =298.15 k, P_0 = 1 bar)

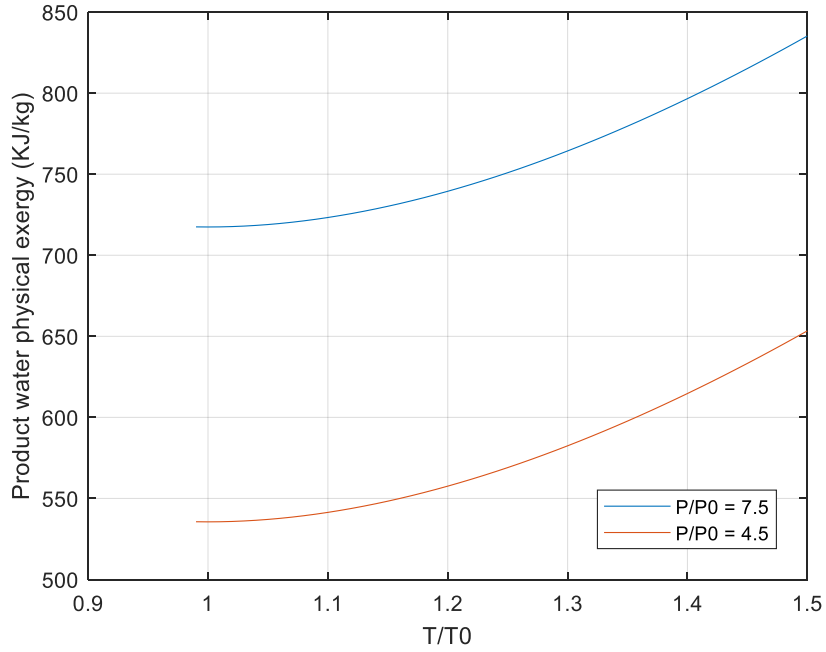

Figure 62. Variation of product water physical exergy with temperature ratio of Nexa™ 1.2 kW PEMFC (T_0 =298.15 k, P_0 = 1 bar)

The product water is also used to humidify the fuel to favour the conduction of hydrogen ions in the membrane and minimise ohmic losses [182]. The water content dramatically influences the membrane conductivity, and it is vital for transporting the reactants and the reaction kinetics in the electrode. The ohmic losses in the membrane at high current density are responsible for a significant fraction of the cell voltage loss if the diffusion of water between the cathode and membrane is insufficient to keep the membrane hydrated.

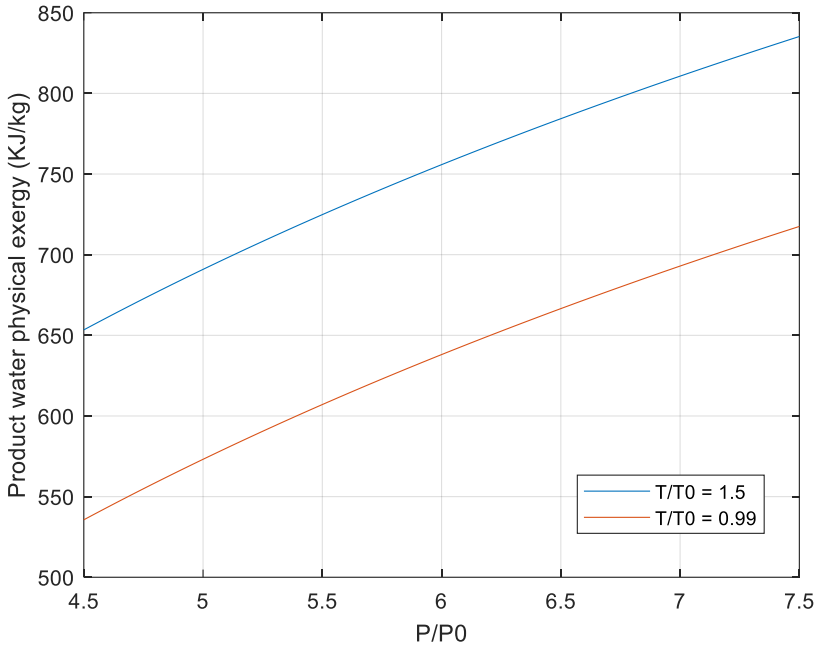

Figure 63. Variation of product water physical exergy with pressure ratio of Nexa™ 1.2 kW PEMFC.

5.2.3 PEM Fuel Cell exergy cost analysis

The exergy cost of a PEMFC is defined as the ratio of the difference between the exergetic cost rate (cost per unit time) of streams entering and exiting the system plus the capital investment and operation and maintenance cost of the PEMFC to the electrical power output. The combination of exergy analysis and exergy cost makes the exergoeconomic analysis. The

method provides a technique to evaluate the costs of inefficiencies and the costs of individual process streams, including intermediate and final products. The exergoeconomic analysis is applicable in feasibility studies, investment decisions, cost-effective equipment section during installation, and exchange or expansion of an energy system [183,184]. It can define a criteria to determine the optimum fuel cell efficiency to operate at an economical rate [185].

In the previous sub-section, an exergy analysis was conducted on the Nexa™ 1.2 kW PEMFC system to examine the effects of temperature, pressure, and humidity on its performance. The exergy cost analysis was performed on fuel cell operation from 0.55 to 0.85 V, air stoichiometry ranging between 2 and 4, pressure ratio p/p_0 from 4.88 to 7.40, and temperature ration T/T_0 from 0.99 and 1.20. The exergy cost of the Nexa™ 1.2 kW PEMFC shows a rate of 115.46 $\pm$ 0.01 \$/GJ in the whole range of temperature and pressure investigated, as shown in Figure 64. Therefore, there was no significant effect on the exergy cost from the variation of operating temperature and pressure. The operating temperature in other fuel cell types such solid oxide fuel cells or even molten carbonate fuel cells should play a more significant role than in a low-temperature PEMFC system (up to 65 °C) [127,146].

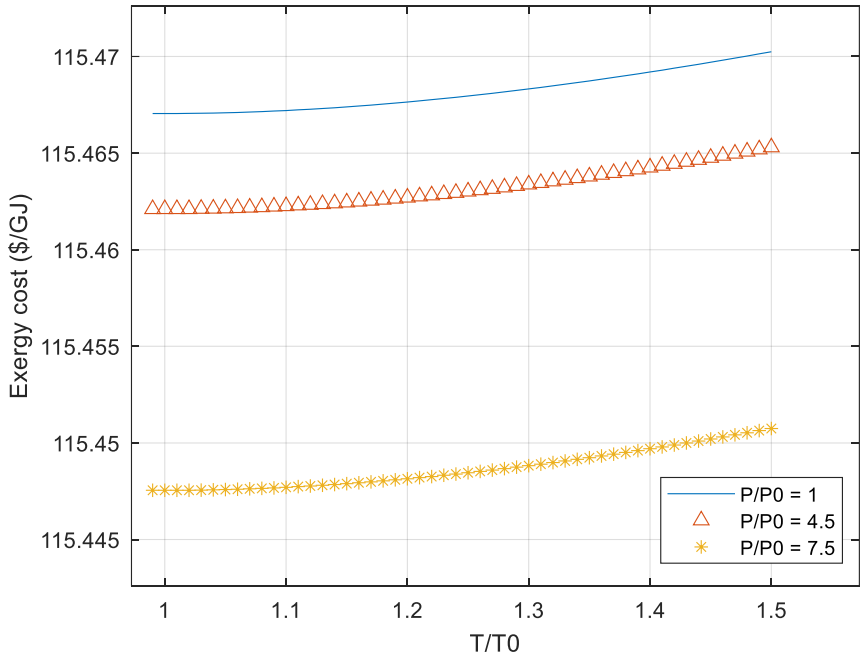

Figure 64. Variation of Nexa™ 1.2 kW PEMFC system exergy cost with temperature and pressure at V = 0.56 V and λ = 3.

Many studies report that hydrogen costs can decrease dramatically over the next decade as hydrogen production, distribution, equipment, and component manufacturing scale up. For some applications, hydrogen can become competitive with other low-carbon alternatives and conventional options. The current hydrogen price of 6.7 US$/kg has been used to produce the results of Figure 64, but the predicted hydrogen price of 1.9 $/kg for 2030 [186] was used in the exergy cost analysis shown by Figure *65*. These results show that the predicted hydrogen price will reduce the fuel cell exergy cost rate to about 101.17 $/GJ, which is a decrease of 12% compared with today's price.

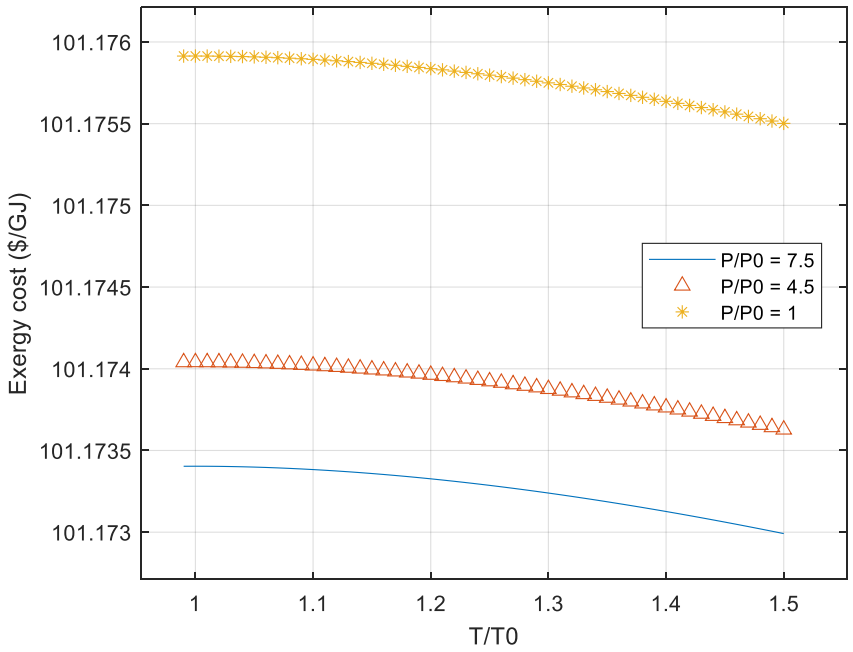

Figure 65. Variation of Nexa™ 1.2 kW PEMFC system exergy cost with temperature and pressure at V = 0.56 V and λ = 3 with reduce hydrogen price of US$ 1.9/kg.

A reduction of about 35 $/GJ can be achieved by operating at a higher stoichiometric ratio of λ = 4 than the recommended ratio of λ = 3, as shown in Figure 66. Nevertheless, one should be extremely careful in setting up the air stoichiometry higher than the recommended value because this decreases the relative humidity of the product air. Hence, a higher risk of cell dehydrating can occur, causing a sharp decrease in the system efficiency [127,187]. Variation in temperature did not influence these results.

The system voltage can also play a key role in its exergy cost, as Figure 67 shows. Reducing the fuel cell voltage from 0.60 V to 0.56 V decreases the exergy cost rate from 115.5 US$/GJ 108.4 US$/GJ. However, the lower the cell voltage, the greater will be the mass flow rates required for reactants and the products to operate the system in order to produce the rated power output of 1.2 kW leading to lower exergetic efficiency. Hence, a gain on the exergy cost of the system can be cancelled. Again, these results were not affected by temperature variation.

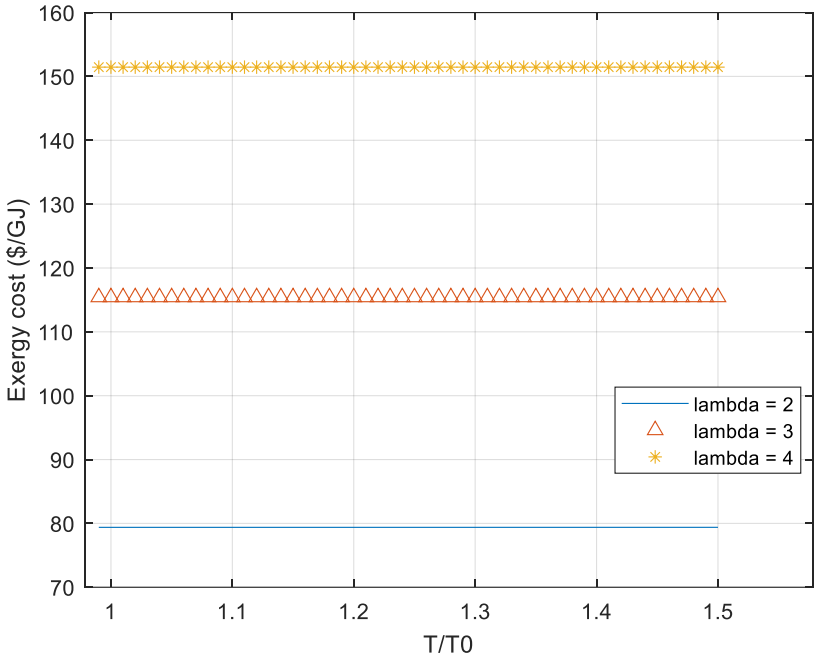

Figure 66. Variation of exergy cost with air/fuel mixture equivalence ratios at 56 V, $p/p_0 = 1$.

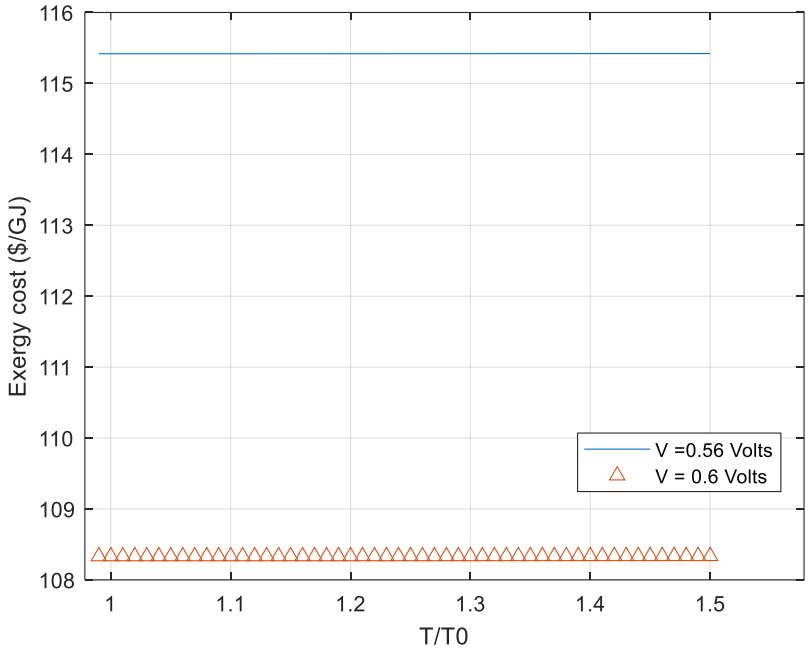

Figure 67. Variation of exergy cost with fuel cell voltage at $\lambda = 3$, $p/p_0 = 1$.

5.3 Improved Power Electronic Interface (PEI) model to optimise voltage, current and power signals.

Preshoot, overshoot and undershoot demonstrate the transient behaviour of the voltage, current and power signals in the Nexa 1.2 kW PEMFC and its power electronics interface. the system output voltage preshoot of 0.5% while the converter shows 0.7%. Both are in the safe operating range. These preshoots were followed by zero overshoot in terms of Nexa voltage but with 6% undershoot, while the converter has 48% overshoot and 13% undershoot, as Figure 68 and Figure 69 show. Although the comparison of overshoot and undershoot indicates that the Nexa 1.2 kW PEMFC performs better than the converter, the converter has settled the voltage at 42 V with less steady state error while the fuel cell settled the voltage at 38 V. The fact that both systems managed to settle the output voltage in less than 18 ms shows that the present model can be used for devices that entail swift change of load requirements. The response is a low pass filter type, meaning that, in addition to the overshoot and undershoot, the rise time, settling time and slew rate – which is the maximum rate of the output voltage change per unit time – are related parameters to analyse these

types of signals. The settling time and slew rate for both fuel cell and the converter were acceptable in terms of output voltage [152].

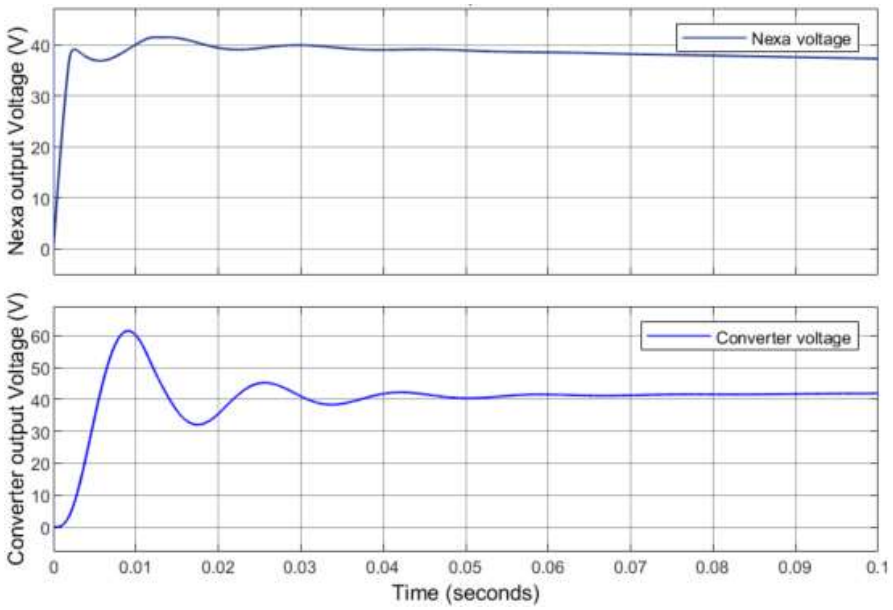

Figure 68. Nexa 1.2 kW PEMFC and converter output voltage signals during 0.1 s from start.

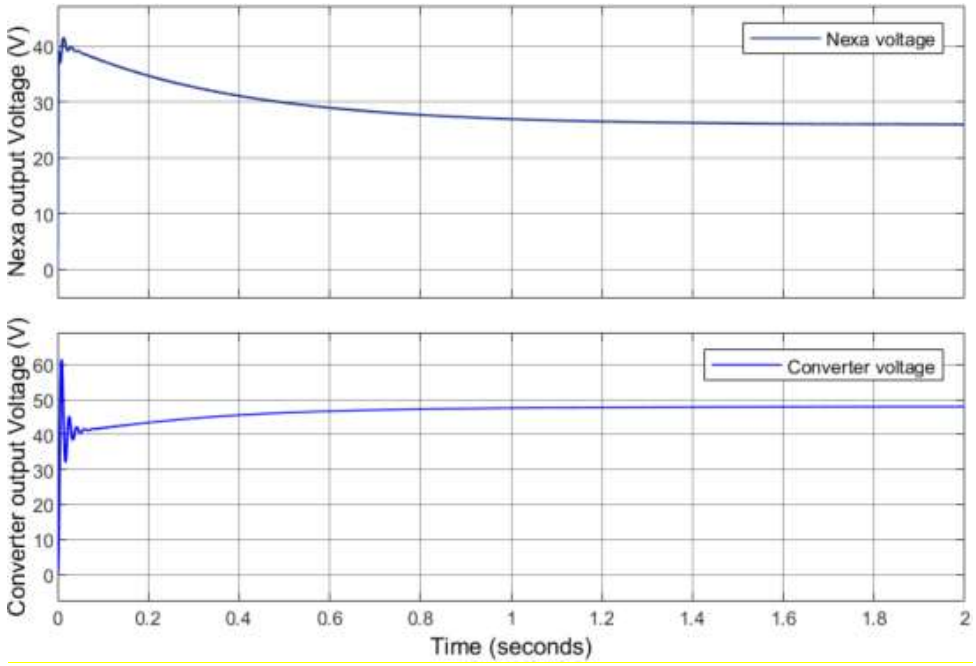

Figure 69. Nexa 1.2 kW PEMFC and converter output voltage signals during 2.0 s from start.

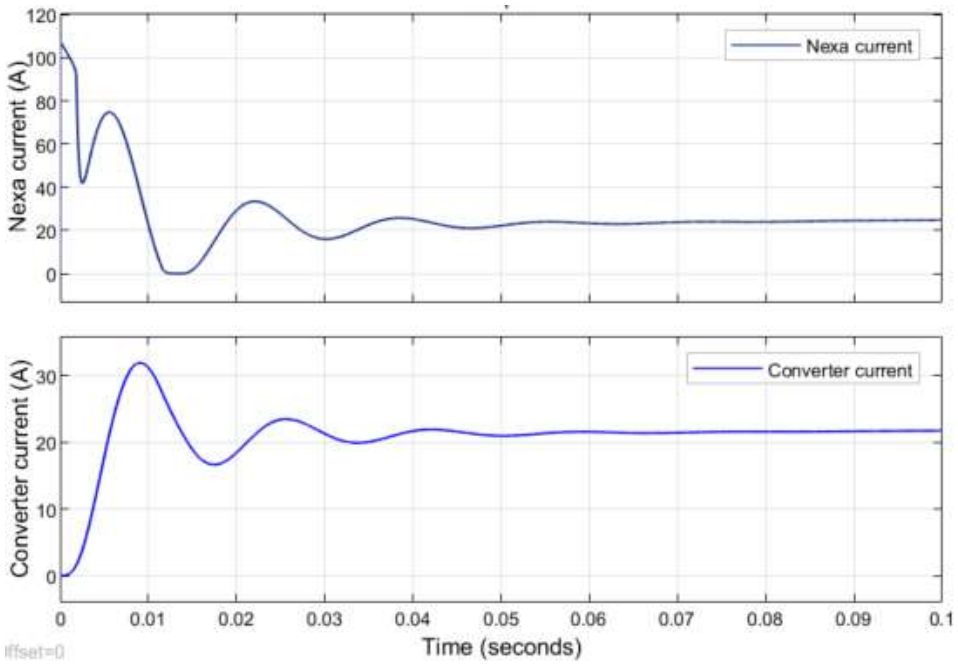

Figure 70. Nexa 1.2 kW PEMFC and converter current signals during 0.1 s from start.

In terms of current, the preshoot of Nexa fuel cell was 48% while the converter had 0.7% preshoot. As the current in Nexa is the dependant variable due to the extent of the input voltage to 22V it tried to reach the new current value of 91 A, but it overshoots it by 16 A, as shown by Figure 70 and Figure 71. The overshoot for fuel cell and the converter were 65% and 49% respectively. In an attempt to correct the overshoot, an undershoot of 32% by the Nexa 1.2 kW PEMFC caused a clipping by exceeding the minimum threshold of 0 A, which can cause a damage to the membrane. As a positive aspect, the overshoot happened with rise time of 68 ns although the falling time took 2.9 ms. The slew rate was as low as 596 µs. The converter overshoot and undershoot were lower than those of the fuel cell and there was no clipping in the signals, and the current ripple of 21% was also lower than that of the fuel cell. Overall, the converter current signal was more stable and with less steady state error than the Nexa 1.2 kW PEMFC.

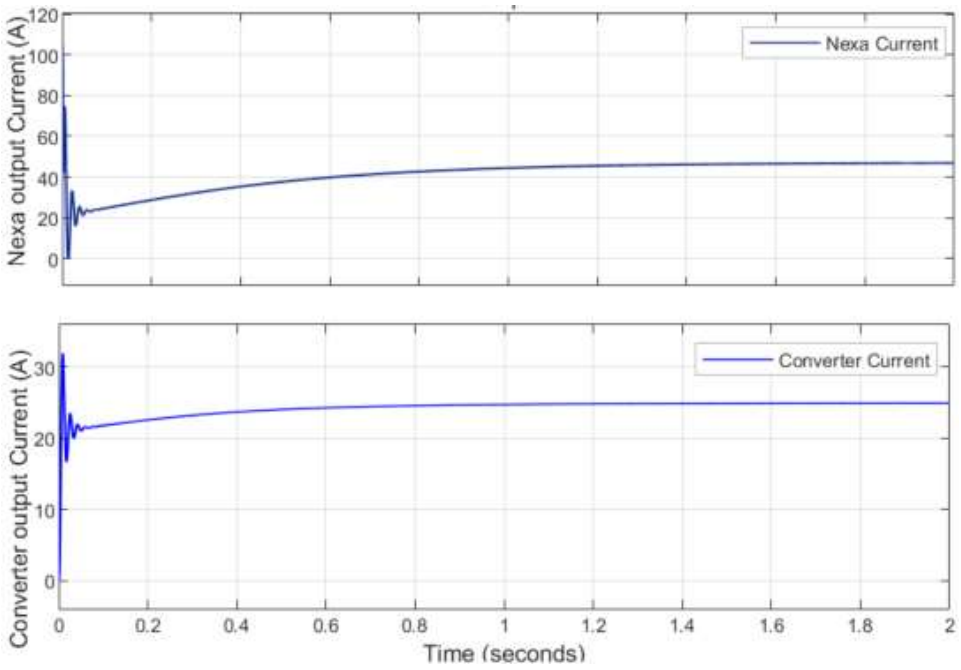

Figure 71. Nexa 1.2 kW PEMFC and converter current signals during 2.0 s from start.

Figure 72, shows Nexa 1.2 kW PEMFC power and the converter and load output during 0.1 s sampling time. The fuel cell power reached 3.2 kW, as consequence of the preshoot effect reaching the voltage of 30.8 V and current of 107 A. This could cause a severe damage to the stack if not corrected. The effect of the swift changes in the current is reflected on the power signal drop below the extended range of 2.0 kW. A second overshoot of 29% took the power to an output value of 2.75 kW, followed by an undershoot of 49% decreasing the power to the minimum threshold of 0 W causing a clipping in the signals before it overshoots again to take the signals close to the set point. The slew rate was as low as 11 ns with a rise time of 379 µs, reflecting the amplitude value after the transition [86,188,189]. The converter load shows an overshoot of 128% because of the extended power set of 2kW, taking the load value to 1.96 kW. This was followed by an undershoot of 134% reaching around 500 W. The slew rate of 275 ms with a rise time of 832 µs, showing a high amplitude of 137 W after high transition of 1.03 kW.

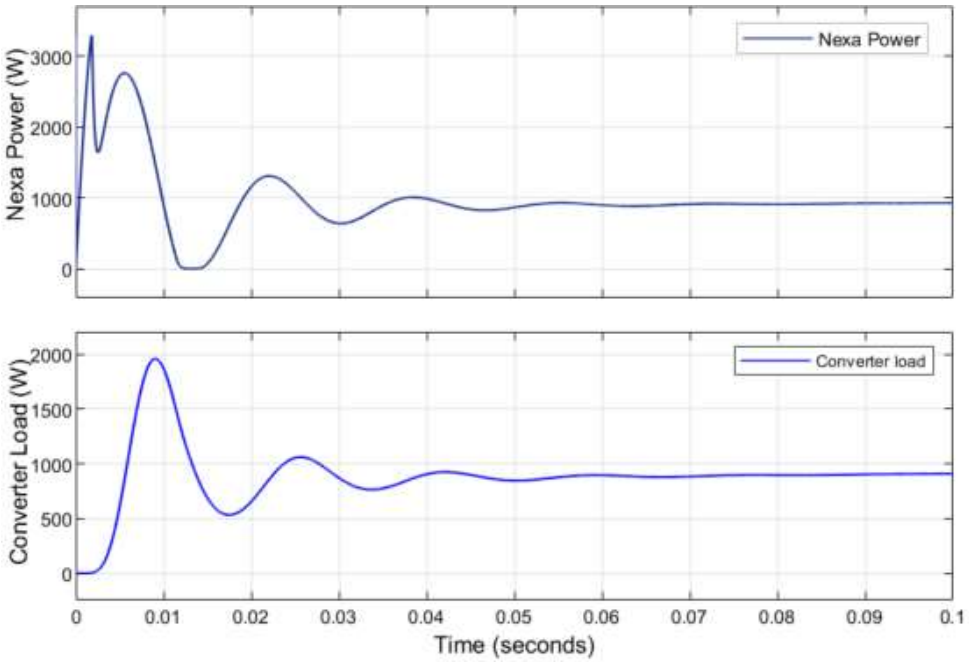

Figure 72. Nexa 1.2 kW PEMFC power and converter load signals during 0.1 s from start.

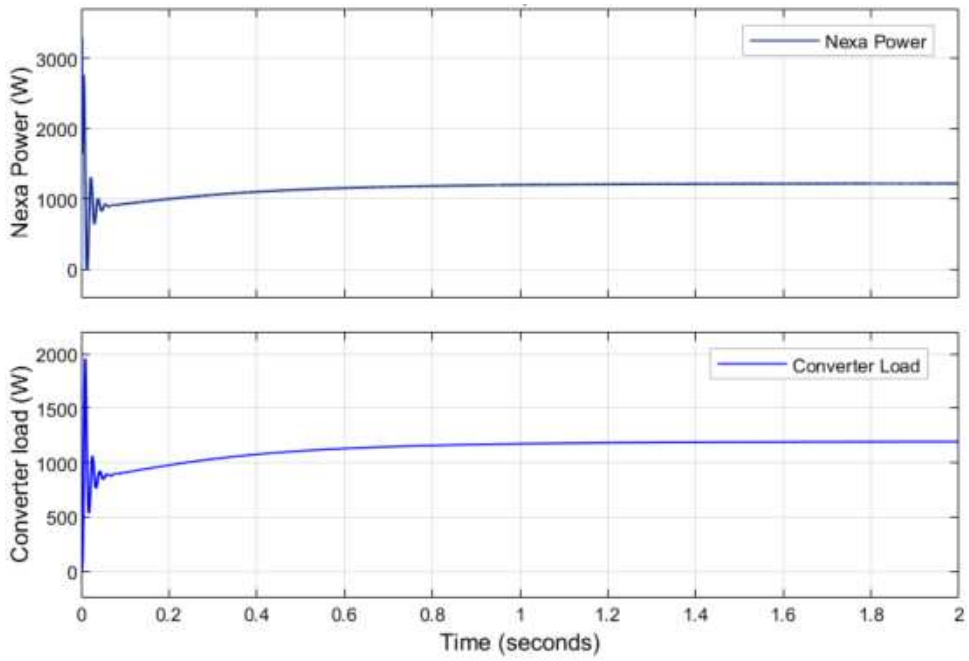

Figure 73. Nexa 1.2 kW PEMFC power and converter load signals during 2.0 s from start.

Figure 73, shows that the power signals managed to reach the setpoint of both and the converter within 2 s. Although the voltage signals have reached the setpoint in less than a sampling period of 0.1 s, the delay in the current signals affected the power signals. The load

in the converter was calculated based on the reference voltage of 48 V and the nominal power of 1.196 kW, while the extended fuel cell power was set to 2 kW.

To conclude with, this chapter covered the results of the three MATLAB/Simulink and M. Script models. The one-dimensional non-isothermal steady state model of 0.5kW PEMFC results were generally found to have a good agreement with the experiments. Model and experiments revealed the maximum overall system efficiency of around 47.5% at 50% of the rated power. The exergoeconomic model of 1.2kW PEMFC revealed that higher operating pressure and cell voltage give a better result than higher operating temperature. The Improved Power Electronic Interface model shows that the preshoot, overshoot and undershoot of the PEI for the electric current were lower than those of Nexa and there was no clipping in the signals. Overall, the PEI current was more stable and with less steady state error than Nexa PEMFC current signals.

6 Conclusion

This PhD project provides a unique scientific contribution to PEMFC technology through a better understanding of temperature, pressure, air stoichiometry, cell voltage and humidity effects and suggests ways to optimise signals and operation, improve performance and efficiency, and reduce cost. The main conclusions of this research are provided next.

6.1 Simulation of the PEM Fuel Cell using MATLAB/Simulink

A one-dimensional non-isothermal model of a PEM fuel cell has been developed, and the effect of design and operating conditions on the cell performance have been investigated. The model simulates the fuel cell output current, voltage and power, analysing the system response to various external loads. The model was validated with experimental data from a commercial Horizon H-500XP fuel cell stack, which main components are a 500 W PEMFC stack, a 12 VDC battery for the start-up and a bank of super-capacitors to supply additional power. In addition, the generated power was dissipated in a variable resistive load, where the voltage was maintained constant by a 48-volt DC-DC boost converter. A controlled current source was used to simulate the variation of fan power consumption with stack temperature, ranging from 36.5W at 23 °C to 52 W at 65 °C.

All results were generally found to have a good agreement between the model and experiments. The stack polarisation curve, stack current and voltage variation with external load showed maximum discrepancies between the model and experiments of 3.1%, 4.2% and 3.1%, respectively. The stack output power variation with the load resistance presented a maximum discrepancy between the model and experiments of 5.7%. Both models and experiments showed a linear dependence of hydrogen consumption with stack current, with a maximum discrepancy of 8.7%. Model and experiments revealed the maximum overall system efficiency of around 47.5% at 50% of the rated power. The maximum discrepancy of the system efficiency variation with output power determined by the model and experiments was 4.6%. Future applications of the model include investigating operating parameters such

as stack temperature, to optimise the system for increased overall efficiency by decreasing fuel consumption and losses.

Although the energy analysis was practical to get an initial image of the performance of PEMFC, exergy and exergoeconomic analyses were applied to produce more in-depth information on fuel cell designs optimisation and costs. The following sub-sections show the conclusions of these analyses.

6.2 Exergy analysis of PEM Fuel Cell using M. Script

The exergy analysis was completed by implementing the derived fundamental governing second law equations for the system into the Nexa™ 1.2 kW PEMFC performance model developed in MATLAB. The model analysed all system components, including the fuel cell stack, air compression, hydrogen supply, built-in humidity exchanger and the cooling system. The total exergy of the reactants and products consists of physical and chemical exergies, which were calculated for each element in the electrochemical process. The results showed that the exergy efficiencies of the system were lower than energy efficiencies. The model provided an improvement of 8% in the fuel cell energy efficiency in comparison with the value declared by the manufacturer, while the exergy efficiency was close to values in published studies.

The model indicated the fuel cell can achieve an increase in power and a reduction of voltage compared with the Nexa™ 1.2 PEMFC system datasheet. It is recommended that the system operates at a stoichiometric ratio lower than 4 to optimise the relative humidity level in the product air and avoid the membrane drying out at high operating temperatures. The system exergy efficiency can be improved by increasing the operating temperature up to 80°C. Although better results were obtained for some analysis was conducted at higher temperatures up to 99°C, this temperature range is not recommended for this system. Higher operating pressure and cell voltage give a better result than higher operating temperature. Product water physical exergy can be improved with increased operating temperature and pressure. However, operation at high temperatures is limited by excessive water evaporation

with consequent drying of the membrane and, thus, reduced conductivity, while operation at increased pressure requires higher power by the compressor.

6.3 Exergy cost analysis of PEM Fuel Cell using M. Script

The exergy cost analyses were performed with cell operation from 0.55 V to 0.85 V, air stoichiometry between 2 and 4, pressure ratio p/p_0 from 7.4 to 4.88, and temperature ratio T/T_0 from 0.99 to 1.2. The temperature variation of the system showed an insignificant impact on the exergy cost. However, the system is regarded as a low-temperature PEMFC system as opposed to other fuel cell systems with higher operating temperatures, which can significantly affect the overall exergy cost. Increasing the air stoichiometry by a third of its recommended value can reduce the exergy cost by 30%, but there are imposed limitations on this strategy by the risk of cell dehydration causing loss of efficiency. Operating voltage increase by 7% can produce a reduction of exergy cost by a similar rate. An estimated reduction of just over 70% on the hydrogen price by 2030 will produce a decrease of the exergy cost by about 12%.

6.4 Improved Power Electronic Interface (PEI) model to optimise voltage, current and power signals.

The Nexa 1.2kW PEM fuel cell voltage, current and power signals were analysed and compared with the same signals from an improved Power Electronic Interface (PEI) model. The PEI consist of a DC-DC converter, control system which includes PID controller and PWM to regulate the duty cycle of the converter to determine the amount of power delivered to the load from the fuel cell. By adjusting the duty cycle based on feedback from the fuel cell, the gain constant K can ensure that the Nexa 1.2 kW PEMFC operates within its optimal range and performance. The conclusion of this section is summarised next.

Nexa 1.2 kW PEMFC shows better voltage signal in terms of overshoot and undershoot comparing to the PEI, however the PEI has settled the voltage at 42 V with less steady state error while the fuel cell settled at 38 V. The settling times of less than 18 ms for both Nexa

and the PEI were acceptable in terms of output voltage. The slew rate values were 19.5ms and 10ms for Nexa and the PEI respectively. The slew is an indicator for the amplitude, and it helps evaluate the best frequency to select. Higher slew rate means better signals as Nexa output voltage shows. The preshoot, overshoot and undershoot of the PEI for the electric current were lower than those of Nexa and there was no clipping in the signals. Overall, the PEI current was more stable and with less steady state error than Nexa PEMFC current signals. Although the voltage signals have reached the setpoint in less than a sampling period of 0.1 s the delay in the current signals affected the power signals, which managed to reach the setpoint of both Nexa PEMFC and the PEI within 2s.

6.5 Recommendations for future work

As overall recommendation, the fuel cell exergy cost can noticeably be improved by adopting a combination of higher temperature, pressure, inlet air stoichiometry and cell voltage. This can be further explored through modelling, taking into consideration the side effects. Moreover, since more emphatic enhancement ca be achieved by lowering the hydrogen price, different cost estimates of the fuel according to various trends and production technologies can also be subject of future studies. In terms of experimental results, it is recommended to use accurate electronic load for better result as well as repeating the experiments to check the accuracy of data collected. Finally, as it is mentioned in Chapter 4 and the Appendix, it is a suggested to further improve the PID controller using PSO logarithm optimisation technique.

To summarise, this chapter shows the conclusion reached of the three models and a recommendation for future work. The steady state model of 05. kW PEMFC and experiments revealed the maximum overall system efficiency of around 47.5% at 50% of the rated power. While the exergoeconomic model of 1.2kW PEMFC illustrate that product water physical exergy can be improved with increased operating temperature and pressure. However, operation at high temperatures is limited by excessive water evaporation with consequent drying of the membrane and, thus, reduced conductivity, while operation at increased pressure requires higher power by the compressor which will increase the operating cost.

The model estimated that a reduction of just over 70% on the hydrogen price by 2030 will produce a decrease of the exergy cost by about 12%. Nexa 1.2 kW PEMFC shows better voltage signal in terms of overshoot and undershoot comparing to the PEI, however the PEI has settled the voltage at 42 V with less steady state error while the fuel cell settled at 38 V. The last section in the chapter recommended that up grading the experimental sets with electronic load as well as repeating the experiments could improve the accuracy of data collected.

References

[1] Xue J, Grift TE, Hansen AC. Effect of biodiesel on engine performances and emissions. Renewable and Sustainable Energy Reviews 2011;15:1098–116. https://doi.org/10.1016/j.rser.2010.11.016.

[2] Shancita I, Masjuki HH, Kalam MA, Rizwanul Fattah IM, Rashed MM, Rashedul HK. A review on idling reduction strategies to improve fuel economy and reduce exhaust emissions of transport vehicles. Energy Convers Manag 2014;88:794–807. https://doi.org/10.1016/j.enconman.2014.09.036

[3] Thomas CE. Fuel cell and battery electric vehicles compared. Int J Hydrogen Energy 2009;34:6005– 20. https://doi.org/10.1016/J.IJHYDENE.2009.06.003.

[4] Alaswad A, Palumbo A, Dassisti M, Olabi A-G. Fuel Cell Technologies, Applications, and State of the Art: A Reference Guide. Reference Module in Materials Science and Materials Engineering 2015. https://doi.org/10.1016/B978-0-12-803581-8.04009-1.

[5] Wilberforce T, Olabi AG. Performance Prediction of Proton Exchange Membrane Fuel Cells (PEMFC) Using Adaptive Neuro Inference System (ANFIS). Sustainability 2020, Vol 12, Page 4952 2020;12:4952. https://doi.org/10.3390/SU12124952.

[6] Wilberforce T, Olabi AG. Design of experiment (DOE) analysis of 5-cell stack fuel cell using three bipolar plate geometry designs. Sustainability (Switzerland) 2020;12. https://doi.org/10.3390/su12114488.

[7] Wilberforce T, Alaswad A, Palumbo A, Dassisti M, Olabi AG. Advances in stationary and portable fuel cell applications. Int J Hydrogen Energy 2016;41:16509–22. https://doi.org/10.1016/j.ijhydene.2016.02.057.

[8] Wilberforce T, Khatib FN, Ogungbemi E, Olabi AG. Water Electrolysis Technology. Reference Module in Materials Science and Materials Engineering 2018. https://doi.org/10.1016/B978-0-12-803581-8.11273-1.

[9] Alaswad A, Omran A, Sodre JR, Wilberforce T, Pignatelli G, Dassisti M, et al. Technical and commercial challenges of proton-exchange membrane (Pem) fuel cells. Energies (Basel) 2021;14. https://doi.org/10.3390/en14010144.

[10] Wisniak J. Historical Notes: Electrochemistry and Fuel Cells: The Contribution of William Robert Grove. Indian J Hist Sci 2015;50. https://doi.org/10.16943/ijhs/2015/v50i4/48318.

[11] Sandstede G, Cairns EJ, Bagotsky VS, Wiesener K. History of low temperature fuel cells. vol. 1. 2010. https://doi.org/10.1002/9780470974001.f104011.

[12] Wang Y, Chen KS, Mishler J, Cho SC, Adroher XC. A review of polymer electrolyte membrane fuel cells: Technology, applications, and needs on fundamental research. Appl Energy 2011;88:981–1007. https://doi.org/10.1016/J.APENERGY.2010.09.030.

[13] Javaid Zaidi SM, Matsuura T. Polymer membranes for fuel cells. Polymer Membranes for Fuel Cells, Hardcover: 2009, p. 1–431. https://doi.org/10.1007/978-0-387-73532-0.

[14] Wang Y, Pang Y, Xu H, Martinez A, Chen KS. PEM Fuel cell and electrolysis cell technologies and hydrogen infrastructure development-a review. This Journal Is Cite This: Energy Environ Sci 2022;15:2288–328. https://doi.org/10.1039/d2ee00790h.

[15] UK government 2015. [Withdrawn] 2010 to 2015 government policy: transport emissions - GOV.UK. GOVUK 2015. https://www.gov.uk/government/publications/2010-to-2015-government-policy-transport-emissions/2010-to-2015-government-policy-transport-emissions (accessed March 17, 2019).

[16] UKH2Mobility. UK H2Mobility | Hydrogen: Fuelling Cleaner Motoring 2012. http://www.ukh2mobility.co.uk/ (accessed March 17, 2019).

[17] Wilberforce T, El-Hassan Z, Khatib FN, Al Makky A, Baroutaji A, Carton JG, et al. Modelling and simulation of Proton Exchange Membrane fuel cell with serpentine bipolar plate using MATLAB. Int J Hydrogen Energy 2017;42:25639–62.

[18] Mokrani Z, Rekioua D, Mebarki N, Rekioua T, Bacha S. Proposed energy management strategy in electric vehicle for recovering power excess produced by fuel cells. Int J Hydrogen Energy 2017;42:19556–75. https://doi.org/10.1016/j.ijhydene.2017.06.106.

[19] Office of public Affairs. Multi-Year Research, Development, and Demonstration Plan. Washington D.C.: 2017.

[20] Kumar A, Sehgal M. Hydrogen Fuel Cell Technology for a Sustainable Future: A Review. SAE Technical Paper Series 2018;1:1–11. https://doi.org/10.4271/2018-01-1307.

[21] Salvi BL, Subramanian KA. Sustainable development of road transportation sector using hydrogen energy system. Renewable and Sustainable Energy Reviews 2015;51:1132–55. https://doi.org/10.1016/j.rser.2015.07.030.

[22] Lilly C. Hydrogen cars - 2020 UK guide to fuel cell vehicles 2020. https://www.nextgreencar.com/fuelcellcars/ (accessed April 4, 2020).

[23] Pivovar B. H2@Scale Overview 2020 DOE Hydrogen and Fuel Cells Program Review 2000.

[24] Martin Saarinen. Hydrogen fuel cell: do hydrogen cars have a future? | Auto Express 2020. https://www.autoexpress.co.uk/car-news/electric-cars/93180/hydrogen-fuel-cell-do-hydrogen-cars-have-a-future (accessed June 26, 2020).

[25] Naylor S. Riversimple Rasa is a super-efficient hydrogen car from Wales - pictures | Auto Express 2016. https://www.autoexpress.co.uk/94371/riversimple-rasa-is-a-super-efficient-hydrogen-car-from-wales-pictures (accessed June 26, 2020).

[26] Burn J. Jaguar Land Rover is developing a hydrogen fuel cell SUV | Auto Express 2020. https://www.autoexpress.co.uk/jaguar/352617/jaguar-land-rover-developing-hydrogen-fuel-cell-suv (accessed June 26, 2020).

[27] Home - FuelCellsWorks 2020. https://fuelcellsworks.com/ (accessed June 6, 2020).

[28] China: Kangsheng & Zhangjiakou Cooperate and Set-Up $141.3 Million Hydrogen Fund - FuelCellsWorks 2019. https://fuelcellsworks.com/news/china-kangsheng-zhangjiakou-cooperate-and-set-up-141-3-million-hydrogen-fund/ (accessed June 6, 2020).

[29] Watson L. JCB heir announces £500m vision to bring 3,000 hydrogen buses to streets of UK - Business Live 2020. https://www.business-live.co.uk/economic-development/jcb-heir-announces-500m-vision-18157075 (accessed June 26, 2020).

[30] Wilberforce T, El-Hassan Z, Khatib FN, al Makky A, Mooney J, Barouaji A, et al. Development of Bi-polar plate design of PEM fuel cell using CFD techniques. Int J Hydrogen Energy 2017;42:25663–85. https://doi.org/10.1016/J.IJHYDENE.2017.08.093.

[31] Wilberforce T, El-Hassan Z, Khatib FNN, Al Makky A, Baroutaji A, Carton JG, et al. Developments of electric cars and fuel cell hydrogen electric cars. Int J Hydrogen Energy 2017;42:25695–734. https://doi.org/10.1016/j.ijhydene.2017.07.054.

[32] Kirubakaran A, Jain S, Nema RK. A review on fuel cell technologies and power electronic interface. Renewable and Sustainable Energy Reviews 2009;13:2430–40. https://doi.org/10.1016/J.RSER.2009.04.004.

[33] Ali DM, Salman SK. A comprehensive review of the fuel cells technology and hydrogen economy. 41st International Universities Power Engineering Conference, UPEC 2006, Conference Procedings 2006;1:98–102. https://doi.org/10.1109/UPEC.2006.367723.

[34] Khatib FN, Wilberforce T, Ijaodola O, Ogungbemi E, El-Hassan Z, Durrant A, et al. Material degradation of components in polymer electrolyte membrane (PEM) electrolytic cell and mitigation mechanisms: A review. Renewable and Sustainable Energy Reviews 2019;111:1–14. https://doi.org/10.1016/J.RSER.2019.05.007.

[35] Wilberforce T, Ijaodola O, Ogungbemi E, Hassan Z El, Thompson J, Olabi AG. Effect of Bipolar Plate Materials on Performance of Fuel Cells. Reference Module in Materials Science and Materials Engineering 2018. https://doi.org/10.1016/B978-0-12-803581-8.11272-X.

[36] Sugla S et al. Fuel Cell Market - Global Size, Share & Industry Analysis [Latest] 2023:328. https://www.marketsandmarkets.com/Market-Reports/fuel-cell-market-348.html (accessed March 18, 2024).

[37] Ahmadi S, Abdi Sh, Kakavand M. Maximum power point tracking of a proton exchange membrane fuel cell system using PSO-PID controller. Int J Hydrogen Energy 2017;42:20430–43. https://doi.org/https://doi.org/10.1016/j.ijhydene.2017.06.208.

[38] Okada O, Yokoyama K. Development of Polymer Electrolyte Fuel Cell Cogeneration Systems for Residential Applications 1 Outline of Polymer Electrolyte Fue Cells n.d. https://doi.org/10.1002/1615-6854.

[39] Omran A, Smith D, Alaswad A, Amiri A, Sodre JR, Lucchesi alessandro. Proton-exchange membrane (PEM) fuel cell system mathematical modelling. SDEWES, Dubrovnik, Croatia, 1/10/19, 2019.

[40] Giorgi L, Leccese F. Fuel Cells: Technologies and Applications. The Open Fuel Cells Journal 2013;6:20.

[41] EG&G Technical Services Inc. Fuel Cell Handbook (Seventh Edition) 2004.

[42] Haile SM. Fuel cell materials and components. Acta Mater 2003;51:5981–6000. https://doi.org/10.1016/J.ACTAMAT.2003.08.004.

[43] Larminie J, Dicks A. Fuel Cell Systems Explained. Wiley; 2003. https://doi.org/10.1002/9781118878330.

[44] Zatoń M, Rozière J, Jones DJ. Current understanding of chemical degradation mechanisms of perfluorosulfonic acid membranes and their mitigation strategies: A review. Sustain Energy Fuels 2017;1:409–38. https://doi.org/10.1039/C7SE00038C.

[45] Erfan Dashtimoghadam MMH-S. Synthesis and characterization of novel proton exchange nanocomposite membranes based on chitosan biopolymer and molecular sieves n.d. http://science24.com/paper/16046 (accessed September 27, 2022).

[46] Besancon BM, Hasanov V, Imbault-Lastapis R, Benesch R, Barrio M, Mølnvik MJ. Hydrogen quality from decarbonized fossil fuels to fuel cells. Int J Hydrogen Energy 2009;34:2350–60. https://doi.org/10.1016/j.ijhydene.2008.12.071.

[47] Karthik Pandiyan G, Prabaharan T. Implementation of nanotechnology in fuel cells. Mater Today Proc 2020;33:2681–5. https://doi.org/10.1016/J.MATPR.2020.01.368.

[48] Wang J, Wang H, Fan Y. Techno-Economic Challenges of Fuel Cell Commercialization. Engineering 2018;4:352–60. https://doi.org/10.1016/j.eng.2018.05.007.

[49] Wang J. Barriers of scaling-up fuel cells: Cost, durability and reliability. Energy 2015;80:509–21. https://doi.org/10.1016/J.ENERGY.2014.12.007.

[50] Johnson B. Power Sources for Space Exploration 2012. http://large.stanford.edu/courses/2012/ph240/johnson1/ (accessed August 5, 2019).

[51] NAVAL Technology. U212 / U214 Submarines - Naval Technology 2019. https://www.naval-technology.com/projects/type_212 (accessed August 5, 2019).

[52] Warshay M, Prokopius PR. THE FUEL CELL IN SPACE: YESTERDAY, TODAY AND TOMORROW. vol. 29. 1990.

[53] Wang J. System integration, durability and reliability of fuel cells: Challenges and solutions. Appl Energy 2017;189:460–79. https://doi.org/10.1016/J.APENERGY.2016.12.083.

[54] Behling N. Solving the fuel cell dilemma. Fuel Cells Bulletin 2012;2012:12–4. https://doi.org/10.1016/S1464-2859(12)70335-8.

[55] Power A, Llc E, Yang Y. PEM Fuel Cell System Manufacturing Cost Analysis for Automotive Applications Have been working on fuel cell manufacturing cost modeling for US DOE, UK Carbon Trust, and commercial clients since 2002. Introduction Overview. 2015.

[56] Sharaf OZ, Orhan MF. An overview of fuel cell technology: Fundamentals and applications. Renewable and Sustainable Energy Reviews 2014;32:810–53. https://doi.org/10.1016/J.RSER.2014.01.012.

[57] Zamel N, Li X. Life cycle analysis of vehicles powered by a fuel cell and by internal combustion engine for Canada. J Power Sources 2006;155:297–310. https://doi.org/10.1016/J.JPOWSOUR.2005.04.024.

[58] Ttopstart. Technology Readiness Levels: a new dimension in Horizon 2020 | ttopstart 2017. https://www.ttopstart.com/news/technology-readiness-levels-a-new-dimension-in-horizon-2020 (accessed August 21, 2019).

[59] GAO-16-410G. GAO-16-410G, Technology Readiness Assessment Guide: Best Practices for Evaluating the Readiness of Technology for Use in Acquisition Programs and Projects. 2016.

[60] Gao F, Jiang SP, Yan Y. Related Titles Proton Exchange Membrane Fuel Cells Modeling Fuel Cells Problems and Solutions, Second Edition Materials for High-Temperature Fuel Cells 2013 Print Hydrogen and Fuel Cells Fundamentals, Technologies and Applications 2010 Print. 2012.

[61] Kinoshita K, Lundquist JT, Stonehart P. Potential cycling effects on platinum electrocatalyst surfaces. J Electroanal Chem Interfacial Electrochem 1973;48:157–66. https://doi.org/10.1016/S0022-0728(73)80257-8.

[62] Yuan X-Z, Zhang S, Wang H, Wu J, Sun JC, Hiesgen R, et al. Degradation of a polymer exchange membrane fuel cell stack with Nafion® membranes of different thicknesses: Part I. In situ diagnosis. J Power Sources 2010;195:7594–9. https://doi.org/10.1016/J.JPOWSOUR.2010.06.023.

[63] Zakaria Z, Kamarudin SK, Timmiati SN. Membranes for direct ethanol fuel cells: An overview. Appl Energy 2016;163:334–42. https://doi.org/10.1016/J.APENERGY.2015.10.124.

[64] Blanchette S. A hydrogen economy and its impact on the world as we know it. Energy Policy 2008;36:522–30. https://doi.org/10.1016/J.ENPOL.2007.09.029.

[65] Zegers P. Fuel cell commercialization: The key to a hydrogen economy. J Power Sources 2006;154:497–502. https://doi.org/10.1016/J.JPOWSOUR.2005.10.051.

[66] EHA. EHA (Europian Hydrogen and Fuel Cell Association) 2019. https://www.h2euro.org/ (accessed August 24, 2019).

[67] Papageorgopoulos D. Fuel Cells R&D Overview. 2019.

[68] Ji M, Wei Z. A Review of Water Management in Polymer Electrolyte Membrane Fuel Cells. Energies (Basel) 2009;2:1057–106. https://doi.org/10.3390/en20401057.

[69] Chen H, Pei P, Song M. Lifetime prediction and the economic lifetime of proton exchange membrane fuel cells. Appl Energy 2015. https://doi.org/10.1016/j.apenergy.2014.12.062.

[70] Pei P, Chen H. Main factors affecting the lifetime of Proton Exchange Membrane fuel cells in vehicle applications: A review. Appl Energy 2014;125:60–75. https://doi.org/10.1016/J.APENERGY.2014.03.048.

[71] Baschuk JJJ, Li X. Mathematical model of a PEM fuel cell incorporating CO poisoning and O<SUB align=right>2 (air) bleeding. International Journal of Global Energy Issues 2003;20:245. https://doi.org/10.1504/IJGEI.2003.003966.

[72] Cheng S, Fang C, Xu L, Li J, Ouyang M. Model-based temperature regulation of a PEM fuel cell system on a city bus. Int J Hydrogen Energy 2015;40:13566–75. https://doi.org/10.1016/j.ijhydene.2015.08.042.

[73] Muñoz PM, Correa G, Gaudiano ME, Fernández D. Energy management control design for fuel cell hybrid electric vehicles using neural networks. Int J Hydrogen Energy 2017;42:28932–44. https://doi.org/10.1016/j.ijhydene.2017.09.169.

[74] Amiri A, Vijay P, Tadé MO, Ahmed K, Ingram GD, Pareek V, et al. Planar SOFC system modelling and simulation including a 3D stack module. Int J Hydrogen Energy 2016;41:2919–30. https://doi.org/10.1016/j.ijhydene.2015.12.076.

[75] Tang S, Amiri A, Tadé MO. System Level Exergy Assessment of Strategies Deployed for Solid Oxide Fuel Cell Stack Temperature Regulation and Thermal Gradient Reduction. Ind Eng Chem Res 2019;58:acs.iecr.8b04142. https://doi.org/10.1021/acs.iecr.8b04142.

[76] Sahraoui M, Tunisie EP De, Halouani K. Two-Dimensional Modeling of Electrochemical and Transport Phenomena in a PEM Fuel Cell 2007.

[77] You L. A parametric study of the cathode catalyst layer of PEM fuel cells using a pseudo-homogeneous model. Int J Hydrogen Energy 2001;26:991–9. https://doi.org/10.1016/S0360-3199(01)00035-0.

[78] Le A, Zhou B. A general model of proton exchange membrane fuel cell. J Power Sources 2008;182:197–222. https://doi.org/10.1016/j.jpowsour.2008.03.047.

[79] Yu D, Yuvarajan S. Electronic circuit model for proton exchange membrane fuel cells. J Power Sources 2005;142:238–42. https://doi.org/https://doi.org/10.1016/j.jpowsour.2004.09.041.

[80] Corrêa JM, Farret FA, Gomes JR, Simões MG. Simulation of Fuel-Cell Stacks using a Computer-Controlled Power Rectifier with the Purposes of Actual High-Power Injection Applications. IEEE Trans Ind Appl 2003;39:1136–42. https://doi.org/10.1109/TIA.2003.814548.

[81] Friede W, Rael S, Davat B. Mathematical model and characterization of the transient behavior of a PEM fuel cell. IEEE Trans Power Electron 2004;19:1234–41. https://doi.org/10.1109/TPEL.2004.833449.

[82] Amphlett JC, Mann RF, Peppley BA, Roberge PR, Rodrigues A. A model predicting transient responses of proton exchange membrane fuel cells. J Power Sources 1996;61:183–8. https://doi.org/10.1016/S0378-7753(96)02360-9.

[83] Kennedy J, Eberhart R. Particle Swarm Optimization. Proceedings of the IEEE International Conference on Neural Networks,4,1942-1948., Perth,WA,Australia: 1995, p. 1942–8. https://doi.org/10.1109/ICNN.1995.488968.

[84] Bouaicha A, Allagui H, Aglzim EH, Rouane A, Mami A. Validation of a methodology for determining the PEM fuel cell complex impedance modelling parameters. Int J Hydrogen Energy 2017;42:12738–48. https://doi.org/10.1016/j.ijhydene.2017.01.114.

[85] Restrepo C, Konjedic T, Garces A, Calvente J, Giral R. Identification of a Proton-Exchange Membrane Fuel Cell's Model Parameters by Means of an Evolution Strategy. IEEE Trans Industr Inform 2015;11:548–59. https://doi.org/10.1109/TII.2014.2317982.

[86] Ahmed OAA, Bleijs JAMAM. An overview of DC–DC converter topologies for fuel cell-ultracapacitor hybrid distribution system. Renewable and Sustainable Energy Reviews 2015;42:609–26. https://doi.org/10.1016/j.rser.2014.10.067.

[87] Falcão DS, Gomes PJ, Oliveira VB, Pinho C, Pinto AMFR. 1D and 3D numerical simulations in PEM fuel cells. Int J Hydrogen Energy 2011;36:12486–98. https://doi.org/10.1016/j.ijhydene.2011.06.133.

[88] Haghayegh M, Eikani MH, Rowshanzamir S. Modeling and simulation of a proton exchange membrane fuel cell using computational fluid dynamics. Int J Hydrogen Energy 2017;42:21944–54. https://doi.org/10.1016/j.ijhydene.2017.07.098.

[89] Yue M, Jemei S, Gouriveau R, Zerhouni N. Review on health-conscious energy management strategies for fuel cell hybrid electric vehicles: Degradation models and strategies. Int J Hydrogen Energy 2019;44:6844–61. https://doi.org/10.1016/j.ijhydene.2019.01.190.

[90] Ahmadi P, Torabi SH, Afsaneh H, Sadegheih Y, Ganjehsarabi H, Ashjaee M. The effects of driving patterns and PEM fuel cell degradation on the lifecycle assessment of hydrogen fuel cell vehicles. Int J Hydrogen Energy 2020;45:3595–608. https://doi.org/10.1016/j.ijhydene.2019.01.165.

[91] Azri M, Nurfatika Abdul Mubin A, Ibrahim Z, Abdrahim N, Rohani Sheikh Raihan S, Malaysia Melaka T. MATHEMATICAL MODELLING FOR PROTON EXCHANGE MEMBRANE FUEL CELL (PEMFC). J Theor Appl Inf Technol 2016;86.

[92] Jiao K, Ni M. Challenges and opportunities in modelling of proton exchange membrane fuel cells (PEMFC). Int J Energy Res 2017;41:1793–7. https://doi.org/10.1002/er.3798.

[93] Heidary H, Kermani MJ, Prasad AK, Advani SG, Dabir B. Numerical modelling of in-line and staggered blockages in parallel flowfield channels of PEM fuel cells. Int J Hydrogen Energy 2017;42:2265–77. https://doi.org/10.1016/j.ijhydene.2016.10.076.

[94] Li W, Zhang Q, Wang C, Yan X, Shen S, Xia G, et al. Experimental and numerical analysis of a three-dimensional flow field for PEMFCs. Appl Energy 2017;195:278–88. https://doi.org/10.1016/j.apenergy.2017.03.008.

[95] Friede W, Rael S, Davat B. Mathematical model and characterization of the transient behavior of a PEM fuel cell. IEEE Trans Power Electron 2004;19:1234–41. https://doi.org/10.1109/TPEL.2004.833449.

[96] Pourrahmani H, Moghimi M, Siavashi M. Thermal management in PEMFCs: The respective effects of porous media in the gas flow channel. Int J Hydrogen Energy 2019;44. https://doi.org/10.1016/j.ijhydene.2018.11.222.

[97] Wu B, Matian M, Offer GJ. Hydrogen PEMFC system for automotive applications. International Journal of Low-Carbon Technologies 2012;7:28–37. https://doi.org/10.1093/ijlct/ctr026.

[98] Saadaoui F, Mammar K, Hazzab A. Water Distribution and the Impact of Relative Humidity in a PEMFC Energy System using Macroscopic Energy Representation by Inversion Control. Majlesi Journal of Electrical Engineering 2021;15:57–68. https://doi.org/10.52547/mjee.15.3.57.

[99] Daud WRW, Rosli RE, Majlan EH, Hamid SAA, Mohamed R, Husaini T. PEM fuel cell system control: A review. Renew Energy 2017;113:620–38. https://doi.org/10.1016/j.renene.2017.06.027.

[100] Garcia-Gabin W, Dorado F, Bordons C. Real-time implementation of a sliding mode controller for air supply on a PEM fuel cell. J Process Control 2010;20:325–36. https://doi.org/https://doi.org/10.1016/j.jprocont.2009.11.006.

[101] Williams JG, Liu G-P, Thanapalan K, Rees D. Design and implementation of on-line self-tuning control for PEM fuel cells. World Electric Vehicle Journal 2008;2:7–17. https://doi.org/10.3390/wevj2040242.

[102] Yu Q, Srivastava AK, Choe S-Y, Gao W. Improved Modeling and Control of a PEM Fuel Cell Power System for Vehicles. Proceedings of the IEEE SoutheastCon 2006, 2006, p. 331–6. https://doi.org/10.1109/second.2006.1629373.

[103] Jianying L, Pengju Z, Fei W. Real -Time DC Servo Motor Position Control by PID Controllers Using Labview. 2009 International Conference on Intelligent Human-Machine Systems and Cybernetics, IHMSC 2009, vol. 1, Department of Electrical Engineering, Inner Mongolia Vocational College of Mechanical Andelectrical Technology, Huhhot, China: 2009, p. 206–9. https://doi.org/10.1109/IHMSC.2009.59.

[104] Zhang J, Liu G, Yu W, Ouyang M. Adaptive control of the airflow of a PEM fuel cell system. J Power Sources 2008;179:649–59. https://doi.org/https://doi.org/10.1016/j.jpowsour.2008.01.015.

[105] Outeiro MT, Chibante R, Carvalho AS, de Almeida AT. A new parameter extraction method for accurate modeling of PEM fuel cells. Int J Energy Res 2009;33:978–88. https://doi.org/10.1002/er.1525.

[106] Benchouia N, Elias HA, Derghal A, Lakhdar K. Modeling and validation of fuel cell PEMFC 2013.

[107] Hosseinpour J, Sadeghi M, Chitsaz A, Ranjbar F, Rosen MA. Exergy assessment and optimization of a cogeneration system based on a solid oxide fuel cell integrated with a Stirling engine. Energy Convers Manag 2017;143:448–58. https://doi.org/10.1016/j.enconman.2017.04.021.

[108] Alaswad A, Omran A, Sodre JR, Wilberforce T, Pignatelli G, Dassisti M, et al. Technical and Commercial Challenges of Proton-Exchange Membrane (PEM) Fuel Cells. Energies 2021, Vol 14, Page 144 2020;14:144. https://doi.org/10.3390/EN14010144.

[109] Wilberforce T, Olabi AG. Design of Experiment (DOE) Analysis of 5-Cell Stack Fuel Cell Using Three Bipolar Plate Geometry Designs 2020;12:4488.

[110] Bejan A, Tsatsaronis G (George), Moran MJ. Chapter 3: EXERGY ANALYSIS. Thermal Design and Optimization 1996:113–65.

[111] Terzi R, Terzi R. Application of Exergy Analysis to Energy Systems. Application of Exergy 2018. https://doi.org/10.5772/INTECHOPEN.74433.

[112] Chitsaz A, Haghghi MA, Hosseinpour J. Thermodynamic and exergoeconomic analyses of a proton exchange membrane fuel cell (PEMFC) system and the feasibility evaluation of integrating with a proton exchange membrane electrolyzer (PEME). Energy Convers Manag 2019;186:487–99. https://doi.org/10.1016/j.enconman.2019.03.004.

[113] Shaygan M, Ehyaei MA, Ahmadi A, Assad MEH, Silveira JL. Energy, exergy, advanced exergy and economic analyses of hybrid polymer electrolyte membrane (PEM) fuel cell and photovoltaic cells to produce hydrogen and electricity. J Clean Prod 2019;234:1082–93. https://doi.org/10.1016/j.jclepro.2019.06.298.

[114] Yilanci A, Dincer I, Ozturka HK. Performance analysis of a PEM fuel cell unit in a solar-hydrogen system. Int J Hydrogen Energy 2008;33:7538–52. https://doi.org/10.1016/j.ijhydene.2008.10.016.

[115] Kazim A. Exergy analysis of a PEM fuel cell at variable operating conditions. Energy Convers Manag 2004;45:1949–61. https://doi.org/10.1016/J.ENCONMAN.2003.09.030.

[116] Sevjidsuren G, Uyanga E, Bumaa B, Temujin E, Altantsog P, Sang D. Exergy Analysis of 1.2 kW NexaTM Fuel Cell Module. Clean Energy for Better Environment, InTech; 2012, p. 3–18. https://doi.org/10.5772/50602.

[117] Lipman TE, Edwards JL, Kammen DM. Fuel cell system economics: comparing the costs of generating power with stationary and motor vehicle PEM fuel cell systems. Energy Policy 2004;32:101–25. https://doi.org/10.1016/S0301-4215(02)00286-0.

[118] Rosen MA, Scott DS. A thermodynamic investigation of the potential for cogeneration for fuel cells. Int J Hydrogen Energy 1988;13:775–82. https://doi.org/10.1016/0360-3199(88)90038-9.

[119] Taner T. Energy and exergy analyze of PEM fuel cell: A case study of modeling and simulations. Energy 2018;143:284–94. https://doi.org/10.1016/j.energy.2017.10.102.

[120] A.J J, A.S A, A J, A.S A. Theoretical Energy and Exergy Analyses of Direct Methanol Fuel Cell. Adv Mater Sci Appl 2015;4:63–75. https://doi.org/10.5963/AMSA0403001.

[121] Mert SO, Dincer I, Ozcelik Z. Exergoeconomic analysis of a vehicular PEM fuel cell system. J Power Sources 2007;165:244–52. https://doi.org/10.1016/j.jpowsour.2006.12.002.

[122] Marandi S, Mohammadkhani F, Yari M. An efficient auxiliary power generation system for exploiting hydrogen boil-off gas (BOG) cold exergy based on PEM fuel cell and two-stage ORC: Thermodynamic and exergoeconomic viewpoints. Energy Convers Manag 2019;195:502–18. https://doi.org/10.1016/j.enconman.2019.05.018.

[123] Guerrero Moreno N, Cisneros Molina M, Gervasio D, Pérez Robles JF. Approaches to polymer electrolyte membrane fuel cells (PEMFCs) and their cost. Renewable and Sustainable Energy Reviews 2015;52:897–906. https://doi.org/10.1016/j.rser.2015.07.157.

[124] Swan DH, Dickinson BE, Arikara MP. Proton Exchange Membrane Fuel Cell Characterization for Electric Vehicle Applications. SAE Technical Paper Series 2010;1. https://doi.org/10.4271/940296.

[125] Wagner N, Schnurnberger W, Müller B, Lang M. Electrochemical impedance spectra of solid-oxide fuel cells and polymer membrane fuel cells. Electrochim Acta 1998;43:3785–93. https://doi.org/10.1016/S0013-4686(98)00138-8.

[126] Lee JH, Lalk TR. Modeling fuel cell stack systems. J Power Sources 1998;73:229–41. https://doi.org/10.1016/S0378-7753(97)02812-7.

[127] Larminie J, Dicks A. Fuel Cell Systems Explained Second Edition. 2nd editio. Chichester: WILEY; 2003.

[128] Büchi FN, Marek A, Scherer GG. In Situ Membrane Resistance Measurements in Polymer Electrolyte Fuel Cells by Fast Auxiliary Current Pulses. J Electrochem Soc 1995;142:1895–901. https://doi.org/10.1149/1.2044211/META.

[129] Hydrogen and Fuel cell Technology Office. Fuel Cell Basics | Department of Energy n.d. https://www.energy.gov/eere/fuelcells/fuel-cell-basics (accessed September 24, 2022).

[130] Ehsani M, Gao Y, Gay SE, Emadi A. Modern Electric, Hybrid Electric, and Fuel Cell Vehicles: Fundamentals, Theory, and Design. 2nd ed. Florida: CRC PRESS; 2004.

[131] Amiri A, Ahmed K, Tadé O. A steady-state and dynamic simulation tool for solid oxide fuel cell operation applications 2019:1–6.

[132] Hamnett A. Mechanism and electrocatalysis in the direct methanol fuel cell. Catal Today 1997;38:445–57. https://doi.org/10.1016/S0920-5861(97)00054-0.

[133] Yalcinoz T, Alam MS. Improved dynamic performance of hybrid PEM fuel cells and ultracapacitors for portable applications 2008. https://doi.org/10.1016/j.ijhydene.2008.01.027.

[134] Barbir F. PEM fuel cells : theory and practice. Second Edi. Academic Press; 2013. https://doi.org/10.1016/B978-0-12-387710-9.01001-8.

[135] Erdinc O, Uzunoglu M. Recent trends in PEM fuel cell-powered hybrid systems: Investigation of application areas, design architectures and energy management approaches. Renewable and Sustainable Energy Reviews 2010;14:2874–84. https://doi.org/10.1016/j.rser.2010.07.060.

[136] Alaswad A, Baroutaji A, Achour H, Carton J, Al Makky A, Olabi AG. Developments in fuel cell technologies in the transport sector. Int J Hydrogen Energy 2016;41:16499–508. https://doi.org/10.1016/j.ijhydene.2016.03.164.

[137] Islam MR, Shabani B, Rosengarten G, Andrews J. The potential of using nanofluids in PEM fuel cell cooling systems: A review. Renewable and Sustainable Energy Reviews 2015;48:523–39. https://doi.org/10.1016/j.rser.2015.04.018.

[138] E. Alizadeh*, S.M. Rahgoshay, M. Rahimi-Esbo MK, S.H.M. Saadat. A novel cooling flow field design for polymer electrolyte membrane fuel cell stack n.d.

[139] O'hayre R, Cha S, Colella W, Prinz F. Fuel cell fundamentals. Third Edit. New Jersey: John Wiley & Sons, Inc; 2009. https://doi.org/10.1007/978-0-387-73532-0_1.

[140] Hall JL. Cell components. Phytochemistry 1987;26:1235–6. https://doi.org/10.1016/s0031-9422(00)82398-5.

[141] S.N. Simons, R.B. King PRP. in Symposium Proceedings Fuel Cells Technology Status and Applications. In: E.H. Camara, editor. In Symposium Porceedings, Chicago: Institute of Gas Technology; 1982, p. 46.

[142] Kazim A. Exergoeconomic analysis of a PEM fuel cell at various operating conditions. Energy Convers Manag 2005;46:1073–81. https://doi.org/10.1016/j.enconman.2004.06.036.

[143] Barbir F, Gómez T. Efficiency and economics of proton exchange membrane (PEM) fuels cells. Int J Hydrogen Energy 1996. https://doi.org/10.1016/0360-3199(96)00030-4.

[144] Fuel Cell Guide - Fuel Cell Costs 2021. http://www.fuelcell.co.uk/fuel-cell-costs/ (accessed September 21, 2021).

[145] Middleton E. The economic case for green hydrogen as a transport fuel – Elgar Middleton 2021. https://www.elgarmiddleton.com/the-economic-case-for-green-hydrogen-as-a-transport-fuel/ (accessed September 21, 2021).

[146] Ebrahimnejad A, Sedighi K, Farhadi M. Exergy Analysis of Direct Methanol Fuel Cell Based on the Experimental Setup. World Appl Sci J 2014;10:1847–56. https://doi.org/10.5829/idosi.wasj.2014.31.10.612.

[147] Cost USIW. News Letter V1 #13 Cost of Water 2001. http://www.waterbank.com/Newsletters/nws13.html (accessed September 21, 2021).

[148] System HFC. User Manual. SpringerReference 2013:1–53. https://doi.org/10.1007/SpringerReference_28001.

[149] Wilberforce T, Biswas M, Omran A. Power and Voltage Modelling of a Proton-Exchange Membrane Fuel Cell Using Artificial Neural Networks. Energies (Basel) 2022;15:5587. https://doi.org/10.3390/en15155587.

[150] Omran A, Lucchesi A, Smith D, Alaswad A, Amiri A, Wilberforce T, et al. Mathematical model of a proton-exchange membrane (PEM) fuel cell. International Journal of Thermofluids 2021;11:100110. https://doi.org/10.1016/j.ijft.2021.100110.

[151] Barbir F. PEM Fuel Cells: Theory and Practice. Second Edi. Elsevier; 2013. https://doi.org/10.1016/B978-0-12-387710-9.01001-8.

[152] Petrocelli R. One-quadrant switched-mode power converters. CERN Accelerator School: Power Converters, CAS 2014 - Proceedings 2018;003:115–39. https://doi.org/10.5170/CERN-2015-003.115.

[153] Bizon N, Thounthong P. Real-time strategies to optimize the fueling of the fuel cell hybrid power source: A review of issues, challenges and a new approach. Renewable and Sustainable Energy Reviews 2018;91:1089–102. https://doi.org/10.1016/j.rser.2018.04.045.

[154] ATLAM Ö, DÜNDAR G. A practical Equivalent Electrical Circuit model for Proton Exchange Membrane Fuel Cell (PEMFC) systems. Int J Hydrogen Energy 2021;46. https://doi.org/10.1016/j.ijhydene.2021.01.108.

[155] Chavan SL. Electrical Equivalent Circuit Modeling And Parameter Estimation For PEM Fuel Cell Sudarshan Chavan 1* , Dhananjay Talange 2 1 2 2017:1–10.

[156] Wang C, Nehrir MH, Shaw SR. Dynamic models and model validation for PEM fuel cells using electrical circuits. IEEE Transactions on Energy Conversion 2005. https://doi.org/10.1109/TEC.2004.842357.

[157] Khubchandani V, Pandey K, Tayal VK, Sinha SK. PEM Fuel Cell integration with using Fuzzy PID technique. 1st IEEE International Conference on Power Electronics, Intelligent Control and Energy Systems, ICPEICES 2016 2017:3–6. https://doi.org/10.1109/ICPEICES.2016.7853450.

[158] Ghasemi J, Rakhtala SM, Rasekhi J, Dokhtala SR. PEM fuel cell system to extend the stack life based on a PID-PSO controller design. Complex Engineering Systems 2022;2:4. https://doi.org/10.20517/ces.2022.02.

[159] Malik S, Dutta P, Chakrabarti S, Barman A, Professor A. Parameter Estimation of a PID Controller using Particle Swarm Optimization Algorithm. International Journal of Advanced Research in Computer and Communication Engineering 2014;3:2278–1021.

[160] Maiti D, Acharya A, Chakraborty M, Konar A, Janarthanan R. Tuning PID and PI/λDδ Controllers using the Integral Time Absolute Error Criterion. 2008 4th International Conference on Information and Automation for Sustainability 2008:1–6.

[161] Jianying L, Pengju Z, Fei W. Real -Time DC Servo Motor Position Control by PID Controllers Using Labview. 2009 International Conference on Intelligent Human-Machine Systems and Cybernetics, IHMSC 2009, vol. 1, Department of Electrical

Engineering, Inner Mongolia Vocational College of Mechanical Andelectrical Technology, Huhhot, China: 2009, p. 206–9. https://doi.org/10.1109/IHMSC.2009.59.

[162] SAHRAIAN M, KODIYALAM S. TUNING PID CONTROLLERS USING ERROR-INTEGRAL CRITERIA AND RESPONSE SURFACES BASED OPTIMIZATION. Engineering Optimization 2000;33:135–52. https://doi.org/10.1080/03052150008940914.

[163] Thanapalan KKT, Williams JG, Liu GP, Rees D. MODELLING OF A PEM FUEL CELL SYSTEM 2008. https://doi.org/10.3182/20080706-5-KR-1001.1739.

[164] Conker Ç. A novel fuzzy logic based safe operation oriented control technique for driving HHO dry cell systems based on PWM duty cycle. Int J Hydrogen Energy 2019;44:9718–25. https://doi.org/10.1016/j.ijhydene.2018.10.243.

[165] Zeng W, Zhu W, Hui T, Chen L, Xie J, Yu T. An IMC-PID controller with Particle Swarm Optimization algorithm for MSBR core power control. Nuclear Engineering and Design 2020;360:110513. https://doi.org/10.1016/j.nucengdes.2020.110513.

[166] Ahmadi S, Abdi Sh, Kakavand M. Maximum power point tracking of a proton exchange membrane fuel cell system using PSO-PID controller. Int J Hydrogen Energy 2017;42:20430–43. https://doi.org/https://doi.org/10.1016/j.ijhydene.2017.06.208.

[167] Ottesen H. Dynamic performance of the nexa fuel cell power module. University of Minnesota Rochester 2004.

[168] Gauchía L, Martínez JM, Chinchilla M, Sanz J. Test bench for the simulation of a hybrid power train. 2007 European Conference on Power Electronics and Applications, EPE 2007. https://doi.org/10.1109/EPE.2007.4417235.

[169] Yun H, Zhao Y, Wang J. Modeling and simulation of fuel cell hybrid vehicles. Undefined 2010;11:223–8. https://doi.org/10.1007/S12239-010-0028-Y.

[170] Mahjoubi C, Olivier J-CC, Skander-mustapha S, Machmoum M, Slama-belkhodja I. An improved thermal control of open cathode proton exchange membrane fuel cell. Int J Hydrogen Energy 2019;44:11332–45. https://doi.org/10.1016/j.ijhydene.2018.11.055.

[171] Marignetti F, Minutillo M, Perna A, Jannelli E. Assessment of fuel cell performance under different air stoichiometries and fuel composition. IEEE Transactions on Industrial Electronics 2011;58:2420–6. https://doi.org/10.1109/TIE.2010.2069073.

[172] Hu Z, Xu L, Li J, Gan Q, Xu L, Ouyang M, et al. A multipoint voltage-monitoring method for fuel cell inconsistency analysis. Energy Convers Manag 2018;177:572–81. https://doi.org/10.1016/J.ENCONMAN.2018.09.077.

[173] Acharya P, Enjeti P, Pitel IJ. An advanced fuel cell simulator. Conference Proceedings - IEEE Applied Power Electronics Conference and Exposition - APEC 2004;3:1554–8. https://doi.org/10.1109/APEC.2004.1296071.

[174] Z. JIN, M. PuYANG QL and DG. DEVELOPMENT OF FUEL CELL HYBRID POWERTRAIN RESEARCH PLATFORM BASED ON DYNAMIC TESTBED. INternation JOuran of Automotive Technology 2008;9:26–32. https://doi.org/10.1007/s12239.

[175] Jin Z, Ouyang M, Lu Q, Gao D. Development of fuel cell hybrid powertrain research platform based on dynamic testbed. Undefined 2008;9:365–72. https://doi.org/10.1007/S12239-008-0044-3.

[176] Alaswad A, Omran A, Sodre JR, Wilberforce T, Pignatelli G, Dassisti M, et al. Technical and Commercial Challenges of Proton-Exchange Membrane (PEM) Fuel Cells. Energies 2021, Vol 14, Page 144 2020;14:144. https://doi.org/10.3390/EN14010144.

[177] Colella WG, Colella, G. W. Market prospects, design features, and performance of a fuel cell-powered scooter. JPS 2000;86:255–60. https://doi.org/10.1016/S0378-7753(99)00486-3.

[178] Amirinejad, M.; Rowshanzamir S; EMH. Effects of operating parameters on performance of a proton exchange membrane fuel cell. J. Power Sources 2006, 161, 872–875. - Google Search. Journal 2006. https://www.google.com/search?q=Amirinejad%252C+M.%253B+Rowshanzamir%252C+S.%253B+Eikani%252C+M.H.+Effects+of+operating+parameters+on+performance+of+a+proton+exchange+membrane+fuel+cell.+J.+Power+Sources+2006%252C+161%252C+872–875.&oq=Amirinejad%252C+M.%253B+Rowshanzamir%252 (accessed September 5, 2022).

[179] Chan SH, Goh SK, Jiang S. A mathematical model of polymer electrolyte fuel cell with anode CO kinetics. Electrochim Acta 2003;48:1905–19. https://doi.org/10.1016/S0013-4686(03)00269-X.

[180] Li X. Thermodynamic Performance of Fuel Cells and Comparison with Heat Engines. Advances in Fuel Cells 2007;1:1–46. https://doi.org/10.1016/S1752-301X(07)80006-8.

[181] Bernardi DM. A Mathematical Model of the Solid-Polymer-Electrolyte Fuel Cell. J Electrochem Soc 1992;139:2477. https://doi.org/10.1149/1.2221251.

[182] Nguyen T V., White RE. A Water and Heat Management Model for Proton-Exchange-Membrane Fuel Cells. J Electrochem Soc 1993;140:2178–86. https://doi.org/10.1149/1.2220792/XML.

[183] Silveira JL, Tuna CE. Thermoeconomic analysis method for optimization of combined heat and power systems. Part I. Prog Energy Combust Sci 2003;29:479–85. https://doi.org/10.1016/S0360-1285(03)00041-8.

[184] Bejan, Adrian, Tsatsaronis, George, Moran M. Thermal design and optimization - Google Books 1996. https://www.google.co.uk/books/edition/Thermal_Design_and_Optimization/sTi2crXeZYgC?hl=en&gbpv=1&dq=Bejan+A,+Tsatsaronis+G,+Moran+M.+Thermal+design+and+optimization.+John+Wiley+%26+Sons,+LTD%3B+1996&pg=PA1&printsec=frontcover (accessed September 19, 2021).

[185] Kazim A. A novel approach on the determination of the minimal operating efficiency of a PEM fuel cell. Renew Energy 2002;26:479–88. https://doi.org/10.1016/S0960-1481(01)00083-0.

[186] Sonal P. How Much Will Hydrogen-Based Power Cost? 2020. https://www.powermag.com/how-much-will-hydrogen-based-power-cost/ (accessed September 14, 2022).

[187] Büchi FN, Srinivasan S. Operating Proton Exchange Membrane Fuel Cells Without External Humidification of the Reactant Gases: Fundamental Aspects. J Electrochem Soc 1997;144:2767–72. https://doi.org/10.1149/1.1837893.

[188] de Bruijn FA, Dam VAT, Janssen GJM. Review: Durability and Degradation Issues of PEM Fuel Cell Components. Fuel Cells 2008;8:3–22. https://doi.org/10.1002/fuce.200700053.

[189] Daud WRW, Rosli RE, Majlan EH, Hamid SAA, Mohamed R, Husaini T. PEM fuel cell system control: A review. Renew Energy 2017;113:620–38. https://doi.org/10.1016/j.renene.2017.06.027.

Appendices

A.1 Publications and Grant Applications

A.1.1. Publications

1. Abdelnasir, O., Smith, D., Alaswad, A., Amiri, A., Sodre, J. R., & Lucchesi, A. (2019). *Proton-exchange membrane (PEM) fuel cell system mathematical modelling*. Paper presented at SDEWES, Dubrovnik, Croatia.

2. Alaswad A, Omran A, Sodre JR, Wilberforce T, Pignatelli G, Dassisti M, et al. Technical and commercial challenges of proton-exchange membrane (Pem) fuel cells. Energies (Basel) 2021;14. https://doi.org/10.3390/en14010144.

3. Omran, A., Lucchesi, A., Smith, D., Alaswad, A., Amiri, A., Wilberforce, T., Sodré, J. R., & Olabi, A. G. (2021). Mathematical model of a proton-exchange membrane (PEM) fuel cell. *International Journal of Thermofluids*, *11*, Article 100110. https://doi.org/10.1016/j.ijft.2021.100110

4. Wilberforce, T.; Biswas, M.; Omran, A. Power and Voltage Modelling of a Proton-Exchange Membrane Fuel Cell Using Artificial Neural Networks. *Energies* **2022**, *15*, 5587. https://doi.org/10.3390/en15155587

5. *Sodre, Jose Ricardo and Omran, Abdelnasir (2023). Exergoeconomic Model of a PEM Fuel Cell. IN: 36th International Conference on Efficiency, Cost, Optimization, Simulation and Environmental Impact of Energy Systems (ECOS 2023). ESP: Curran Associates Inc. Proceedings.*

A.1.2. Grant Applications

The following is a seed-corn grant from ASTUTE: £1493.13

Project Title: Development of innovative Proton Exchange Membrane fuel cell for the automotive industry

Introduction: my main input in the grand application includes the discussion of the idea, agreeing to do the experimental part as well as the writing up of the grand application and the future grant application and publications.

PI: Tabbi Wilberforce, Co-PI: Abed Alaswad, PhD student: Omran, Abdelnasir

Background: Heavy goods vehicles (HGVs) account for ~17% of UK greenhouse gas (GHG) emissions from road transport and ~21% NO_x emissions from just 5% of vehicle miles. The transport sector contributes around 25% of all Europe's GHG emissions, with road transport providing almost three-quarters of this figure. Meeting climate change targets will require GHG emissions reductions across all sectors of the economy, including road freight. EU regulations covering CO2 emissions produced by lorries have been introduced; after 2025, HGV manufacturers will be legally bound to a 15 per cent reduction in CO2, rising to 30 per cent by 2030. All fossil-fuelled vehicles will be banned from European cities by 2050. Scotland, for instance, will ban the sales of new petrol/diesel vehicles by 2032 and the UK by 2040.

Proposal: This project will address issues impeding the commercialisation of fuel cell electric vehicles from design to testing. **The project aim**s to experimentally determine the performance of a novel Proton Exchange Membrane fuel cell. The design considerations will also include ease and cost of manufacture, integration requirements within existing trucks and vehicles and total life cycle requirements.

Objectives:

1) Development: Develop a novel PEM fuel cell using open-pore cellular foam material as bipolar plate material and polybenzimidazole (PBI) as the membrane material.
2) Testing: Test the performance of the novel fuel cell at varying operational conditions.
3) Dissemination: Present work at the Sustainable Energy and Environmental Protection Conference in October 2020 and submit the ASTUTE report. Start applications for grants and journal paper draft in November 2020.

A.2 Project Plan

Table 1. First-year PhD project plan

Project name	Timescale		Research Question		Key Work Goals	Study Materials/Equipment	Skills Acquired	Output Conferences	Publications	Grants
	Start date	Finish date								
1. Test rig set up (500W PEMFC)	07/01/2019	30/04/2019	How to assemble and test the H-500W PEMFC rig.	1.	Check equipment.	Lab PC/ PEMFC Manual. Books	PEMFC test rig assembly and test			
				2.	Order extra parts	PC/Online orders				
				3.	Assemble the PEMFC rig.	Tools/ manuals.		Abstract to SDEWES2019		
				4.	Prepare test procedure.	Manuals, websites, journals.	Working Safely			
				5.	Test the rig.	Following procedures and RA.	Conducting RA			
				6.	Collect data.	Excel				

2. Literature Review (Fuel cell)	01/05/2019	26/07/2019	What is a fuel cell? And how it operates?	1.	Review Fossil fuel and its effect on Climate Change.	Journals Websites Books		
				2.	Review fuel cells.	Journals Websites Books		
				3.	PEMFC applications.	Journals Websites Books		Review journal paper (in progress)
				4.	R&D of PEMFC.	Journals Websites Books		
3. Literature Review of Hydrogen as an alternative fuel.	29/07/2019	04/10/2019	What is the future of hydrogen fuel?	1.	Hydrogen applications.	Journals Websites Books	Article and poster at SDEWES2019	
				2.	Hydrogen productions.	Journals Websites Books		

					Journals Websites Books		
4. Test rig set up (1.2 kW PEMFC)	07/10/2019	06/03/2020	How to assemble and test the Ballard 1.2kW PEMFC test rig.	1. Order parts.	PC/Online	Journal Submission to IJHE (Rejected)	
				2. Assemble parts.	Test rig Following procedure and RA.		
				3. Test rig.			
5. Writing Qualifying Report	09/03/2020	03/08/2020	Does the work completed so far and work planned enough for a successful PhD project?	1. Literature Review.	Journals Websites Books		Revise the journal paper and send it to the Thermofluid journal
				2. PhD research plan.	MS Office/ Proposal		
				3. Methodology.	MS word		
				4. Four years plan	MS Office/ Proposal		

5.	Preparing two test rigs.	Tools/ Manuals
6.	Prepare testing procedure and Risk Assessment.	Websites/ Manuals
7.	Run the experiment and collect data.	PC, test rig/ Testing procedure and RA
8.	Analyse data.	Excel
9.	Validated Mathematical steady-state modelling for H-500W PEMFC.	Test rig/ MATLAB Simulink
10.	Followed pieces of training	See Appendices

Table 2. Second-year PhD Project Plan

Project name	Timescale		Research Question		Key Work Goals	Study Materials/Equipment	Skills Acquired	Output Conferences	Publications	Grants
	Start date	Finish date								
1. Develop and test an improved PEMFC rig.	04/08/2020	30/12/2020	How to develop the PEMFC System?	1	Check existing equipment.	Lab PC/ PEMFC Manual. Books	1. How to conduct a process fault diagnosis.			
				2	Order parts.	PC/Online orders				
							2. Identify how to fix the fault.			
				3	Assemble the upgraded equipment	Tools/ manuals.				
				4	Prepare test procedure.	Manuals, websites, journals.	Working Safely			
				5	Test the rig.	Following procedure and RA.	Conducting RA	Journal paper to Energies journal		

				6	Collect data.	Excel	
2. Test the performance with various operation conditions	01/01/2021	14/03/2021	How to optimise a PEMC?	1	Running a trial test using humidified membrane		
				2	Operating the fuel cell at varying conditions.	Test rig	Optimisation technics
				3	Running tests using the lab view control system.		
				4	Optimising a fuel cell using the new test procedure.		
3. Comparing the experimental results with numerical	15/03/2021	30/06/2021	How to validate numerical and experimental data?	1	Collecting data		

data to ascertain the margin of error.								
				2	Analyse data.	Excel		
				3	Develop a mathematical model for comparison.	MATLAB		
4. Literature review and paper draft.	01/07/2021	03/08/2021	How to publish a new work?	1	Review the literature	PC/Online	Writing for publications	Journal paper Submission
				2	Analyse data.			
				3	Progression report submission			

Table 3. Third-year PhD Project Plan

Project name	Timescale		Research Question		Key Work Goals	Study Materials/Equipment	Skills Acquired	Output Conferences	Publications	Grants
	Start date	Finish date								
1. Test rig Upgrade (Nexa 1.2kW PEMFC system)	04/08/2021	31/10/2021	How to upgrade and test the Nexa 1.2kW PEMFC system for thermal and humidity control?	1	Check equipment.	Lab PC/ PEMFC Manual. Books	PEMFC test rig upgrade and test			
				2	Order extra parts	PC/Online orders	Characterisation of PEMFC			
				3	Upgrade PEMFC rig.	Tools/ manuals.				
				4	Prepare test procedure.	Manuals, websites, journals.	Working Safely			
				5	Test the rig.	Following procedure and RA.	Conducting RA		Journal Paper to Energies journal	

				6	Collect data.	Excel	
2. Develop an Exergoeconomic model for PEMFC optimisation	01/11/2021	28/02/2022	How to optimise PEMFC using the Exergoeconomic model?	1	Get training	Journals Websites Books	
				2	Literature Review.	Journals Websites Books	
				3	Build the model	Journals Websites Books	MATLAB
3. Validate the model and analyse the data	01/03/2022	07/05/2022	How can a model improve performance?	1	MATLAB/Experimental setup.	Journals Websites Books	
				2	Hydrogen productions.	Journals Websites Books	
				3	Hydrogen storage.	Journals Websites Books	
4. Thesis Writing up	08/05/2022	15/10/2022	Optimisation of PEMFC	1	Background	PC/Online	Journal paper Submission
				2	Aims and objectives		

3 Experimental setup and methodology

4 Results

5 Discussion and conclusion

Using Mendeley for referencing

5. Extension

Extra chapter

16/10/2022

30/06/2023

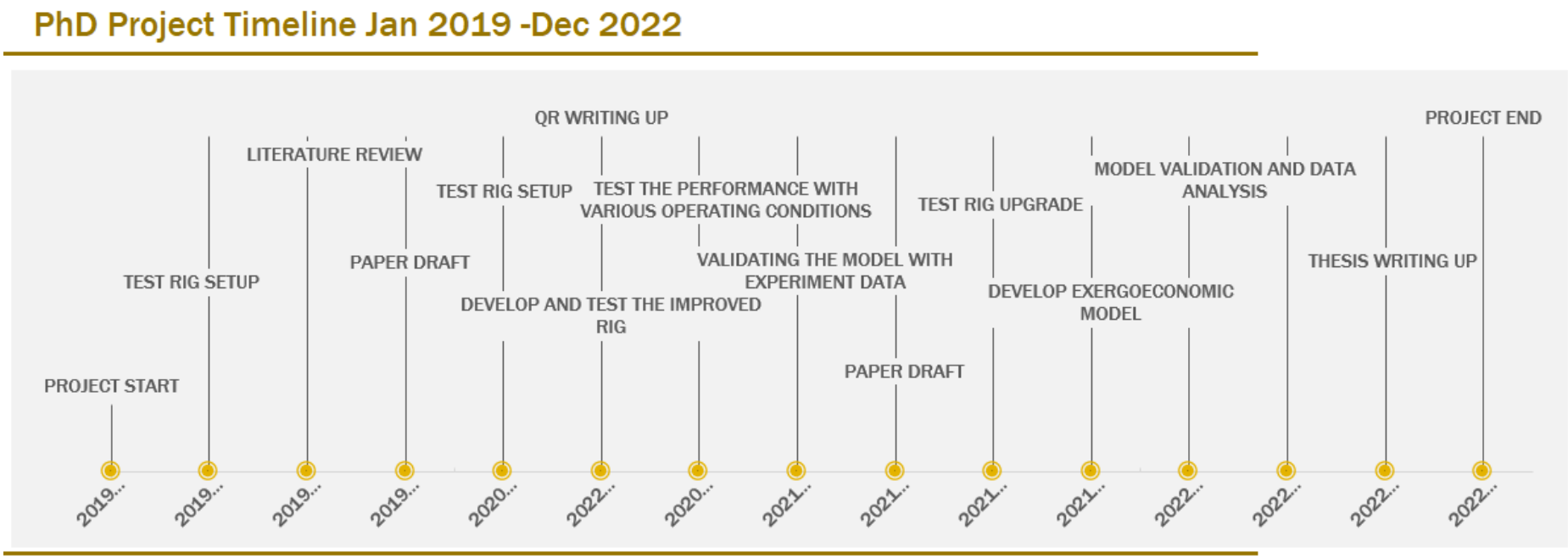

Fig. 1. Timeline of the PhD project

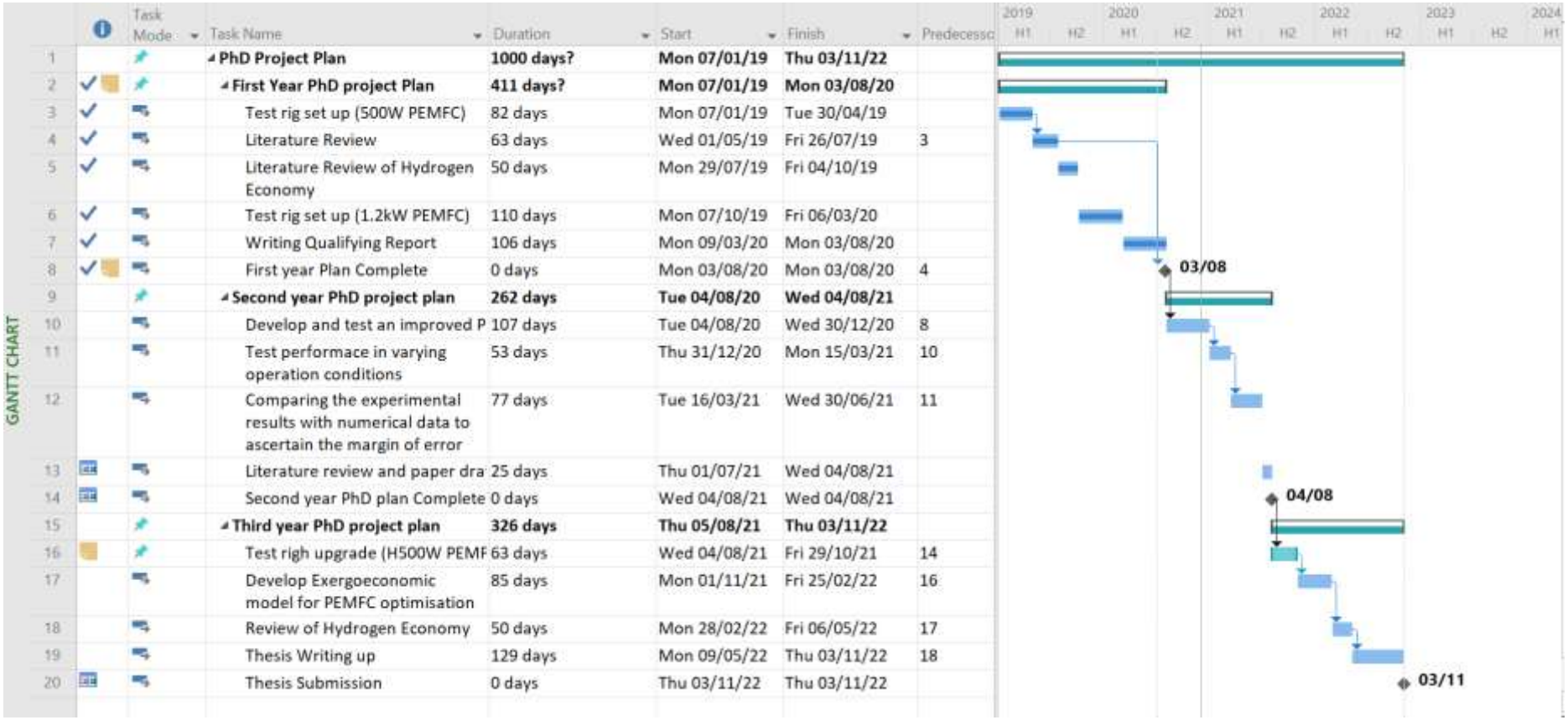

	Task Name	Duration	Start	Finish	Predecessors
1	**PhD Project Plan**	**1000 days?**	**Mon 07/01/19**	**Thu 03/11/22**	
2	**First Year PhD project Plan**	**411 days?**	**Mon 07/01/19**	**Mon 03/08/20**	
3	Test rig set up (500W PEMFC)	82 days	Mon 07/01/19	Tue 30/04/19	
4	Literature Review	63 days	Wed 01/05/19	Fri 26/07/19	3
5	Literature Review of Hydrogen Economy	50 days	Mon 29/07/19	Fri 04/10/19	
6	Test rig set up (1.2kW PEMFC)	110 days	Mon 07/10/19	Fri 06/03/20	
7	Writing Qualifying Report	106 days	Mon 09/03/20	Mon 03/08/20	
8	First year Plan Complete	0 days	Mon 03/08/20	Mon 03/08/20	4
9	**Second year PhD project plan**	**262 days**	**Tue 04/08/20**	**Wed 04/08/21**	
10	Develop and test an improved P	107 days	Tue 04/08/20	Wed 30/12/20	8
11	Test performace in varying operation conditions	53 days	Thu 31/12/20	Mon 15/03/21	10
12	Comparing the experimental results with numerical data to ascertain the margin of error	77 days	Tue 16/03/21	Wed 30/06/21	11
13	Literature review and paper dra	25 days	Thu 01/07/21	Wed 04/08/21	
14	Second year PhD plan Complete	0 days	Wed 04/08/21	Wed 04/08/21	
15	**Third year PhD project plan**	**326 days**	**Thu 05/08/21**	**Thu 03/11/22**	
16	Test righ upgrade (H500W PEMF	63 days	Wed 04/08/21	Fri 29/10/21	14
17	Develop Exergoeconomic model for PEMFC optimisation	85 days	Mon 01/11/21	Fri 25/02/22	16
18	Review of Hydrogen Economy	50 days	Mon 28/02/22	Fri 06/05/22	17
19	Thesis Writing up	129 days	Mon 09/05/22	Thu 03/11/22	18
20	Thesis Submission	0 days	Thu 03/11/22	Thu 03/11/22	

Fig. 2. Gantt Chart of the PhD

A.3 Exergoeconomic M. Script code

Theoretical electrical power

```
 % Im   = 36.59;                % in Ampere
 % Vm   = 29.20;                % in Volt
 % E_Ext = Im*Vm;               % in Watt
 Ith = 1: 46;
 Ica =
[3.38,3.81,4.51,5.92,7.20,11.02,12.93,12.66,16.24,12.66,18.28,19.29,19.23,19.02,24.13,24.56,26.42,26.09,25.38,30.34,31.6
8,36.59];
 Vca =
[38.57,38.42,37.94,36.91,36.36,35.51,35.52,35.88,34.60,35.88,34.48,34.17,34.30,34.17,32.32,32.24,31.07,30.95,31.14,30.77
,30.10,29.20];
 Ee = Ica.*Vca;
 yyaxis left
 plot(Ica,Vca,'*')
 ylabel('Stack Voltage (V)')
 hold on
 I1 =  -0.2997;
 I2 =   39.44;
 Vth = I1*Ith+I2;
 plot(Ith,Vth)
 xlabel('Current (A)')
 yyaxis right
 plot(Ica,Ee,'o')
 hold on
 p1 =     -0.3072;
 p2 =      39.6;
 p3 =      0.4246;
```

```
Eth = p1*Ith.^2 + p2*Ith + Ith
```

```
Eth = 1×46

10^3 ×

    0.0403    0.0800    0.1190    0.1575    0.1953    0.2325    0.2691 ⋯
```

```
plot(Ith,Eth)
ylabel('Power (Watt)')
grid on
legend('Experiment Voltage','Curve fit voltage (Theory)','Experiment Power','Curve fit Power (Theory)')
legend('Position',[0.31032,0.80959,0.41648,0.19436])
```

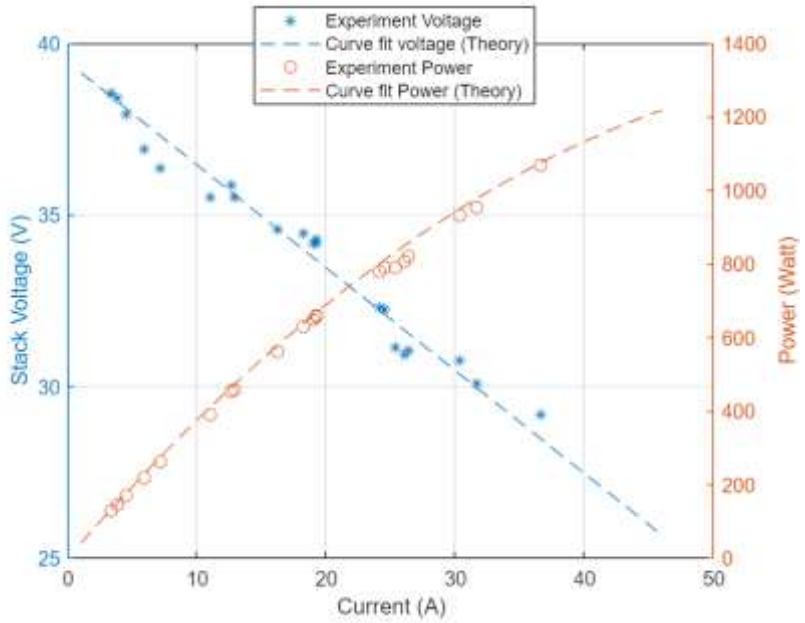

Constants

```
P0   = 1;             % standard pressure (atm).
T0   = 298.15;        % ambient standard temperature (K)
```

Variables

```
T = T0 * 0.94:0.01:1.2;
P = P0 * 7.40:-0.01:4.88;


% J = 0.001:0.001:0.79;
% Ica = J*120;                    % in Ampere 1:0.5:46;
% Vca  =  (0.001:0.001:0.79)*47;  % Stack voltage
% Vca = 29.2;                   % in Volt 43:-0.2:25;
lambda  = 3;
```

Current Density

```
 %J = 0:0.01:0.8;                     % current density (A/cm^2),120 is the area of the cell in cm^2.
 %Ica = J*120;
F    = 96485.33212;           % Faraday's constant (F) in C/mole
mH2  = 47*Ica/(2*F);          % the mass flow rate of Hydrogen
Ee    = Ica .* Vca;           % The total theoretical electrical power output of the Nexa
E_Aux = Ee - E_Ext;           % in Watt

%plot(J,Vca)
%hold on
%plot(J,Ee)
```

Mass Flow rates

```
Vc      = 26;
m_airR  = 3.57e-7*lambda*Ee/Vc;
m_H2R   = 1.05e-8 * (Ee/Vc);
m_O2    = 8.29e-8 * (Ee/Vc);
m_airP  = m_airR - m_O2;
m_H2O_P = 9.34e-8 * (Ee/Vc);
```

Physical Exergy

```
Cp   = 1.005;         % constant specific heat
k    = 1.4;           % Specific heat ratio
 Xe_ph = Cp*T0*(T/T0-1-log(T/T0)+((k-1)/k)*log((P/P0)));           % Physical exergy: or  thermo mechanical exergy
```

Reactant Air Exergy

```
%Xe_ch is chemical exergry, R : reactance, P: Product
Xne_ch_O2_R = 124000;                          % standard chemical exergy kJ / kg
Xne_ch_N2_R = 25714;                           % standard chemical exergy kJ / kg
xn_O2_R   = 0.207;                             % molar fraction of component n
xn_N2_R   = 0.775;                             % molar fraction of component n
R     =   8.3145;                               % universal gas constant kJ / kmolK
Xe_ch_O2 = xn_O2_R*Xne_ch_O2_R+R*T0*xn_O2_R*log(xn_O2_R);
Xe_ch_N2 = xn_N2_R*Xne_ch_N2_R+R*T0*xn_N2_R*log(xn_N2_R);
Xe_ch_air_R = Xe_ch_O2 + Xe_ch_N2;
XairR = m_airR*(Xe_ch_air_R+Xe_ph);
```

Reactant Hydrogen

```
Xne_ch_H2_R = 118050000;                          % standard chemical exergy kJ / kg
xn_H2_R     = 1;                                  % molar fraction of component n
Xe_ch_H2_R = xn_H2_R*Xne_ch_H2_R+R*T0*xn_H2_R*log(xn_H2_R);
XH2R = m_H2R*(Xe_ch_H2_R+Xe_ph);
```

Product Air Exergy

```
XairP = m_airP*(Xe_ch_air_R+Xe_ph);            % This what I found Xe_ch_air_R
```

Product Water

```
Xne_ch_H2O_P = 50550;
xn_H2O_P     = 1;
Xe_ch_H2O_P = xn_H2O_P*Xne_ch_H2O_P+R*T0*xn_H2O_P*log(xn_H2O_P);
XH2OP = m_H2O_P*(Xe_ch_H2O_P+Xe_ph);
```

Exergy Efficiency

```
eta = Ee./((xirr+XH2R)-(XairP+XH2OP))*100
```

Exergoeconomic Constants

```
CF = 0.9;               % The project function rate is 90%.
ir = 0.7 ;              % The annual inerest rate is 7%.
ny = 5 ;                % The number of years life of PEM FC.
PEMcost = 250;          % PEM FC cost based on the annual average cost of mass production $/kW of powr output.
OM = 30 ;               % The annual operation and maintenance cost $/kW yr.
AIRcost = 0.011;        % The cost of air in $/kg.
H2Ocost = 1;            % The water cost in $/m3.
H2cost = 10;            % The hydrogen cost in $/kg.
```

```
Syr = 8760*3600          % Converting the year to seconds.
```

Exergy cost

```
OMcost = (OM*Ee)/Syr;                       % The cost of annual operation and maintenance cost of Nexa 1.2kW ($/s).
CRF = (ir*(1+ir)^ny)/((1+ir)*ny-1);         % The capital recovery factor.
ACC = OMcost*CRF;                           % The annual capital cost.
CIcost = (ACC.*Ee)/(CF.*Syr);               % The capital investment cost.
FCcost = CIcost.*OMcost;                    % The total investment cost.
%EeCost = ((AIRcost*XairR)+(H2cost*XH2R)-(H2Ocost*XH2OP)-(AIRcost*XairP)+FCcost)/Ee; % Exergetic power cost ($GJ).
```

A.4 Improved Closed Loop Boost Converter Design Parameters

Variables

```
outpV = 48;      % Output voltages (V) of the boost converter.

BCFrq = 10000;   % Boost converter frequency (Hz).

ExMaxP = 2000;   % The maximum power of Nexa (W).

ExinV = 22;      % The input voltage (V) which is the max input Voltage of nexa.
```

Equations

```


ExMaxI = ExMaxP/outpV ;                 % To find the maximum current.
Delt_outpV = 0.01*outpV ;               % Delta output voltage.

Delt_LodI = 0.01*ExMaxI*(outpV/ExinV) ; % calculating Delta of the load current to resistance.
```

Calculating the values of inductance, capacitor, load and duty cycle

```
D_cycVal = (outpV-ExinV)/outpV;                                  % The duty cycle value.

CapVal = (ExMaxI*(1-(ExinV/outpV)))/(BCFrq*Delt_outpV) ;         % Capacitor value.

IndVal = (ExinV*(outpV-ExinV))/(Delt_LodI*BCFrq*outpV) ;         % Inductance value.



RsisVal = outpV/ExMaxI ;                                         % Resistance load value.
Cr = 1-D_cycVal ;                                                % Part of the I-rip calculations.

T_s = D_cycVal/BCFrq;                                            % Calculating the switching period.

I_rip = D_cycVal*(Cr)^2 ;                                        % Calculating the current ripples.

                                                                 % Calculate the Voltage ripples.
```

A.5 PSO algorithms optimisation M. Script code

A.5.1 PSO Optimisation code for Nexa 1.2 kW PEMFC

Define the details of the design problem

```
% nVar = 2;                      % number of variables
nVar = 3;

%Ymax = [10 10 10];              %upper Bound

 Ymax = [999 999 999];

Ymin = [0 0 0];                  % lower bound
```

```
fobj = @optimising;              % Objective function Name
```

Define the PSO parameters

```
% P = 19;                  % number of particles for initialization

noP = 19;

% maxIter = 99;            % maximum iterations

maxIter = 999;


wMax = 0.9;                % maximum and minimum inertial
wMin = 0.4;


0₁ = 2;                    % constant related to position and velocity

0₂ = 2;

Cmax =(Ymax -Ymin ). * 0.2;

 Cmin = - Cmax;
```

Initialize the particles

```
for k = 1: noP
    Swarm.Particles(k).z = (Ymax - Ymin).* rand(1,nVar) + Ymin;

    Swarm.Particles(k). y = zeros (1, nVar);

    Swarm.Particles(k). PBEST.z = zeros(1, nVar);
```

```
    Swarm.Particles(k). PBEST.O = inf;


    Swarm.GBEST.z = zeros (1, nVar);
    Swarm.GBEST.O = inf;
end
```

Main loop

```
for t = 1: maxIter
```

Calculate the objective value

```
    for k = 1 : noP
        currentX = Swarm.Particles(k).z;
        Swarm.Particles(k). O = fobj(currentz);
```

Update the PBEST

```
        if Swarm.Particles(k). O < Swarm.Particles(k). PBEST.O
            Swarm.Particles(k). PBEST.z = currentz;
            Swarm.Particles(k). PBEST.O = Swarm.Particles(k). O;
        end
```

```
        % Update the GBEST
        if Swarm.Particles(k).O < Swarm.GBEST.O
            Swarm.GBEST.z = currentz;
            Swarm.GBEST.O = Swarm.Particles(k).O;
        end
    end

    % Update the z and y vectors
    w = wMax - t .* ((wMax - wMin) / maxIter);

    for k = 1 : noP
        Swarm.Particles(k).y = w .* Swarm.Particles(k).y + 0₁ .* rand(1,nVar) .* (Swarm.Particles(k).PBEST.y -
Swarm.Particles(k).y) + 0₂ .* rand(1,nVar) .* (Swarm.GBEST.y - Swarm.Particles(k).y);
```

Check velocities

```
        index1 = find (Swarm.Particles(k).y > Cmax);
        index2 = find (Swarm.Particles(k).y < Cmin);

        Swarm.Particles(k). y(index1) = Cmax (index1);
        Swarm.Particles(k). y(index2) = Cmin (index2);
```

```
        Swarm.Particles(k).z = Swarm.Particles(k).z + Swarm.Particles(k). y;
```

Check positions

```
        index1 = find (Swarm.Particles(k).z > Ymax);
        index2 = find (Swarm.Particles(k).z < Ymin);

        Swarm.Particles(k).z(index1) = Ymax (index1);
        Swarm.Particles(k).z(index2) = Ymin (index2);

    end
```

Showing Results

```
    outmsg = ['Iteration# ', num2str(t) , ' Swarm.GBEST.O = ' , num2str(Swarm.GBEST.O)];
    disp(outmsg);

    cgCurve(t) = Swarm.GBEST.O;
end
```

```
semilogy(cgCurve);
xlabel('Iteration#')
ylabel('Weight')
```

A.5.2 Cost function code

```
function cost = optimising(kk)
% kk=[0 0.16694 ];
assignin('base','kk',kk);
% assignin('base','kk', (2));
% [~,~]=sim('PSO_optimising_PID',[0 1]);
sim('PSO_optimising_PID');
% cost= e(length(e));
% cost= ITAE (length(ITAE));
cost= ITSE (length (ITSE));
% cost= ISE (length (ISE));
% cost = IAE (length (IAE));
end
```

A.5.3 The complete PSO optimisation model built up in Simulink linked to the code through a workspace block.

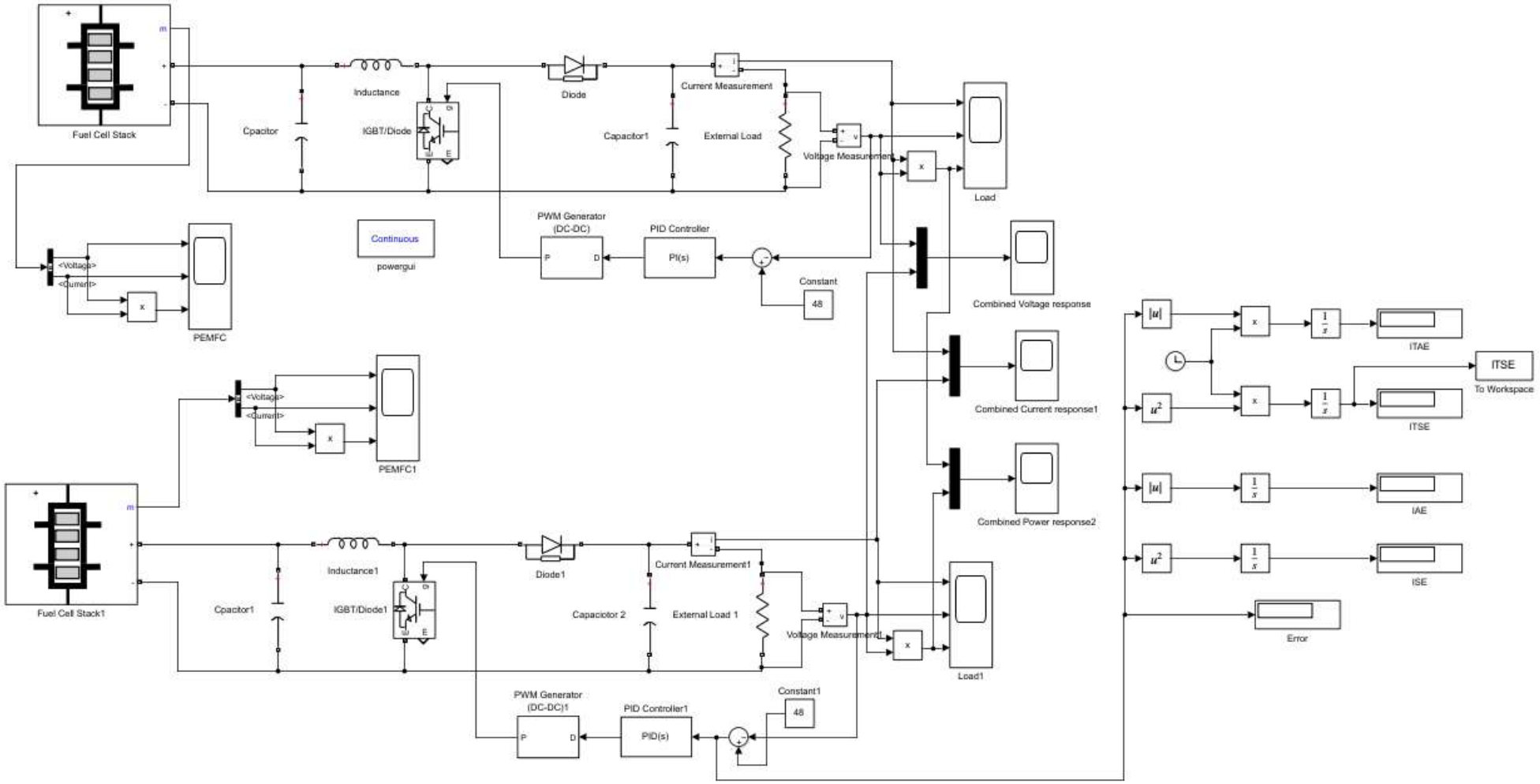

A.6 PSO algorithm for PID optimisation

As future work, the PID model can be further enhanced by using Particle Swarm Optimisation (PSO) code. One of the drawbacks of using the PID controller to control and maintaining the voltage at a fixed reference is that the coefficients are limited and do not consider the changes on important PEM fuel cell parameters such as fuel pressure, water content in the membrane and stack temperature. Combining the PID controller with a PSO algorithm will help to reduce these limitations.

In 1995, the PSO method was introduced to the field of optimisation. The uniqueness of PSO is that it can be used to provide solutions to optimise problems with unimodal or multimodal landscapes. Some of the PSO parameters are iterations, velocity, particle, swarm size, acceleration and random coefficients. The group of particles move in an s-dimensional space where the solution should be found. Each particle (P) has allocation (Z) corresponding to a possible solution, velocity (y) and the best private location alongside the best global swarm location (h) achieved so far. The best global position is shared by all particles, which move to find the best location in the search space. The velocity of particles is updated in time steps of (t), which is added to the value in the previous location so that particles can move to their new locations according to [158,166]:

$$Z(t+1) = Z(t) + y(t+1) \qquad (A.1)$$

The new velocity is updated form the previous one as:

$$y(t+1) = \omega y(t) + L(0,\theta_1).\big(p(t) - z(t)\big) + L(0,\theta_2).d\big(h(t) - z(t)\big) \qquad (A.2)$$

where L (e, f) is a random variable of uniform distribution in the interval [e, f]. ω is a parameter known as inertia coefficient, which show the dependence of the new velocity on the previous one. The parameters θ_1 and θ_2 represent the importance of $p(t)$ and $h(t)$, respectively. Moreover, in all iterations there is an upper limit (C_{max}) and lower limit (C_{min}) to the velocity factor y(t) of all particles. Based on an uniform distribution, the particles are assigned an initial

position (coordinates) in the search space as well as initial velocities that are drawn randomly for the interval $[-Y_{max}, Y_{min}]$.

The POS optimisation code has been built using M. Script. Although the template is an open source, the information has been filled according to the improved PID model here developed. Another important part of the PSO optimisation code is a suitable cost function for optimisation. Although researchers have shown many suitable cost functions, to evaluate the best one for this model the available cost functions have been collected and modelled in Simulink. After running the model, the cost function with the less error value has been selected which is the Integral Time Square Error (ITSE) (Fig. A.1) [162].

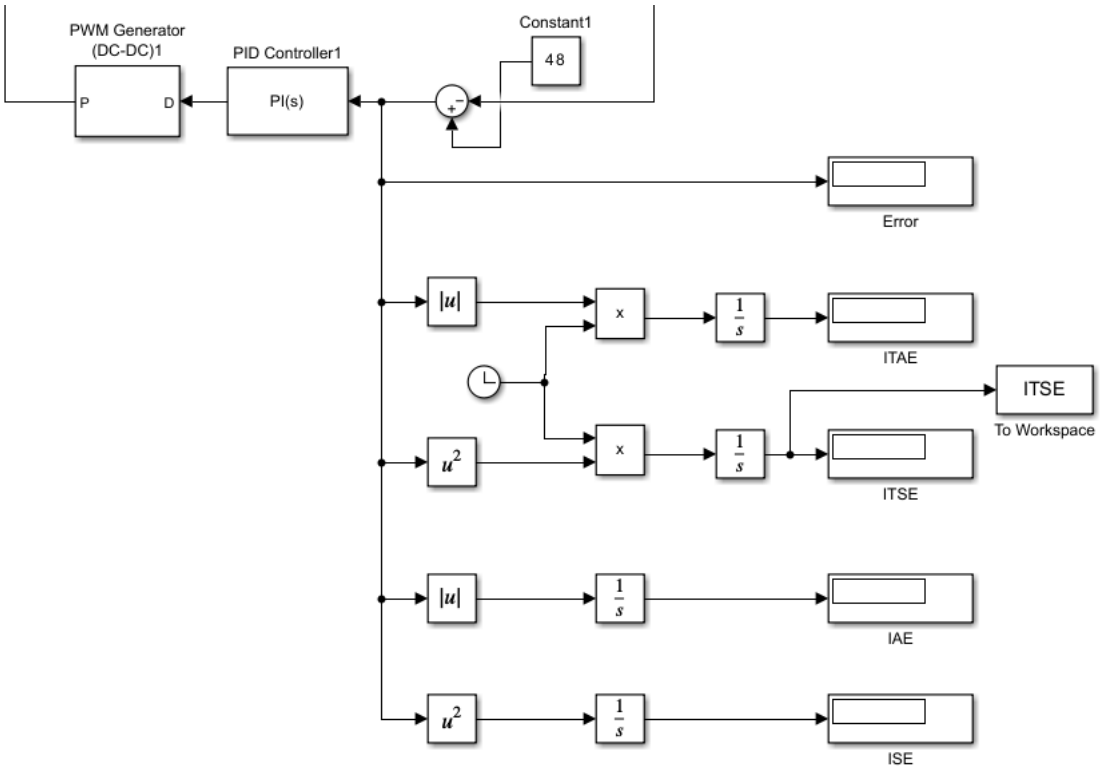

Figure A.1. Selection of the right PSO optimisation cost function (ITSE).

The reason for this selecting ITSE is that the response of the model is of slow decaying type. The ISTE is defined as follows [162]:

$$ISTE = \int_0^x t^2\, e(t)^2 dt \qquad (A.3)$$

The PSO optimisation algorithm to enhance the PID has the values of kp, ki and kd as shown in Table 11. The parameters of the PSO have been chosen as shown in Tab. A.1.

Table A.1. PSO parameters.

PARAMETER	VALUE
Number of particles	19
Number of iterations	999
Inertial interval $\boldsymbol{\omega}$	$(0.4, 0.9)$
Space interval Y_{min}	(0 0 0)
Space interval Y_{max}	(999 999 999)
Constant numbers θ_1 and θ_2	2